Aus dem
Max-Planck-Institut
für Neurobiologie

Role of the posterior insular cortex in cardiorespiratory interoception during fear

Dissertation
zum Erwerb des Doctor of Philosophy (Ph.D.) an der Medizinischen Fakultät der Ludwig-Maximilians-Universität München

vorgelegt von
Caroline Weiand

aus
München / Deutschland

Jahr
2026

Mit Genehmigung der Medizinischen Fakultät der
Ludwig-Maximilians-Universität München

Erstes Gutachten:	Prof. Dr. Dr. Elisabeth Binder
Zweites Gutachten:	Dr. Nadine Gogolla
Drittes Gutachten:	Prof. Dr. Lars Kellert
Viertes Gutachten:	Priv. Doz. Dr. Mathias Kunz

Dekan: Prof. Dr. med. Thomas Gudermann

Tag der mündlichen Prüfung: 15.01.2026

Table of content

Abstract

Interoception refers to the sensing, processing, regulation and prediction of internal signals. During fear, baseline, homeostatic interoceptive processes are disrupted in favor of changes, which are required to avoid danger and harm. However, when fear becomes pathological, these processes are altered. A growing body of literature suggests important interactions between different interoceptive measures and emotion regulation. Most prominently, cardiac and respiratory interoception have been implicated in fear and anxiety. An additional cardiac measure commonly used to reflect internal arousal state is heart rate variability which has been implicated to reflect trait anxiety. Furthermore, imaging studies have revealed the insular cortex as an important interoceptive hub. Importantly, the insular cortex has shown to not only be crucial in normal interoceptive processing but to also display a markedly altered activity in patients with anxiety disorders. Interestingly, anxiety disorders are associated with disruptions of brain-body communication.

Bodily signals are transmitted via cranial nerves and processed in the brainstem, before reaching cortical levels. The most important components of this lower order processing are the vagus nerve and the nucleus of the solitary tract (NTS). On the cortical level, the posterior insular cortex (pInsCtx), also called the visceral cortex, receives, processes, and influences these internal as well as external cues. This ability, along with its interconnection properties, makes it a central cortical region that is heavily involved in interoception. Additionally, the pInsCtx has been shown to play a crucial part in the processing of aversive emotions. As such, it has been identified to play an important role in fear and extinction learning. Moreover, studies implicated pInsCtx in the perception and regulation of cardiac signals by suggesting a tight coupling during fear.

This study aims to advance current knowledge of body-brain interactions during fear by characterizing pInsCtx interactions with cardiac and respiratory measures during fear and anxiety.

Wireless telemetry in freely moving mice was utilized to measure cardiac signals via electrocardiogram (ECG) recordings as well as respiration via measurements of changes in intrapleural pressure. The ECG signals further allowed for calculation of the heart rate variability. Additionally, bulk calcium recordings via fiber photometry were employed to measure neuronal pInsCtx activity. To obtain a comprehensive picture of pInsCtx-body

interactions, measurements were taken during undisturbed settings in the home cage, during conditioned fear learning and fear extinction, and innate fear paradigms. Furthermore, to explore differences between signaling in the brainstem versus the pInsCtx, additional fiber photometry recordings from the NTS were obtained in a subset of animals. Lastly, brain-body interactions were probed for directionality and utility in predictive analyses.

My results indicate that activity in the pInsCtx reflects different interoceptive computations compared to the brainstem. They further suggest that pInsCtx and body relationship is not only cue- and behaviour- dependent, but also changes depending on internal fear state. I found a significant positive interaction between the pInsCtx and heart rate variability during fear learning, highlighting the potential of the pInsCtx to reflect arousal rather than purely autonomic signaling. Intriguingly, my findings provide evidence for the emergence of a lateralization in the pInsCtx during fear learning. Moreover, directionality analyses reveal fear-state dependent changes in pInsCtx-body interactions. Finally, my data indicates an important role of the interaction between pInsCtx and respiration as a feature of successful fear extinction. Overall, this study corroborates the role of pInsCtx in fear and processing of bodily signals, adding insights into bidirectional cardiorespiratory influences and emotional lateralization.

List of figures and tables

List of abbreviations

Abbreviation	
aInsCtx	Anterior insular cortex
ADF	Augmented Dickey-Fuller
BIC	Bayesian information criterion
BLA	Basolateral amygdala
Bpm	Beats per minute
Brpm	Breaths per minute
CeA	Central nucleus of the amygdala
CNS	Central nervous system
CS-	Conditioned stimulus (neutral)
CS+	Conditioned stimulus (aversive)
ECG	Electrocardiogram
EPM	Elevated plus maze
GC	Granger causality
HRV	Heart rate variability
InsCtx	Insular cortex
KPSS	Kwiatkowski–Phillips–Schmidt–Shin
mInsCtx	Medial insular cortex
MVGC	Multivariate Granger causality
NTS	Nucleus of the solitary tract
PAG	Periaqueductal grey
pInsCtx	Posterior insular cortex
PNS	Parasympathetic nervous system
RMSSD	Root-mean-square of successive differences
SAN	Sinoatrial node
Sd	Standard deviation
SEM	Standard error of mean
SNS	Sympathetic nervous system
SSR	Sum of squared residuals
US	Unconditioned stimulus
VAR	Vector autoregression model

1. Introduction

This section covers four main topics. First, fear and anxiety disorders will be introduced, describing underlying autonomic and neural networks. Second, general characteristics of physiological signals with an emphasis on cardiac and respiratory signals, will be outlined. Third, the neuroanatomy and roles of the insular cortex will be summarized. Tying the previous chapters together, interoception will be discussed. Finally, the questions this study aims to address are summarized.

1.1 Fear and anxiety disorders

Fear and anxiety are both terms referring to emotions and behaviors that are elicited by threat perception[1]. However, while fear is defined as a short-lived emotional state in response to a specific danger or in anticipation of an immediate threat, anxiety refers to a more sustained state of fear, usually elicited by unspecific, future threats[1–4]. In general, a healthy perception of fear and the accompanying display of behavioural responses is a necessary asset to ensure the survival of an individual. However, when fear and anxiety are dysregulated and become more intense and unspecific, it can turn pathological and develop into an anxiety disorder. The latest estimations from the World Health Organization (WHO) from 2023 reported that approximately 4% of the global population are suffering from an anxiety disorder, which along with depression, makes it the most common mental disorder globally[5,6]. Several treatment options are available for anxiety disorders, including medication, psychotherapy, and exposure therapy[7]. In exposure therapy, patients are presented with the subject or situation that triggers their anxiety (or fear) in a safe environment to form new associations[8,9]. This form of therapy can be further investigated, particularly in rodent research, using a paradigm called fear extinction. In fear extinction, animals are repeatedly exposed to a conditioned stimulus (CS+), like a tone, which had previously been learned to be associated with an aversive unconditioned stimulus (US), like a foot shock or an air-puff[1,10]. Exposure therapy and fear extinction of conditioned fear both show a reduction in negative association to the trigger or stimulus, thus making it a useful model for studying mechanisms of recovery from anxiety. However, not every patient responds to treatment in the same manner. Due to this fact, the high prevalence of anxiety disorders and the significant burden they cause on an individual and global level, it is crucial to study underlying mechanisms of the disease for aiding in the advancement of efficient treatment options.

1.1.1 Sex differences in fear conditioning and extinction

Women have been found to be about twice as likely to develop an anxiety disorder than men[11]. Furthermore, women have been reported to have a higher disease severity and are diagnosed more often with comorbid psychiatric diseases like eating, and mood disorders compared to men[11–13]. However, in basic research, female animals have oftentimes not been included, due to concerns about potentially higher variability because of the estrous cycle[14]; studies have since shown that overall variability of results is not higher when using female rodents compared to male rodents[15,16]. Concerning research about fear, some evidence from rodent studies including males and females in cued fear conditioning have predominantly shown no effect of sex differences in freezing response to CS+ presentations[17–20]. Fear extinction studies, on the other hand, have shown inconsistent findings, showing either no overall difference[21–23] or a higher resistance to fear extinction in females compared to males[17,24,25]. Using healthy human subjects, Rattel et al. (*2019*)[26] could show that cue-triggered intrusive memories are more pervasive in women compared to men, which, additionally, was indicative of reduced fear extinction[26]. Taken together, these studies indicate a need to focus more attention on mechanisms underlying fear acquisition and extinction in females.

1.1.2 Neural networks of fear and anxiety

Fear networks in the brain have largely been identified thanks to fear conditioning studies in rodents. The main regions which have been shown to consistently play key roles in fear include the amygdala, the periaqueductal grey (PAG), the ventral hippocampus (vHC) and the medial prefrontal cortex (mPFC)[27].

The amygdala has been shown to be crucial for not only fear but also extinction learning[28,29]. Although the amygdala consists of several sub-nuclei, studies most often focus on the two major sub-nuclei, which are the basolateral amygdala (BLA) and the central nucleus of the amygdala (CeA)[30]. The BLA plays an important role in forming associative fear memories and in the extinction thereof, while the CeA is particularly involved in mediating fear responses[28,31–36].

The CeA has additionally been found to be an important relay site, transmitting information to several downstream regions, among which is the PAG[37,38]. The PAG is primarily known for its crucial roles in autonomic regulation and mediation of defensive behaviours[39–41]. Moreover, a study by Signoret-Genest et al (*2023*), showed how these properties are strongly interacting by inducing immobility-associated bradycardia[42]. The next component of the fear network is the vHC which is related to emotion and stress in general, with an emphasis on its important role in contextual fear[43,44]. And, lastly, the main role of the mPFC

is the top-down control of fear regulation[45,46]. Interestingly, Etkin and Wager (*2007*) additionally summarized that across different forms of anxiety disorders and during fear the two main brain regions displaying an increased activity in patients compared to controls were the amygdala and the InsCtx[47]. An overview of the insula's specific role in fear and anxiety can be found in *chapter 1.3.2* Role of the insular cortex.

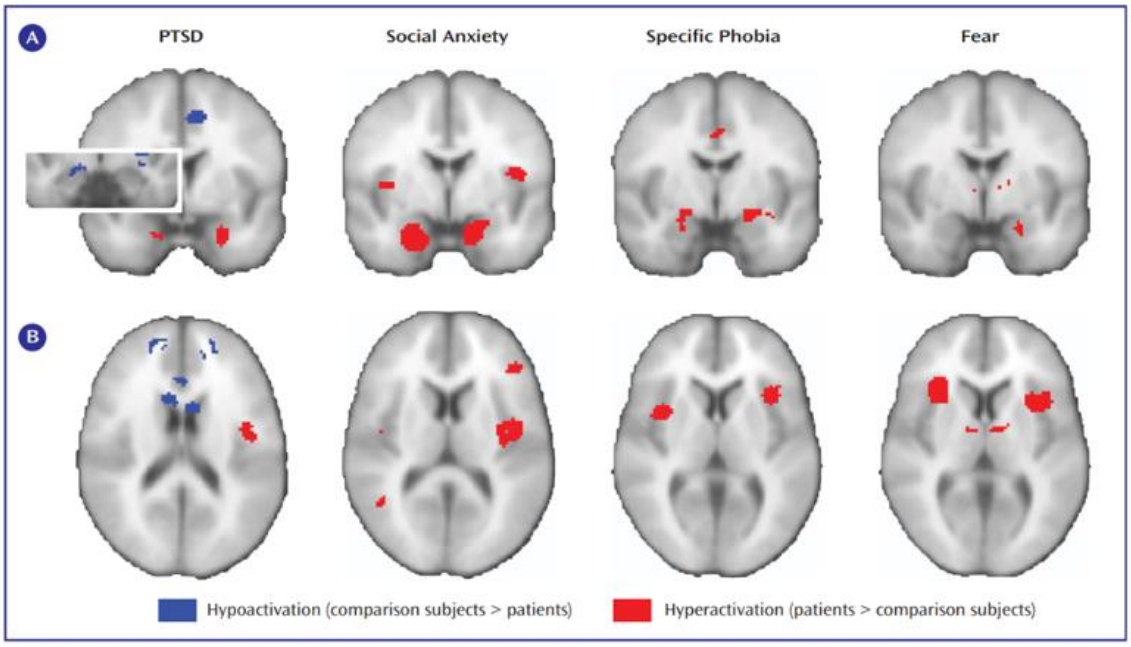

Fig. 1: **Activation patterns in fear and anxiety.**
During fear and anxiety, the amygdala (A) and insular cortex (B) display increase activation in patients suffering from PTSD, social anxiety or specific phobias compared to healthy controls. Hypoactivation is indicated in blue, hyperactivation in red. From Etkin and Wager, 2007 [47]

1.1.3 Autonomic networks involved in fear

Fear and anxiety can affect multiple organs apart from the brain, including the heart, lungs and digestive system. Interestingly, when healthy individuals were asked to describe where they predominantly felt changes in their body during different emotions, subjects overwhelmingly highlighted their chest area during fear or anxiety[48] (*Fig. 1*). Thus, it is of special interest to investigate cardiac and respiratory functions in connection with aversive emotional experiences.

Strikingly, breathing is the only internal bodily function which can be controlled intentionally, which opens the possibility to leverage this aspect to influence the internal states of an individual. It indeed has been shown that conscious breathing regulation holds the capability of modulating emotional states[49]. Therefore, breathing is already being explored for its possible therapeutic value and applied in the form of breathing exercises and breathing meditation[50–52].

Another useful proxy of internal state is heart rate variability (HRV). HRV can be used to gauge the general arousal state of an individual. It has been shown that high HRV is correlated with lower anxiety and, more generally, a better ability of emotion regulation[53,54]. Remarkably, a recent study was further able to show that high HRV is correlated with a high symptom burden decrease after fear extinction[55].

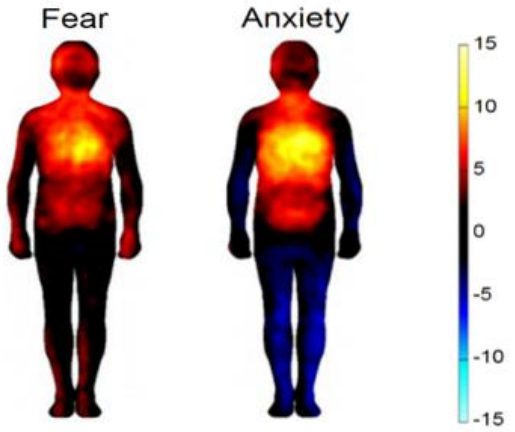

Fig. 2: **Bodily sensations during fear and anxiety.**
Bodily signal changes that were associated with fear and anxiety as reported by study participants. The self-reported measures were topographically mapped. Warm colors indicate increases and cool colors decreases. *Adapted from Nummenmaa et al., 2014* Nummenmaa et al., 2014.

Alongside behavioural impacts and emotional distress, fear and anxiety are also accompanied by physiological changes like alterations of cardiac and respiratory functions (for review see: Steimer, 2002[56]). These physiological changes can sometimes have severe impacts on physical health. For instance, anxiety is one of the main risk factors for the development of cardiovascular diseases[57,58]. Furthermore, respiratory dysregulation has been shown to be present in several different anxiety disorders[59]. This relationship of anxiety and physical health is also true in the reverse, in that physiological diseases can cause or exacerbate fear and anxiety disorders. In this context, it has been shown that patients suffering from cardiac or pulmonary diseases have a higher prevalence rate of anxiety compared to the general population[60,61]. The highly comorbid nature of fear-related disorders with physical health does not only present additional challenges, but also provides more avenues of studying and ultimately treating them.

1.2 Physiological signals

Physiological signals encompass a plethora of different signal modalities and dimensions. This subchapter will introduce the autonomic nervous system (ANS) and give an overview over cardiac and respiratory signals as well as their regulation in the central nervous system (CNS).

1.2.1 The autonomic nervous system

The ANS is a component of the peripheral nervous system which regulates visceral processes and consists mainly of the sympathetic (SNS) and the parasympathetic nervous systems (PNS)[62]. Both these branches are motor pathways that are tightly connected with the CNS (*Fig. 6*). The SNS and PNS pathways are composed of two neurons: a preganglionic neuron in the CNS and a postganglionic neuron in the periphery[62,63].

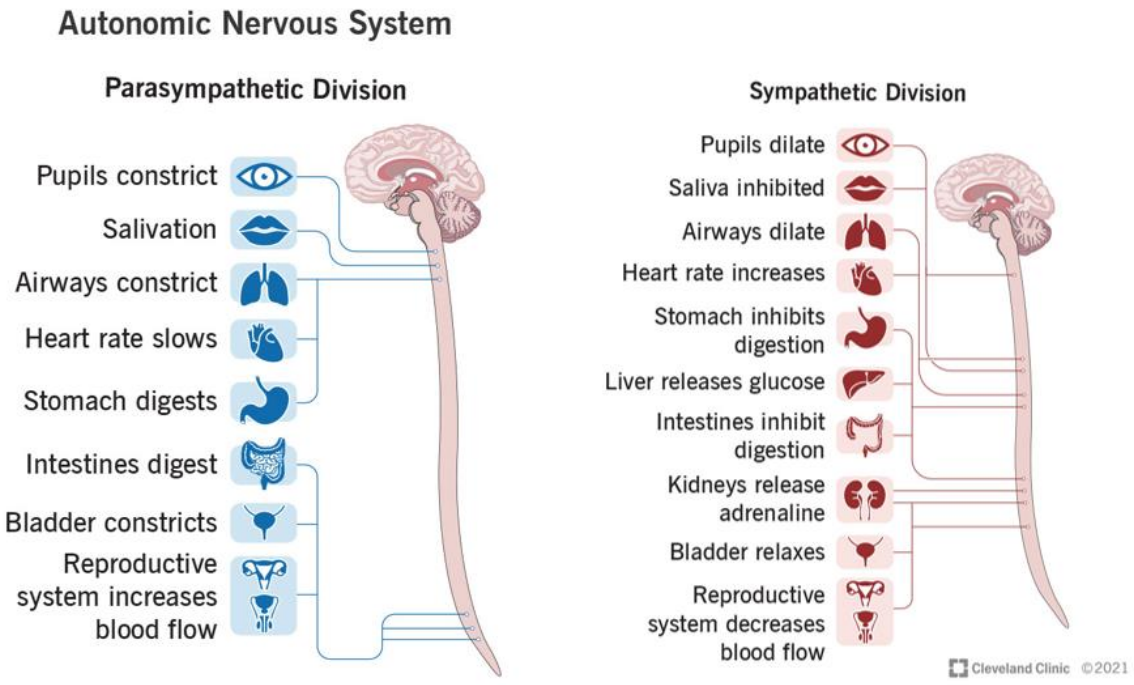

Fig. 3: **Autonomic nervous system.**
Functions classically associated with activity of either the parasympathetic (left) or sympathetic (right) division of the ANS as well as the location of the postganglionic neuron. *From Cleveland Clinic, 2021.*

Regarding their function, SNS activation is known to initiate an overall arousal. This state is commonly known as the 'fight or flight' response and is characterized by an increased physiological activity, like elevated heart and respiratory rates (*Fig. 3*). On the other hand, PNS activity is known as the 'rest and digest' phase, and its activity leads to a decrease in physiological activity; a slowed heart rate and contraction of airways are characteristic for

this state[64,65] (*Fig. 3*). Interestingly, studies in humans suggest a laterality in the CNS regarding the control of the autonomic nervous system. As such, the right hemisphere has been shown to be mainly involved in the control of sympathetic activity and the left to be predominantly involved in the control of parasympathetic activity[66–68].

1.2.2 Cardiac signals

The average heart rate of mice (C57BL/6 mouse strain) measures between 550 - 700 beats per minute (bpm)[69,70]. This rate is determined by the sinoatrial node (SAN), which functions as the heart's pacemaker (for review see: Turner et al., 2021)[71]. The SAN triggers electrical impulses that lead to contractions of the heart. The spontaneously initiated activity of the SAN is controlled by the ANS, which acts on the ion channels of the SAN's pacemaker cells. Regulation of the SAN by the PNS can be observed as phasic, abrupt, and fast changes in heart rate, whereas regulation by the SNS causes slow and tonic beating of the heart. The modulation of SAN activity produces fluctuations in heart rate and is thus responsible for the variability of heart rate.

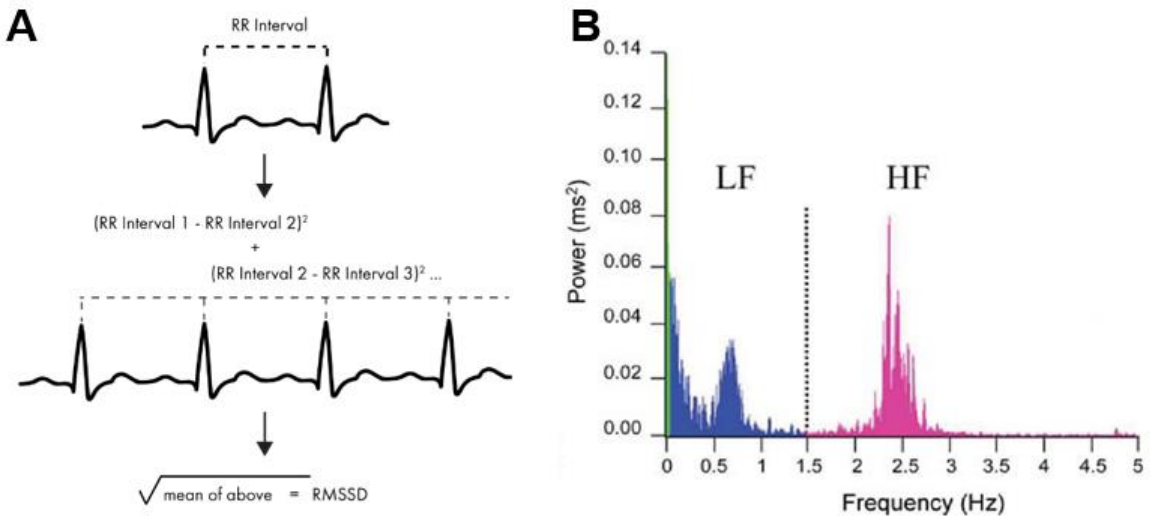

Fig. 4: **Heart rate variability measures.**
A) Illustration of the calculation of RMSSD (root-mean-square of successive differences. *Adapted from imoitions.com/blog/learning/best-practice/heart-rate-variability and*
B) Spectral analysis of heart rate frequency of FVB/N mice of a three-minute recording period. *From Thireau et al., 2008*[74]*.*

Heart rate variability (HRV) can be divided into two different domains[72]. Firstly, there is the time domain of HRV, which is based on descriptive statistics. One HRV measure in the time domain is the root-mean-square of successive differences (RMSSD) which is calculated from RR intervals that are detectable with ECG recordings (*Fig. 4A*). RMSSD is calculated from so called normal RR peaks (NN). NN peaks exclude any ectopic beats, which

are irregular beats which are not elicited by the SAN[72–74]. RMSSD can be assessed even from short term ECG recordings and is mainly a representation of vagally mediated SNS activity[75]. Furthermore, RMSSD can be leveraged in humans as a measure to assess physiological arousal[76,77]. In general, a high RMSSD is indicative of a low arousal state, whereas a low RMMSD indicates high physiological arousal of an individual. Moreover, a negative correlation between freezing and heart rate variability has been shown in mice, indicating similar interpretational value as in human[78].

The second domain of HRV is the frequency domain and is based on Fast Fourier Transformation (FFT)[72,74]. Time is converted into harmonics of frequencies and amplitudes by decomposition of the periodic oscillations of heart beats. The resulting frequency bands are indicative of the main modulators acting on the SAN[72,74].

In the mouse, the low frequency band (LF) spans across 0.1-1.5 Hz and blood pressure is the main physiological contributor to this rhythmicity[69,79]. It further indicates a regulation of the heart rate by both PNS and SNS, albeit there being a dominance of the tonic SNS. High frequency (HF) is predominantly influenced by the respiratory rhythm as well as the phasic PNS. HF is defined as frequencies between 1.5-5 Hz (*Fig. 4*B)[69,74,79]. Overall, mouse HRV has been found to be mostly related to HF[80].

1.2.3 Respiratory signals

Baseline frequency of breathing in C57BL/6 mice is around 500 breaths per minute (brpm) in both male and female mice[81] (*Fig. 5A*). During each breath, both the SNS and the PNS is involved. Sympathetic nerves fire during the inspiration phase and parasympathetic ones during expiration[82]. Apart from the breathing rate, the rhythmicity of respiration holds valuable information. This rhythm has been shown to modulate oscillatory patterns in various brain regions[83–86]. In freely moving mice, average breathing frequencies can range between 1Hz and 15Hz[87–89]. Respiration frequencies differ with behaviour, generally showing frequencies between 1Hz and 6Hz during sleep and periods of quiescence and low activity and frequencies between 8Hz to 15Hz during high activities like running and jumping[89]. Most notably, during fearful freezing mice show a characteristic steady breathing power around 4 Hz[88] (*Fig. 5B*). This 4 Hz rhythm is reflected in brain oscillations and interestingly, has been shown to have functional roles in freezing regulation. 4 Hz oscillations in the prefrontal cortex, for example, have been shown to predict the onset of freezing and even alter freezing and fear extinction outcomes[90,91].

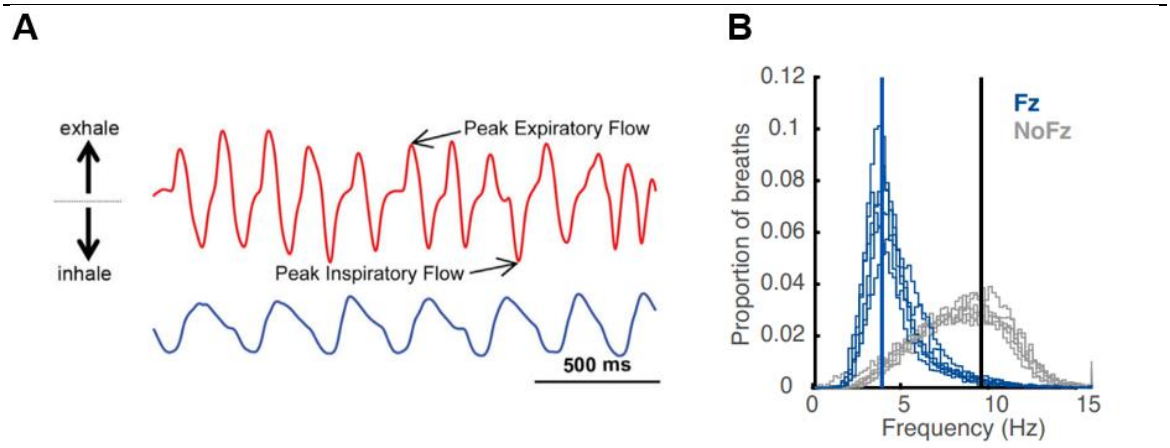

Fig. 5: **Single breaths and respiratory frequencies in mice**
A) Example of single breaths during wakefulness (top, red) and sleep (bottom, blue). Direction of in- and exhales is indicated on the left, and breathing peaks are indicated in the trace. *From Schreck et al., 2022* [92]
B) Respiratory frequencies distribution of animals during freezing (Fz, blue), and all other timepoints (NoFz). *From Bagur et al., 2021*[88]

1.2.4 Neuronal regulation of cardiorespiratory activity

The first relay station for bodily signals when entering the CNS is the brainstem[93,94]. Within the brain stem, key nuclei sense, transmit, and regulate cardiorespiratory activity in both a bottom-up and top-down fashion[95] (*Fig.* 6). The nucleus serving as the primary region to receive visceral inputs is the nucleus of the solitary tract (NTS)[96]. One of the major pathways of how visceral inputs reach the NTS is via cranial nerves[97]. Two important cranial nerves, which are involved in cardiorespiratory signaling, are the IXth (CN IX, glossopharyngeal nerve) and Xth cranial nerve (CN X, vagus nerve)[98]. The vagus nerve constitutes the main part of the PNS, making up 75% of its entirety, and carrying information from the body to the NTS and vice versa[99]. Visceral signals from chemo- and baroreceptors originating in the heart and the lungs project to the NTS via cranial nerves before their signaling is being relayed to cardiac and respiratory control centers in the medulla[100]. On the path back to the body, the NTS additionally holds the important function as the last convergence site of descending signals before the output is split into sympathetic and parasympathetic responses[100–102].

Both afferent and efferent signaling is needed for control of cardiac function. On the way from the body to the brain, afferents from the heart project to the NTS which further relays the signals to the principal components of cardiac control centers which are the nucleus ambiguous (NA) and the ventrolateral medulla (VLM). Subsequently, the VLM exerts top-down control on the heart, which is mainly mediated through influencing the SNS[103].

Likewise, control of respiration is achieved through an interplay of top-down and bottom-up signaling. In both signaling directions, respiration is centrally controlled by small nuclei in the medulla and pons that are organized into dorsal (DRC) and ventral respiratory columns (VRC)[104,105]. The VRC can further be divided into several nuclei that are highly functionally specialized, regulating rhythmic or motoric properties of respiration, and thus holding crucial roles in both afferent and efferent signaling[104,106–108].

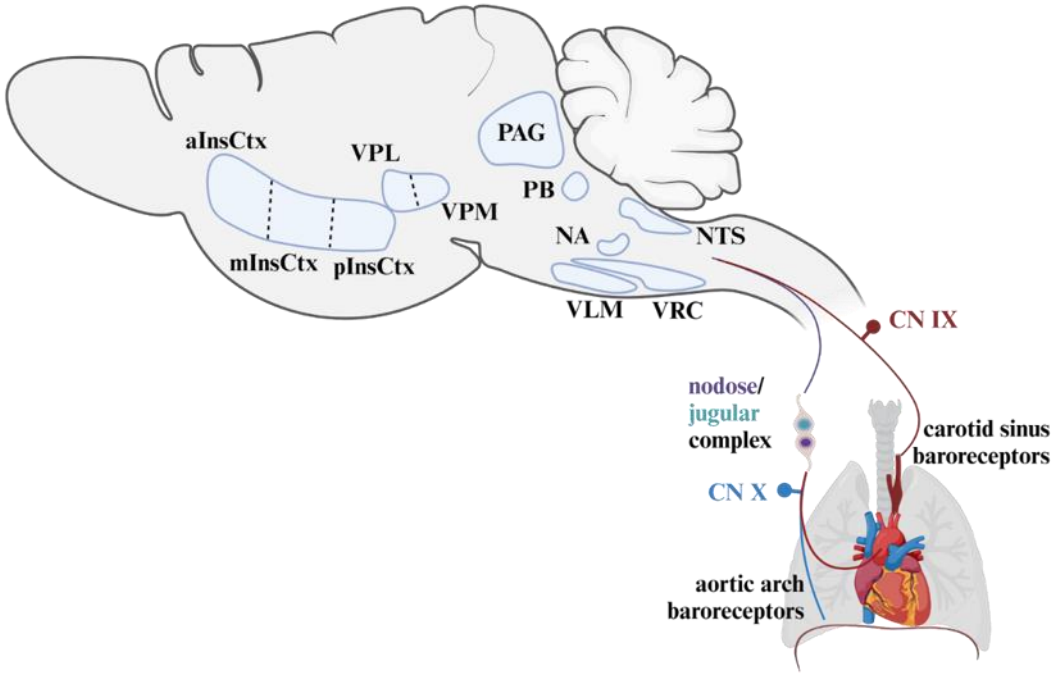

Fig. 6: **Brain regions and cranial nerves involved in the regulation of cardiorespiratory activity.**
Abbreviations left to right: aInsCtx (anterior insular cortex), mInsCtx (medial insular cortex), pInsCtx (posterior insular cortex), VPL/VPM (ventral posterolateral/ -medial nucleus of the thalamus), PAG (periaqueductal grey), PB (parabrachial nucleus), NA (nucleus ambiguous), VLM (ventrolateral medulla), VRC (ventral respiratory columns), NTS (nucleus of the solitary tract), CN IX (glossopharyngeal nerve), CN X (vagus nerve). *Created with BioRender.*

For higher order control of cardiorespiratory activity, signals are further propagated from the brainstem to subcortical and cortical regions, which in turn exert top-down control on bodily functions (*Fig.* 6). In the midbrain, two regions are especially heavily involved in the regulation of cardiorespiratory control. These are the parabrachial nucleus (PB) and the periaqueductal gray (PAG), with the PB being the essential relay center for the propagation of cardiorespiratory signals. Both the PB and the PAG have the capability of modulating cardiac and respiratory functions via direct and indirect pathways[109,110]. Notably, the PAGs modulatory action has been found to be tied to its prominent role in regulation of defensive behaviours[111–113].

Subsequently, cardiorespiratory signals reach subcortical levels, most prominently the thalamus, which receives direct inputs from the NTS. The ventral nuclei of the thalamus (ventral posterolateral and ventromedial nuclei) constitute the main site of transmission and integration of autonomic signals in the thalamus [114].

Lastly, autonomic signals get transmitted to the posterior insular (pInsCtx), which is also known as the viscerosensory cortex. Crucially, the insular cortex is not only a recipient of sensory inputs but also integrates those signals and exerts top-down control on heart and respiratory rates [115–117].

1.3 Insular cortex

The insular cortex (InsCtx) is an intriguing brain region to study as it is one of the main integration hubs in the brain. In this chapter, the characteristic neuroanatomy, cytoarchitecture, and structural connectivity of the InsCtx will be summarized. Furthermore, an overview about functions and pathologies that have shown to heavily involve the insula cortex, will be given.

1.3.1 Neuroanatomy and cytoarchitecture

In humans, the InsCtx is located inside the lateral sulcus and underneath the frontal, parietal and temporal lobes. In rodents, and more specifically mice, the InsCtx is located on the outside surface, above the rhinal fissure (*Fig.* 7)[118–120].

The InsCtx can be divided into several sub regions. One way of division is by anatomical location into an anterior (aInsCtx), a medial (mInsCtx), and a posterior (pInsCtx) part. The aInsCtx and pInsCtx are divided by the central insular sinus in humans, and at bregma 0.0 in mice. The mInsCtx roughly encompasses the area between bregma +1 and 0 in a mouse brain. In humans, the mInsCtx is defined as the area around the central insular sinus. In both cases, mInsCtx exhibits a blend of features and connectivity patterns from aInsCtx as well as pInsCtx[119,121–123].

Additionally, three distinct subregions are identifiable by their cytoarchitecture[118,119]. They are characterized by the amount of cortical layer IV granular neurons. Consequently, a granular section, a dysgranular section, and an agranular section can be found in the InsCtx. The granular section contains all layers, the dysgranular a thinner layer IV, and the agranular section is missing the IVth layer completely[119]. Whilst the distinction into these cytoarchitectural sections is arranged diagonally within the human InsCtx, in mice, they

are stacked in a dorso-ventral direction along the anterior-posterior axis of the InsCtx[118,119]. Therefore, even though morphological nomenclature shows consistency between humans and the model system of the mouse, there are differences in how borders of anatomically defined sub regions are drawn. It is therefore more informative to refer to the granularity and connectivity with other brain regions rather than the macroscopic location when comparing functional research results from humans and rodents. This will be beneficial in building a comprehensive understanding of the various functions and connectivity patters of the InsCtx.

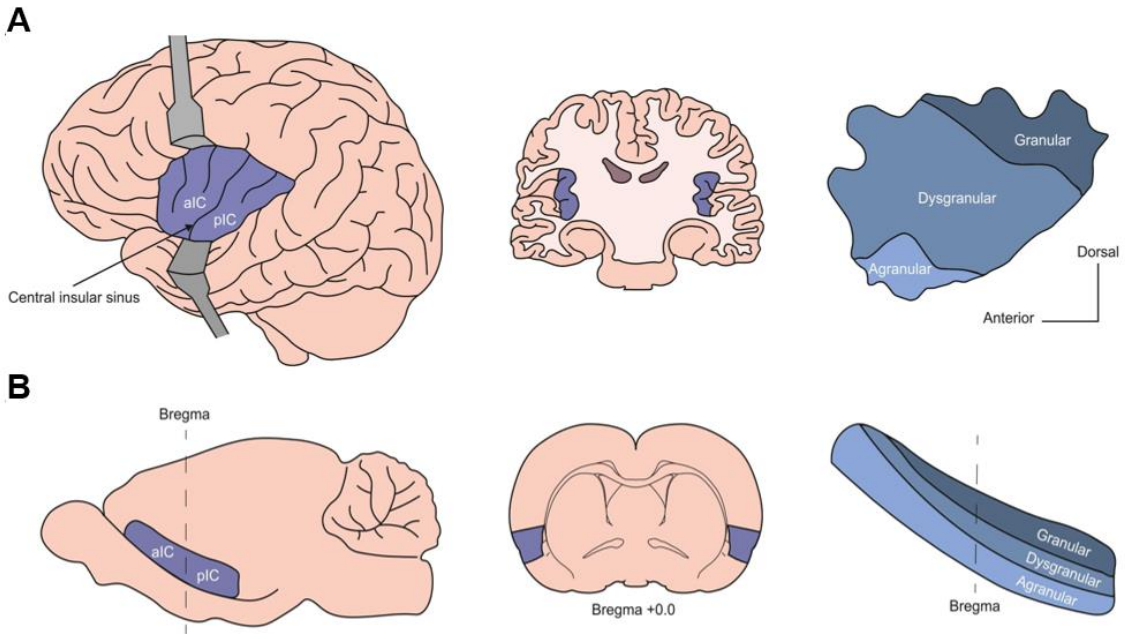

Fig. 7: **Anatomical location and cytoarchitecture of human and mouse insular cortex.** A) Location of the human insular cortex underneath the parietal and temporal lobes (left, middle) and granularity of anterior-dorsal axis (right). B) Location of the mouse insular cortex on the cortical surface (left, middle) and granularity of anterior-posterior axis. *From McGregor & LaLumiere, 2023* McGregor & LaLumiere, 2023.

As described earlier, the insular cortex is a highly interconnected brain region (*Fig. 8*). A comprehensive mapping study which I carried out in collaboration with a second PhD student of my laboratory[121] highlighted that aInsCtx, mInsCtx, and pInsCtx all exhibit strong intra-insular connectivity as well as more specialized brain wide interactions. Overall, major regions of connectivity for all sub regions that have also been shown to be functionally connected are the sensory cortex, the amygdala and the thalamus[119,124–127].

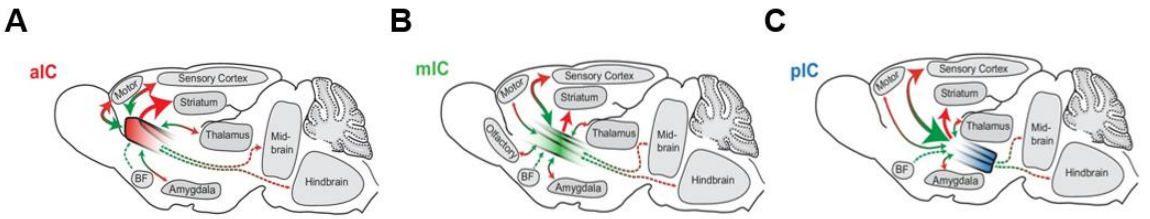

Fig. 8: **Major connectivity patterns of the mouse insular cortex.**
A) Bi- and unidirectional connectivity of the anterior insular cortex (aIC)
B) Bi- and unidirectional connectivity of the medial insular cortex (mIC)
C) Bi- and unidirectional connectivity of the posterior insular cortex (pIC). Abbreviation: BF (basal forebrain), Motor (motor cortex). *Adapted from Gehrlach, Weiand et al., 2020*[121].

1.3.2 Role of the insular cortex

The insular cortex (InsCtx) is best known for its role as integration hub, which receives and propagates external and internal cues[116,119,128,129]. This property enables the InsCtx to be implicated in an array of different functions but also pathologies. For instance, InsCtx has been shown to play crucial roles in addiction, eating disorders, self-awareness and emotions, and anxiety and interoception[118,130–132]. Interoception encompasses the processes of bodily signals, which informs individuals about their internal state. A broader explanation of the sense of interoception, with an emphasis on the unique and important role of the InsCtx will be given in chapter *1.4. Interoception*. Involvement of the insular cortex in aversive emotions like fear and anxiety has been shown using both conditioned and innate fear paradigms. Existing studies in rodents outline a crucial role of especially the posterior insular cortex in conditioned fear[133,134]. Furthermore, studies have shown that pInsCtx activity plays important roles in sustained fear states as well as in the regulation and consolidation of conditioned fear[132,134–137].

1.4 Interoception

Interoception comprises the sensing, interpretation, integration, and regulation of internal signals of an individual[128,138,139]. Interoception involves internal signals as well as a variety of brain regions (*Fig. 9*). It can further have both an unconscious and conscious component, which helps to not only achieve automatic homeostasis of internal states, but also enables individuals to exert voluntary control on certain aspects[140,141]. Moreover, dysregulation of interoceptive processes has been proposed to play a crucial role in variety of mental disorders, especially disorders of altered emotion processing[142–145].

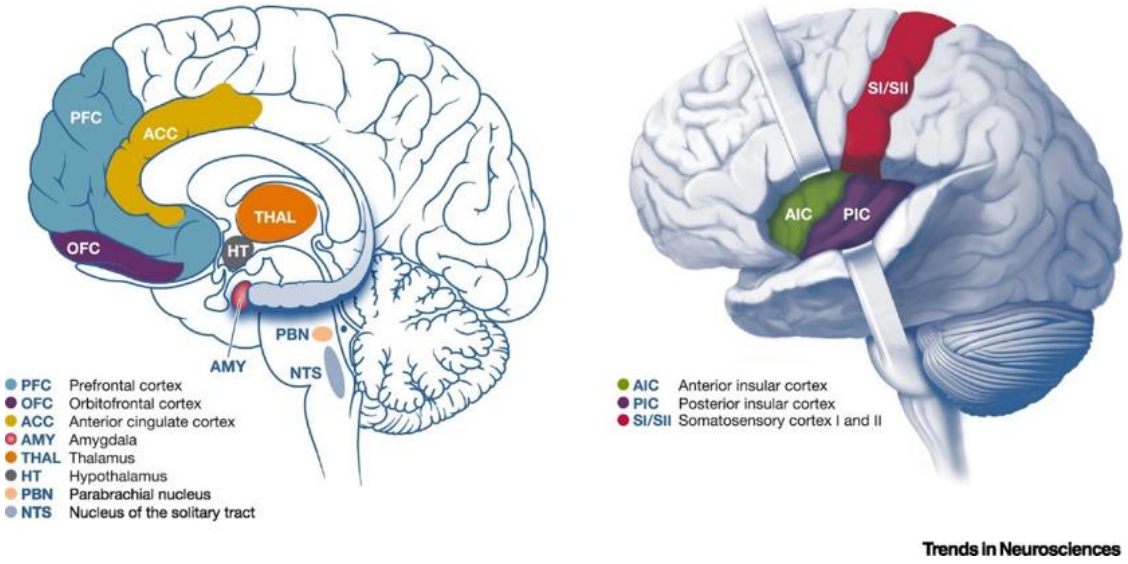

Fig. 9**: Brain regions involved in interoception.**
Brain regions that have been found to play important roles in interoceptive processes in humans. Abbreviations are explained below the brain schematics. *From W.G. Chen et al., 2021*[139]

1.4.1 Interoception research in humans

Research on interoception traditionally relies on conscious processes and involves verbal feedback. Therefore, most insights on this topic were and are gained from human studies.

The most commonly used tasks in humans are the heartbeat perception task to assess cardiac interoception and respiratory load tasks[146,147]. Both tasks require study participants to report their internal signals by either counting their own heartbeats or judging the severity of respiratory challenges. Therefore, key terms used in human studies investigating interoception are interoceptive awareness and accuracy. Interoceptive awareness describes the metacognitive aspect while interoceptive accuracy describes actual performance on the interoceptive task[139,148,149]. Multiple studies have shown that both these interoceptive dimensions of accuracy and awareness are altered in psychiatric diseases[150–

[152]. Furthermore, a study which investigated both the cardiac and the respiratory interoceptive dimensions found that specific measures from either were predictive of anxiety symptoms[153]. For cardiac interoception, the measure predicting a low anxiety score was awareness while for respiration it was accuracy. These findings highlight the need for investigating multiple interoceptive sensations in order to gain a better understanding of these intricate processes.

1.4.2 Insular cortex and interoception

The most frequently reported interoceptive hub is the insular cortex. This is not only due to its highly interconnected nature, but it has consistently been shown that activity in the InsCtx in humans increases during interoceptive tasks and interoceptive predictions[154–157]. Intriguingly, it has been proposed that patients suffering from anxiety may additionally exhibit alterations in predictive interoceptive signaling[158,159]. Indeed, in human studies, the insular cortex has not only been found to be active during the anticipation of an aversive stimulus, but also to be more active in individuals with high trait anxiety[160–163]. In addition to those findings, other studies have specifically addressed the interoceptive dimension in these predictive processes and showed that the InsCtx activity is not only a crucial component in interoceptive tasks but also appears to be the key region to display alterations in patients suffering from psychiatric disorders[164–168]. Moreover, some of the studies pointed towards potential lateralization effects based on an individual's trait-anxiety[161,162].

1.4.3 Interoception research in the rodent model

As mentioned previously, interoception research mostly focused on human studies in the past. However, thanks to new developments of tools and techniques that enable scientists to precisely interrogate biological systems, studying interoception in rodents is becoming increasingly feasible. Leveraging model systems like mice will aid in gaining a mechanistic understanding of processes underlying interoception and help build a comprehensive understanding.

In the past years, basic research has been able to show that InsCtx activity represents and predicts bodily states[169–171]. Most studies, however, focused on homeostatic functions rather than emotional functions[172]. A limited number of studies has come out showing a link between heart rate and fear behaviour in mice. First, studies showed that fearful freezing induced an immediate bradycardic response[42,134]. The study by Klein et al. (2021), which came from my laboratory and I was involved in as co-author, found that pInsCtx activity exhibited an initial decrease at the onset of freezing, similar to the decrease in

heart rate[134]. Furthermore, after pairing of a conditioned stimulus (CS+) to a foot shock, the correlation between pInsCtx activity and heart rate was significantly higher in the time after the first CS+ presentation compared to the time before. Finally, this study linked body-pInsCtx interaction during fear conditioning by showing that both pInsCtx inhibition and vagus nerve stimulation (VNS) bidirectionally modulated fear extinction. Further evidence linking InsCtx and cardiac signals in emotion regulation comes from a study identifying the pInsCtx as one of the main regions responding to heart rate changes induced by peripheral optogenetic pacing[173]. This study not only demonstrated that an artificial heart rate increase induced anxious behaviour on an elevated plus maze (EPM) and in the Vogel conflict task, but also that inhibition of pInsCtx eliminated the anxiogenic effect of heart rate increases. In summary, first evidence suggests the relationship between the pInsCtx and cardiac signals play an important role during fear responses.

1.5 Aims of the study

One major bottleneck in studying interoception in animal models is obtaining multiple precise readouts across different interoceptive dimensions without restraining the animals, and thus, compromising their natural behaviour. In this study, neuronal activity recordings were combined with measurements of ECG and intrapleural pressure in freely moving mice. The goal of this study was to generate a comprehensive characterization of interactions of the posterior insula cortex with both cardiac and respiratory signals during emotional behaviour. This aim can further be divided into three main parts:

I. Characterization of body-pInsCtx interactions during neutral and fear states

To gain a better understanding of general interactions between cardiac and respiratory signals and the pInsCtx, baseline measurements were taken in the mice' home cage environment to keep possible influences and disturbances of the animals and their internal state at a minimum. Furthermore, assessment of interactions of the pInsCtx with the periphery was obtained during different stages of fear and extinction learning, to decipher possible differences. Lastly, interactions were measured during innate fear behavior on an elevated plus maze (EPM).

II. Comparison of pInsCtx with NTS activity

The brainstem and especially the nucleus of the solitary tract (NTS) are critical in the perception, propagation and control of bodily signals. Consequently, to compare pInsCtx activity with lower order processes of interoception, activity in the NTS was compared to the activity in the pInsCtx during fear and extinction conditioning.

III. Exploring the data for its predictive value

To investigate if and how pInsCtx and body interplay could be leveraged to understand the directionality of interaction and its potential of predicting extinction success, the data was probed accordingly.

2. Material and Methods

2.1 Animals

All procedures described were conducted in accordance with the German Animal Welfare Act regulations from the Government of Upper Bavaria (Animal licenses AZ: 55.2-2532.Vet_02-21-29 and AZ: 55.2-1-54-2532-56-2014). Mice used in this study were wild-type C57BL/6 and transgenic *Camk2a*-Cre (B6Cg-Tg(Camk2a-cre)T29-1Stl/J) mice. For viral tracing experiments, mice were between the ages of 3-11 months when undergoing surgery. For behavioral experiments, the age range was between 3 and 6 months. Animals were either single or group-housed in individually ventilated and clear plexiglass cages (GM500, Tecniplast) with bedding and nesting material. Before surgeries, additional cage enrichment consisted of a wooden tunnel. After surgeries the mice could no longer use the wooden tunnels due to implanted optic fibers and were instead provided with other enrichment sources like tissue paper, wooden sticks, and red-tinted plastic houses. All mice used in this study had ad libitum access to food and water. Animals were kept on a reverse light/dark cycle with the dark phase between 10AM and 10PM.

2.2 Surgeries

All surgeries were conducted under sterile conditions. The analgesic metamizole (0.2 mg/g bodyweight, s.c.) was administered to the animal 30 minutes prior to the start of surgery. For induction of anesthesia, the mouse was placed in a transparent anesthesia chamber which had been pre-flooded with a 3-4% (v/v) isoflurane and 1% oxygen mix. To prepare mice for the surgical procedures, fur on the head and abdomen and chest area was shaved off and the skin disinfected with 80% Ethanol and a povidone iodine solution. To prevent the eyes from drying out, they were covered with eye ointment (Bepanthen; Bayer Vital GmbH).

During surgery, mice were placed on a heating pad which was set to 38°C to keep their body temperature stable. Anesthesia was maintained at a 1-3% isoflurane/oxygen mixture via a breathing mask.

Mice were monitored and provided with wet food for at least five days post-surgery. Daily administration of the analgesia Carprofen (5 mg/kg body weight, s.c.) was continued for two days after surgery and prolonged if necessary.

2.2.1 Wireless telemetry transmitter implantation

2.2.1.1 Transmitter preparation

The extra-small wireless telemetry transmitter HD-X11 (Data Science International, DSI) (*Fig. 10A*) was switched on with a magnet 1-2 hours prior to surgery for stabilization of the electronic components. The transmitter was implanted in the activated state which allowed for real time placement verification. To prepare the ECG leads, they were first shortened to a length appropriate for implantation. Utilizing a sterile scalpel blade, silicone tubing around the stainless-steel wires was cut and pulled to the tip of the lead to expose 0.5-1 cm of wire. To secure the silicone tubing in place, 7/0 non-absorbable braided silk suture (Fine science tools, FST) was tied around it at both ends surrounding the bare wire with a 1-1 knot and excess silicone at the top of the lead was cut down. The pressure catheter was hydrated by placing it in warm, sterile saline (0,9 % NaCl) 15 minutes before implantation.

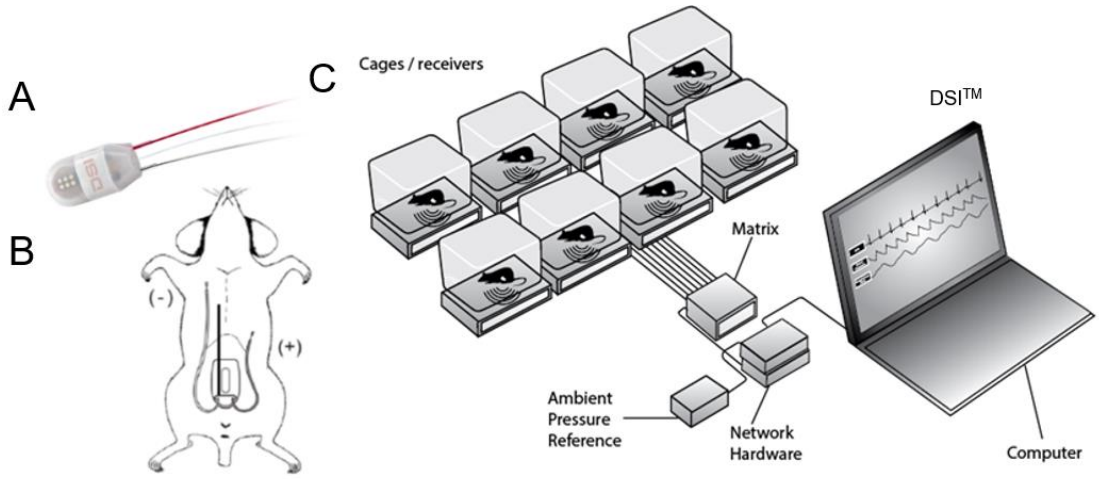

Fig. 10: **Wireless telemetry**
A) Transmitter which was implanted (HDX-11; ECG leads in red and grey, pressure catheter in white). B) Schematic depiction of transmitter position in the abdomen and placement of ECG leads and pressure catheter (along the esophagus into the intra-pleural cavity). C) General Setup and components of the DSI wireless telemetry system**.** *Adapted from Data Science International (DSI)*

2.2.1.2 Transmitter implantation

After surgery preparation, as described above, the mouse was placed on their back to expose their abdomen, onto the heating pad and their extremities were lightly fixated with surgical tape. Starting at the sternum, an approximately 1.5-2 cm long caudal incision of the skin and abdominal wall was made. Using wet cotton-swabs, the intestines were carefully retracted to expose the left hepatic lobe and the stomach. Next, the hepatic lobe was

retracted as well to expose the esophagus. Utilizing a 25G injection needle, a small incision was made in the outer longitudinal muscular layer surrounding the esophagus. The muscular layer was further loosened up to the level of the intrathoracic part before the pressure catheter was inserted into the incision of the muscle layer. After optimal placement for detection of intrapleural pressure was achieved, the catheter was fixated by application of a small patch of cellulose paper and tissue adhesive (Vetbond). After implantation of the pressure catheter, the abdominal cavity was irrigated with warm, sterile saline and organs were gently massaged back into their original position. Next, the transmitter body was placed on top of the intestines parallel to the longitudinal axis and secured to the abdominal wall using Vetbond. To externalize the ECG leads from the abdominal cavity, a 18G infusion needle was used to pierce through the abdominal wall to the left and right of the caudolateral part of the incision. The leads were passed through the lumen of the infusion needle to draw them out of the abdomen. Small skin incisions were made at the left caudal rib region and the right pectoral muscle for positioning of the positive and the negative lead respectively (*Fig. 10B*). After tunneling the leads subcutaneously to the positioning sites, they were secured underneath the upper muscle layer with Lambert stitches at both ends using a 7/0 prolene suture thread (Ethicon). Lastly, surplus lead was fixed to the inside of the abdominal wall using Vetbond and all of the incisions were closed using 6/0 mersilk suture thread (Ethicon) and Vetbond. Wounds were covered with iodine solution and since implantation was combined with a brain surgery, the mouse was turned on its belly and transferred into the stereotactic apparatus (Stoelting). The protocols for the immediately following stereotaxic surgery can be found in the next chapter *2.2.2 Stereotaxic surgeries under 2.2.5 and 2.2.6*.

2.2.2 Stereotaxic surgeries

Animals used for viral tracing experiments underwent surgeries in a stereotactic apparatus. For animals that would be used in behavioral experiments, Injections and fiber implantations in the apparatus were in some cases preceded by implantation of a telemetric transmitter in their abdomen, as described in section 1.2.1.

2.2.3 Viral constructs

Viral constructs used in this study were acquired from UNC Vector Core (Gene Therapy Center, University of North Carolina at Chapel Hill, USA). All viral constructs were packaged in an adeno-associated viral vector (AAV) of differing serotypes. The virus used for anterograde tracings in transgenic mice was AAV2/5-EF1α-DIO-eYFP (5.6×10^{12} vg/ml). In wild-type mice, AAV5-Camk2α-eGFP (4.3×10^{12} gc/ml) was used. The calcium indicator

used for fiber photometry experiments was packaged into an AAV9- Camk2α-jGCaMP8m-WPR.

2.2.4 Preparation of optic fibers

Optic fibers for fiber photometry were custom made. The glass fibers used had a core diameter of 200 µm and a numerical aperture (NA) of 0.48. Firstly, fibers were cut into pieces with the straight edge of a crystal knife. Next, the fibers were glued into zirconia ferrules with 4-6 mm of the glass fiber exposed. The cold-curing polymer Paladur (Kulzer GmbH) was used to accelerate the drying process. Lastly, the fiber side that would be connected to the laser patch cable was shortened and polished utilizing diamond lapping (polishing) sheets of the coarseness of 6, 3 and 1 µm in this order. To ensure adequate quality of laser throughput, fibers that did not produce a round laser beam or had a transmission power of less than 75% were discarded.

2.2.5 Virus injections

After receiving pre-surgery care, as described in the beginning of the chapter 2.2 Surgeries, mice were placed in the stereotax and their head secured with ear-bars and nose-clip. For tracing surgeries, the skin above the skull was incised with a scalpel blade and retracted to the sides of the head to enable access to the skull. For all other surgeries, the scalp was completely removed. A local anesthetic (2% Lidocaine, 2 drops) was applied to the surface of the skull, before removing the periosteum with cotton-swabs. Using bregma as absolute zero, the anatomical planes (anterior-posterior (AP), medio-lateral (ML) and dorsoventral (DV) were aligned. After leveling the head, injection sites were marked, and craniotomy was performed using an electric drill (Foredom). For tracing experiments the craniotomy was performed unilaterally in either the left or the right hemisphere above the posterior insular cortex, pInsCtx (AP -0.5, ML +/-4.1). For fiber photometry experiments, trepanation sites were unilaterally above pInsCtx (AP -0.4, ML +/-4.5) and NTS (AP -7.6, ML +/-0.3) of the same hemisphere. After the craniotomy, the brain surface was kept hydrated by application of sterile saline and correct head leveling was confirmed or re-adjusted if necessary.

Virus injections were performed using glass pipettes (0.5 mm inner diameter, 1 mm outer diameter) that were pulled with a P-97 micropipette puller (Sutter Instrument). The glass pipette was attached to a 1 µl Hamilton micro-syringe and filled with mineral oil before being secured to a Micro4 precision pump (World Precision Instruments) at the stereotax. Viral constructs being injected are described in section 1.2.2.1. Viruses for tracing experiments were injected at a rate of 50 nl/min. For anterograde tracings, transgenic mice were

injected with 80 nl AAV5-DIO-eYFP. Wild-type mice received injections of 70 nl AAV5-CamKIIα-GFP. For fiber photometry surgeries, 300 nl of the calcium indicator were injected at a rate of 100 nl/min. Injection depths (DV axis) were -4 mm for pInsCtx injections and -4.55 mm from brain surface or from skull level? for the NTS. After injection, the glass pipette remained at the injection site for 6-10 minutes to allow for proper virus diffusion.

The next step in the procedures for fiber photometry surgeries were implantation of optic fibers which is described in 1.2.2.4 Optic fiber implantation.

Tracing surgery mice received s.c. injections of the analgesic Carprofen (5 mg/kg body weight). Afterwards, tracing surgeries were concluded by suturing the skin, discontinuing the anesthesia and removing the mice from the stereotax. Lastly, mice were placed into their home cage with supplemental warmth and wet food provided. They were monitored closely until the return of full consciousness and mobility.

2.2.6 Optic fiber implantation

For fiber photometry surgeries, optic fiber implantations were performed following the virus injections. First, to increase friction to help the glue adhere to the bone surface, the skull was lightly scored with a scalpel blade. Subsequently, the fibers were implanted at the same AP and ML coordinates as the injection. DV coordinates were 0.5 mm less than that of the injections so the laser would cover the injection site fully during experiments. Optic fibers were secured in place with super glue and the polymer Paladur. To cover the exposed skull and, further secure the fibers in place to prevent light spillage, the wound and fibers were covered with denture self-curing cement (C&B super bond; Generique International) mixed with ivory black pigment (Kremer Pigmente). Implantation was followed by injection of the analgesia Carprofen (5 mg/kg body weight), discontinuation of anesthesia, removal from the stereotax and previously described post-operative care. To warrant complete recovery and proper virus expression, behavioural experiments were conducted 2-3 weeks after surgery for fiber photometry measurements. For optogenetic manipulations experiments began 4-5 weeks post-surgery.

2.3 Behavioral experiments

Prior to behavioral experiments, mice were handled for 5-10 minutes over a period of 3 to 5 days, until they were fully comfortable with the experimenter. In case of multiple mice being kept in one cage, cage mates were handled simultaneously. All behavioural experiments were tracked using the software ANY-maze. After conclusion of experiments, data

was analyzed with custom written Python scripts as well as GraphPad Prism 10. Furthermore, all other recording systems were connected to the software using TTL (Transistor-Transistor Logic)-triggers.

2.3.1 Cage recordings

Baseline recordings were obtained in a fresh cage with monitoring of behaviour, physiological signals and calcium bulk signal. Recordings were conducted after handling and the day prior to habituation and training of the fear conditioning paradigm. Post fear conditioning recordings were conducted three days after the extinction retrieval test.

2.3.2 Fear conditioning and fear extinction

A classical Pavlovian auditory fear conditioning and extinction paradigm was used (see Results: *Fig. 12C)*. Ventilated behaviour boxes (Ugo Basile©) that were equipped with loudspeakers, a front view camera and the experimental chamber (16 cm x 16 cm) were utilized to control the measures and the environment surrounding the mice during experiments. The DSI (Data Science International) receivers were placed centrally underneath the chamber. Fear conditioning was carried out in a different context than fear extinction. The context during fear conditioning consisted of no smell (cleaning with water), no wall patterns and a metal grid floor. During fear extinction, ethanol was used as a smell (cleaning with water and subsequently with 70% ethanol), striped wallpaper was added to the left and right side of the chamber and a white plastic served as the floor. During the stages of fear conditioning two different 30-second-long tones were used as conditioned stimuli (CS) and were presented at predetermined random intervals and orders (Table.1). The neutral tone, termed CS-, was a 60 dB loud white noise. The tone that was coupled with the unconditioned stimulus (US) during the training stage were 60 dB loud pips (7.5 kHz, 250 ms and repeated at 2 Hz) and termed CS+. The US was a 0.4 mA strong electrical foot shock that was administered for the last second of the tone during training via the metal grid floor.

Table 1: **Timepoints of CS presentations.**
Starting timepoints of tone presentations (CS+ top, CS- bottom) per stage

	Habituation	**Training**	**Recall**	**Extinction**	**Retrieval**
CS+ start (s)	180, 380, 630, 850	180, 340, 510, 800, 1040	380, 540	180, 250, 350, 430, 540, 610, 730, 830	180, 250
CS- start (s)	240, 540, 700, 910	250, 400, 660, 900, 1120	300, 450		

On the first day of the paradigm, habituation, and fear training were conducted. For habituation, mice were placed in the experimental chamber for 1000 seconds. During this time span, four CS+ and four CS- were presented. 60 to 120 minutes after habituation, training (duration: 1200 seconds) was conducted. During training five CS- and five CS+ were presented, and CS+ was paired with the US. The fear recall session (duration: 300 seconds) was conducted 24 hours after training. The mice were presented with both tones twice, with the CS+ not being coupled to a foot shock anymore. On day three of the paradigm, the context switched, and the fear extinction was performed. During extinction (duration: 900 seconds) the CS+ was presented eight times so the animals would learn to no longer associate the tone with the US. Lastly, on day four, extinction retrieval was tested by presenting the CS+ twice during a time span of 310 seconds.

The DSI transmitter was switched on and the fiber photometry cables were connected to the implanted fibers before the mice were placed into the experimental chamber. The conditioning sessions were started once the physiological signals were stably recorded. This took approximately five seconds after mice had been placed into the chamber.

2.3.3 Elevated Plus Maze (EPM)

The Elevated Plus Maze (EPM) consists of four arms that are arranged like a plus sign at a height of 60 cm. Two opposing arms are closed (walls on the side) and the other two are open (see Results: *Fig. 12C*). The length of two opposing arms including the center zone measures 55 cm. The EPM was placed behind black curtains in a dark room with a light above to illuminate the apparatus. At the start of the experiment, the cables for calcium recordings with fiber photometry were attached to the implanted fibers before the mice were placed in the center of the EPM facing towards one of the closed arms. Mice were left to explore the EPM for 600 seconds and their behavior, physiological, and calcium signals were recorded. After each experiment the EPM was cleaned with water and ethanol. EPM tests were run five days after fear conditioning.

2.4 Wireless Telemetry

For measurements of physiological signals with the DSI (Data Science International) wireless telemetry system, receivers that were connected with the other system components, were placed underneath the experimental setup (*Fig. 10C*). For baseline recordings in the home cage as well as for fear conditioning, a receiver was placed underneath the cage, or experimental chamber, respectively. The EPM was equipped with one receiver underneath each of the arms to ensure a complete and seamless coverage of the entire maze.

Before the start of experiments, the transmitter was switched on by holding a magnet close to the animal. Recordings of physiological measures were acquired with the accompanying software Ponemah©. A TTL pulse was utilized to mark the beginning and endpoint in the Ponemah© data file. The pulse was triggered by the start of the experiment which was centrally controlled with the AnyMaze© software. After each experiment, the transmitter was switched off with the magnet. Finally, after animals were sacrificed, the transmitters were explanted, sterilized and reused. After conclusion of the behavioural experiments, recordings were pre-processed in the Ponemah© software. To achieve an automatic detection of single breaths, both a low and high pass filter were applied to the pressure channel to filter out ambient pressure and artefacts derived from heart beats. Whenever the automatic detection of the software failed to mark an R peak in the ECG signal or single breaths in the pressure channel, they were marked manually. Unclear or missing signal parts were excluded. Additionally, the one second of foot-shock during fear conditioning training was excluded to excise the foot shock related artifact. Data was saved in one second bins. Further processing, analysis and visualizations of acquired physiological data was conducted with custom written Python scripts as well as GraphPad Prism 10 software.

2.5 Fiber photometry

Fiber photometry is a technique that is used to record calcium activity on a population level within a specified brain region[174]. Viral constructs containing genetically encoded calcium indicators (GECIs) are utilized to elicit fluorescence. The most widely used calcium indicator is GCamP (G: from green fluorescent protein (GFP), CaM: calcium modulated domain, P: peptide sequence) which is a green fluorescent protein-based calcium sensor that changes its color according to the intracellular calcium concentration[175,176]. In general, a viral construct of an AAV coding for the GECI is injected into the region of interest and an optic fiber is implanted above the desired recording site. GCamP infected neurons are being excited by a 465nm laser which in turn produces an emission of calcium bound GCamP which is getting picked up by a Photodetector[175] (*Fig. 11A*). Additionally, an isobestic signal is excited with a wavelength of 405nm which functions as a control signal. In recent years there have been considerable advances in the kinetic profiles of GCamP indicators, making them faster and more event bound, helping to provide a temporally more precise representation of bulk activity[177] (*Fig. 11B*). The calcium indicator used in this study was jGCaMP8m[177].

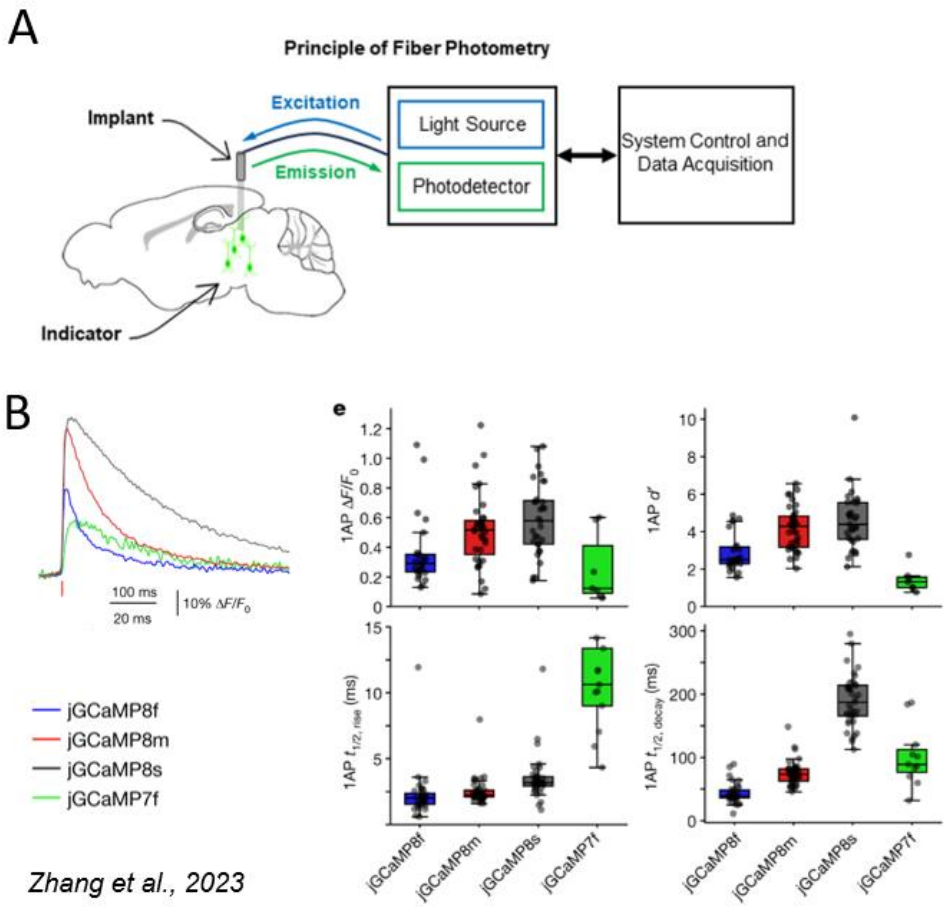

Fig. 11 **: Fiber photometry method and calcium indicators.**
A) Schematic depicting the general principle of fiber photometry. *From Byron & Sakata, (2023)*[175]
B) Exemplary traces of response of different calcium indicators in cells in the mouse visual cortex upon stimulation (left) and the respective kinetic properties (right): top left: response amplitude, top right: sensitivity, bottom left: half-rise time, bottom right: half-decay time. *Adapted from Y. Zhang et al., 2023*[177].

For experiments including calcium measurements, fiber photometry cables were connected to the implanted fibers before mice were placed into the experimental setup. After experiments were concluded, calcium signals were pre-processed utilizing the in-built functionality of the Doric Neuroscience Studio software. The first 20 seconds of recordings were discarded, to remove the initial signal drop due to photo-bleaching. The signal was further normalized to the control channel. Finally, ΔF/F signals were exported from the Doric Neuroscience Studio and further analyses and visualizations were conducted with custom written Python scripts as well as the GraphPad Prism 10 software.

2.6 Histology

2.6.1 Perfusions and sectioning

Mice were transcardially perfused with 4% PFA after being terminally overdosed with a Ketamin-Xylazin anesthesia mix (100 mg/kg body weight ketamine; 16 mg/kg body weight Xylazin). Timepoints of perfusion depended on the experimental procedures that were conducted beforehand. After injections of the anterograde tracer, mice were perfused exactly 4 weeks after the surgery. After behavioural experiments, mice were sacrificed as soon as the experiments were concluded.

Immediately following perfusion, brains were extracted and suspended in 4% PFA at room temperature for 36-48 hours. Sectioning was performed with a Vibratome (VT100 S; Leica Biosystems). Brains from mice that had undergone behaviour experiments were cut into coronal sections of a thickness of 70 µm, starting a few sections before and ending a few sections after the injection site. Those sections were mounted using a mix of Mowiol and 0.2 mg/mL DAPI and left to dry overnight in the dark at room temperature before imaging for verification of correct injection and implantation sites. Brains from tracing mice were first embedded in a 3% agarose/water mix before being cut coronally at 70 µm thickness, starting from the posterior end (brainstem). All sections were collected in 96-well plates that had been filled with 1 X PBS beforehand. Until immunohistochemistry staining, the sections were kept at -20°C.

2.6.2 Immunohistochemistry

To enhance the fluorescent signal of anterograde tracings, GFP immunostaining was applied on mounted slides. After mounting every second slice from previously sectioned brains (for details see 1.7.1 Perfusions and sectioning) on slides, they were left to air dry. Next, sections were washed three times for 10 minutes with 1 X PBS before blocking them for 30 minutes at room temperature with 10% normal goat serum + 1% Triton X-100 in 1 X PBS. Afterwards, the 1st antibody (Chicken anti-GFP, Biozym cat.# GFP-1010; Dilution 1:500) in 1% normal goat serum + 0.3% Triton X-100 in 1 X PBS was applied and after adding a coverslip, the slides were kept at 4°C overnight. The next day, the coverslips were removed, and the sections washed three times for 15 minutes in 1 X PBS. The following steps were all conducted using a dark chamber to avoid bleaching damage. The 2nd antibody (Goat anti chicken Alexa Fluor 488, Invitrogen A-11039; Dilution 1:250) in 1% normal goat serum + 0.3% Triton X-100 in 1 X PBS was applied onto the slides and kept at room temperature for 2 hours. Lastly, the sections were washed three times for 15

minutes in 1 X PBS and mounted with DAPI fluoromount-G. Slides were left at room temperature overnight before scanning with a fluorescent microscope.

2.7 Statistics

2.7.1 Pearson's correlations

Exclusively clean signal measurements were utilized in analyses. Animals in this study did not all show clean signals for all of the measurements throughout all of the stages of the experimental paradigm (breathing rate, heart rate, heart rate variability, pInsCtx and NTS activity). Since Pearson's correlations were exclusively calculated within animals, animal numbers for average responses differ from animal numbers in correlations. For definition of statistical significances and of Pearson's correlation strength, see Table 2 and

Table 3. Statistics of correlations involved two separate analysis steps. Firstly, Pearson's correlation analyses were conducted per animal to obtain within-individual correlations (One point in a Pearson's correlation plot represent the correlation of a single animal). Afterwards, one sampled t-tests were run to assess significance of the individual correlations on a population level. In figure legend descriptions, this combination of analyses is referred to as 'Pearson's correlation'.

2.7.2 Multivariate Granger Causality

Calculation of Multivariate Granger causality (MVGC) was conducted per animal. First, bodily signals of heart rate in beats per minute (bpm), heart rate variability in RMSSD, breathing rate in breaths per minute (brpm), and pInsCtx activity in fluorescence normalized to isobestic fluorescence (ΔF/F) were tested for stationarity with the Kwiatkowski–Phillips–Schmidt–Shin (KPSS), and Augmented Dickey-Fuller test (ADF). If stationarity was not significant, the data was transformed by differencing it once. Next, lag selection was achieved using the Bayesian Information Criterion (BIC), and Vector Autoregression model (VAR) fitting was computed. Last, a Sum of Squared Residuals (SSR) based chi^2 Granger causality (GC) test was performed. Following these steps, the average lag over all animals was computed and p-values thereof calculated with Fisher's combined probability test. A workflow diagram can be found in *3.3.1Directionality of neuronal and physiological signals, Fig. 24.*

2.7.3 Formulas and general statistics

Fear extinction performance indices were calculated with the following formula:

$$\text{Extinction performance index} = \frac{\text{freezing during recall} - \text{freezing during late extinction}}{\text{freezing during recall} + \text{freezing during late extinction}}$$

For calculation of the RMSSD the following formula was used with normal-normal peaks (NN) and a rolling window of 10 seconds:

$$\text{RMSSD} = \sqrt{\frac{1}{\text{N}-1} \sum_{n=1}^{N-1} (NN_{n+1} - NN_n)^2}$$

Table 2: **Definition of statistical significances**

P value	Significance
ns	Not significant
*$p \leq 0.05$	Weak
**$p \leq 0.01$	Moderate
***$p \leq 0.001$	Strong
****$p \leq 0.0001$	Very strong

Table 3: **Definition of Pearson's correlation strength**

Correlation coefficient (Pearson r)	Strength
±0 – ±0.1	Negligible
±0.1 – ±0.3	Low
±0.3 – ±0.5	Moderate
±0.5 – ±1.0	High

3. Results

3.1 Interaction between neuronal and physiological signals during fear

To investigate the intricate relationship between brain and body during emotional behaviour, pInsCtx activity as well as cardiac and respiratory signals across different emotional states were characterized. I measured bulk calcium signals as a proxy for neuronal activity in the pInsCtx (*Fig. 12A*) utilizing fiber photometry. In parallel, I recorded ECG as well as intrapleural pressure as a readout of breathing utilizing wireless telemetry (*Fig. 12B*). I recorded those signals as well as the animals' behaviour during emotionally neutral conditions, in the home cage, as well as during fear and extinction learning, and during EPM exploration, as a test of innate fear (*Fig. 12C*).

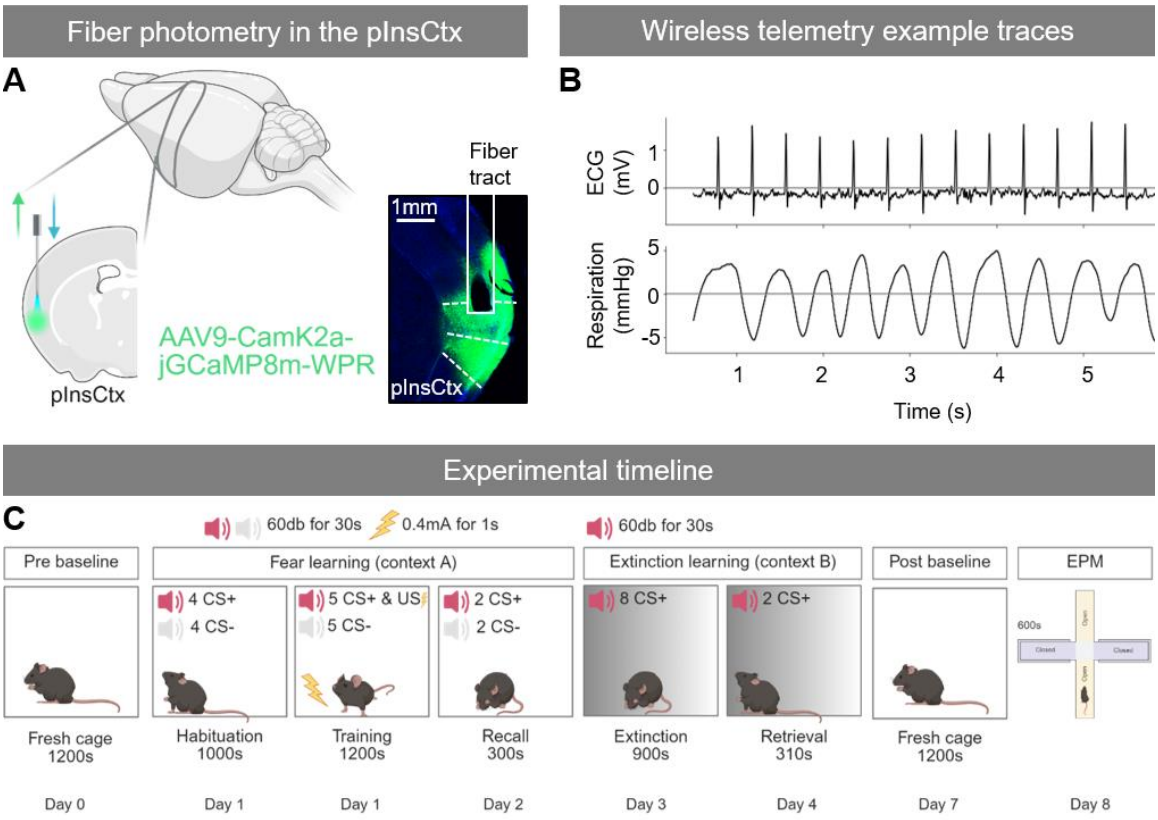

Fig. 12 **: Methods and experimental timeline.**
A) Schematic of injection and implantation site in the posterior insular cortex (pInsCtx) for fiber photometry (left, created with BioRender) and example from one animal with fiber placement and pInsCtx indicated in white (right).
B) Example traces of ECG and intrapleural pressure recordings using the DSI wireless telemetry setup.
C) Experimental timeline showing the different stages of the experiment: home cage recordings, fear and extinction learning, EPM exploration test (Created with *BioRender*)

First, a baseline was established with animals being recorded in home cage settings. In the following days, fear and consecutive extinction learning was conducted. Three days after completion of the fear and extinction learning paradigm, a post baseline was recorded in home cage settings. To conclude behavioural experiments, the day after post baseline recordings, innate fear was assessed on an elevated plus maze (EPM). A detailed explanation of measuring techniques as well as behavioural paradigms can be found in the methods section.

3.1.1 Interactions of the posterior insular cortex with the body in fear learning

First, I sought to address how pInsCtx activity and bodily signals interact during baseline conditions in the home cage of the animals when arousal and emotion state were kept as neutral as possible (*Fig.* 12*C, Day 0*). Under baseline conditions, the heart rate (in beats per minute or bpm), heart rate variability (HRV, assessed as RMSSD, see *2.7 Statistics*), breathing rate (in breaths per minute or brpm), as well as activity in the posterior insular cortex (pInsCtx, assessed as ΔF/F) was on average not statistically significant across periods of mobility or immobility (*Suppl. Fig.* 1*A*). Heart and breathing rates showed a weak positive correlation, and heart rate and HRV displayed an anti-correlation (*Suppl. Fig. 1B*). This inverse relationship between heart rate and HRV was expected, since these two measures have been shown to typically exhibit an anti-correlation[178]. Finally, no correlation between pInsCtx activity and the aforementioned bodily signals could be observed (*Suppl.* Fig*. 1C*). Overall, baseline recordings revealed that in a neutral state, pInsCtx and bodily signals showed no meaningful interactions.

Next, the relationships during emotionally arousing states were investigated to identify whether and how their interactions differ from neutral baseline states. Therefore, interactions were characterized during fear and extinction learning in the auditory fear conditioning paradigm (*Fig. 12C, Day 1 - 4*). Bodily signals and neuronal activity in the pInsCtx were assessed during conditioned stimuli (CS+ and CS-) and during the conditioned fear response (freezing) (*Fig. 13A*).

Assessment of freezing throughout the different stages of fear conditioning revealed that animals spent significantly more time freezing to CS+ (aversive cue) compared to CS- (neutral cue) during fear recall (*Fig. 13B*). This result indicates a successful fear learning, since the animals display the ability to differentiate between the two tones. However, animals did not spend less time freezing during the CS+ in retrieval (retrieval of extinction

memory) than during the CS+ in recall (recall of fear memory, *Fig. 13B*). Therefore, extinction training cannot be regarded as successful. As this chapter focuses on the two different types of emotional learning, an emphasis is placed on the stages of training and extinction, in which the learning occurs.

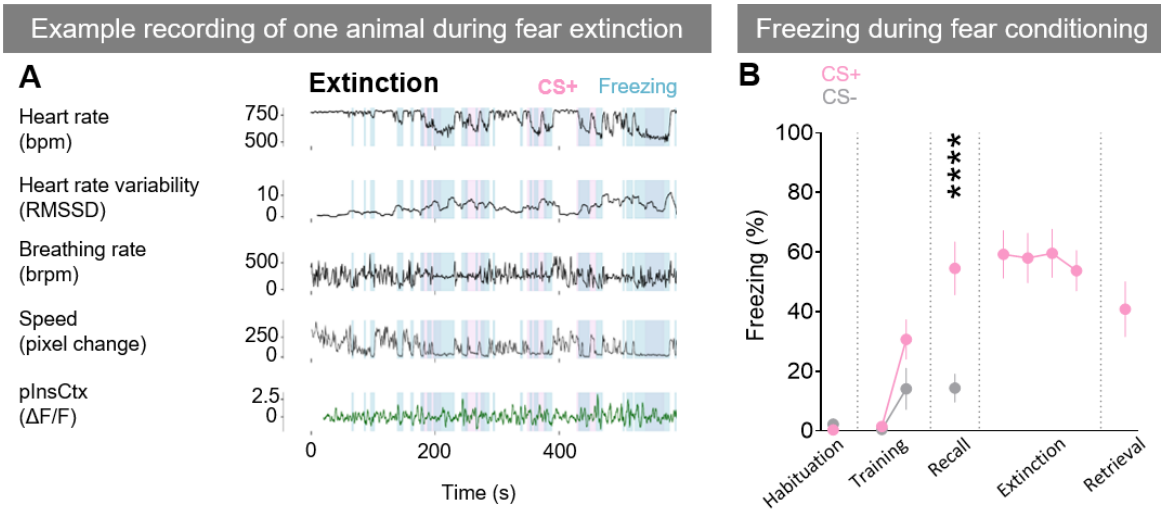

Fig. 13 **: Fear conditioning measurements and freezing responses.**
A) Example traces of all recorded parameters during the first 600 seconds of an extinction session of one animal. Recorded parameters (top to bottom): heart rate (bpm), heart rate variability (RMSSD), breathing rate (brpm), speed (pixel change) and pInsCtx activity (ΔF/F). CS+ presentations are shown in pink freezing episodes in blue.
B) Percentage of time spent freezing to aversive conditioned stimuli (CS+, pink) and the neutral conditioned stimulus (CS-, grey) of all animals (n = 11 mice). Each data point represents two pooled CS presentations.
Statistics:
Comparison of CS+ vs. CS- across Habituation, Training and Recall with 2way ANOVA: interaction factor **p = 0.002; post-hoc Sidak's multiple comparisons: Recall: ****p<0.0001, Habituation and Training: ns.
Difference of freezing during the first two CS+ in training to the last two CS+ in training calculated with a RM one-way ANOVA of comparison of CS+ across fear conditioning: ANOVA summary ****p<0.0001; post-hoc Tukey's multiple comparison test: Training first 2 CS+ vs. Training last 2 CS+ *p = 0.02. Averaged freezing responses show the mean; error bars show SEM.

3.1.1.1 Characterization of bodily signals and posterior insular cortex activity during the conditioned fear cue in training

To gain a better understanding of the interactions between the body and posterior insula cortex during the process of emotional learning, the emotionally salient times of tone presentations (30 seconds of CS+) were characterized (*Fig. 14A*). First, the training stage was assessed. In this stage animals learn to associate the CS+ with the foot shock (US). Characterization of average changes during all CS+ presentations compared to the baseline (10 seconds preceding CS+) revealed a significant decrease of RMSSD (*Fig. 14C*). Heart and breathing rate as well as pInsCtx activity did not show overall changes (*Fig. 14A,*

B, D). However, onset of CS+ was accompanied by a sharp but very transient increase in pInsCtx activity (*Fig. 14D, E*). Interestingly, none of the bodily signals showed a significant change towards the CS+ onset (*Suppl. Fig. 2*). Together, these results demonstrated that RMSSD and pInsCtx activity respond to CS+ during training.

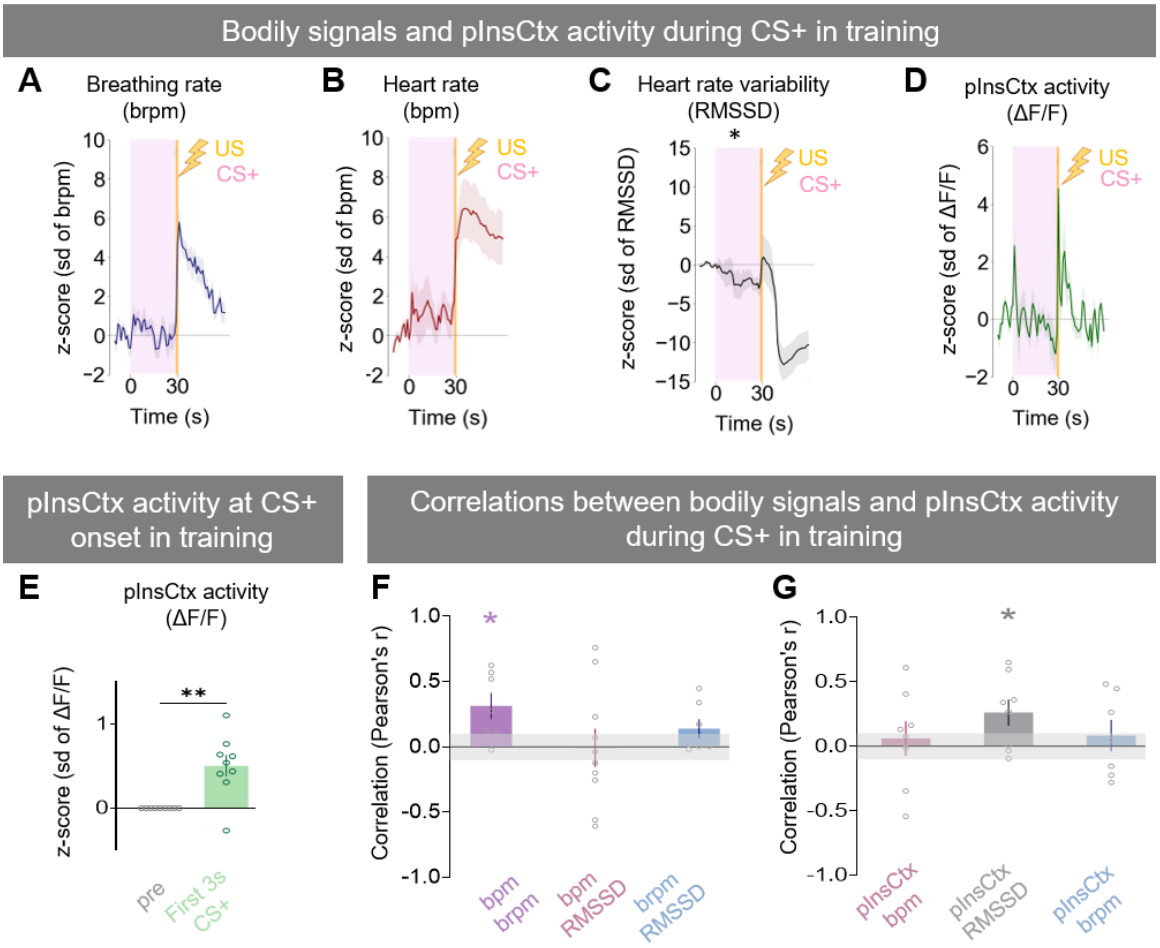

Fig. 14**: Fear learning initiates interactions between pInsCtx and HRV.**
A - D: Averaged responses of bodily signals of breathing rate (brpm), heart rate (bpm), heart rate variability (RMSSD), and pInsCtx activity (ΔF/F) of all animals to all 5 CS+ presentations in training. Responses are z-scored to the 10 seconds of baseline before CS+ onset. Statistics: comparison of baseline (10 seconds preceding CS+) vs. CS+ with paired t-test.
A) Response of breathing rate (brpm, n=8), baseline vs. CS+ ns.
B) Response of heart rate (bpm, n=11), baseline vs. CS+ ns.
C) Response of heart rate variability (RMSSD, n=11), baseline vs. CS+ *p=0.02.
D) Response of pInsCtx activity (ΔF/F, n=9), baseline vs. CS+ ns.
E) Response of pInsCtx activity (ΔF/F, n=9) at the onset of CS+ (first 3 seconds), z-scored to the 10 seconds of baseline before CS+ onset (pre). Comparison of baseline (10 seconds preceding CS+ vs. first 3 seconds of CS+ with paired t-test **p = 0.004.
F) Pearson's correlations between bodily signals (as in A - C); bpm and brpm (n=7) CS+ mean r=0.31, *p=0.02; bpm and RMSSD (n=10) ns; brpm and RMSSD (n=7) ns.
G) Pearson's correlations between bodily signals and pInsCtx; pInsCtx and RMSSD (n=8) mean r =0.26, CS+ p*=0.04; pInsCtx and bpm (n=8) ns, pInsCtx and brpm (n=7) ns.
Averaged values show the mean, shading and error bars show SEM.
A - D: Vertical pink bars indicate the duration of CS+ presentations (30 seconds); yellow line and lightning bolt indicate time point of foot shock (US).
F and G: horizontal grey bars between -0.1 and 0.1 indicate area in which the mean Pearson's r values indicate no correlation.

Subsequently, possible interactions between bodily signals (*Fig. 14F*) as well as between pInsCtx and bodily signals (*Fig. 14G*) during emotional states were investigated. Towards this goal, within-animal correlations between the recorded variables during CS+ periods were analysed. During CS+ presentations, heart and breathing rate displayed a positive correlation, as in the case of the neutral emotional state during baseline recordings in the home cage (*Fig. 14F, Suppl. Fig. 1B*). Interestingly, unlike during the neutral state, there was no inverse relationship found between bpm and HRV during CS+ in training (*Fig. 14F, Suppl.* Fig. *1B*). Most importantly, HRV now displayed a positive correlation with pInsCtx activity during CS+ in training (*Fig. 14G*). Taken together, analysis of body-pInsCtx interactions revealed that HRV and pInsCtx are coupled during fear learning but not during baseline recordings.

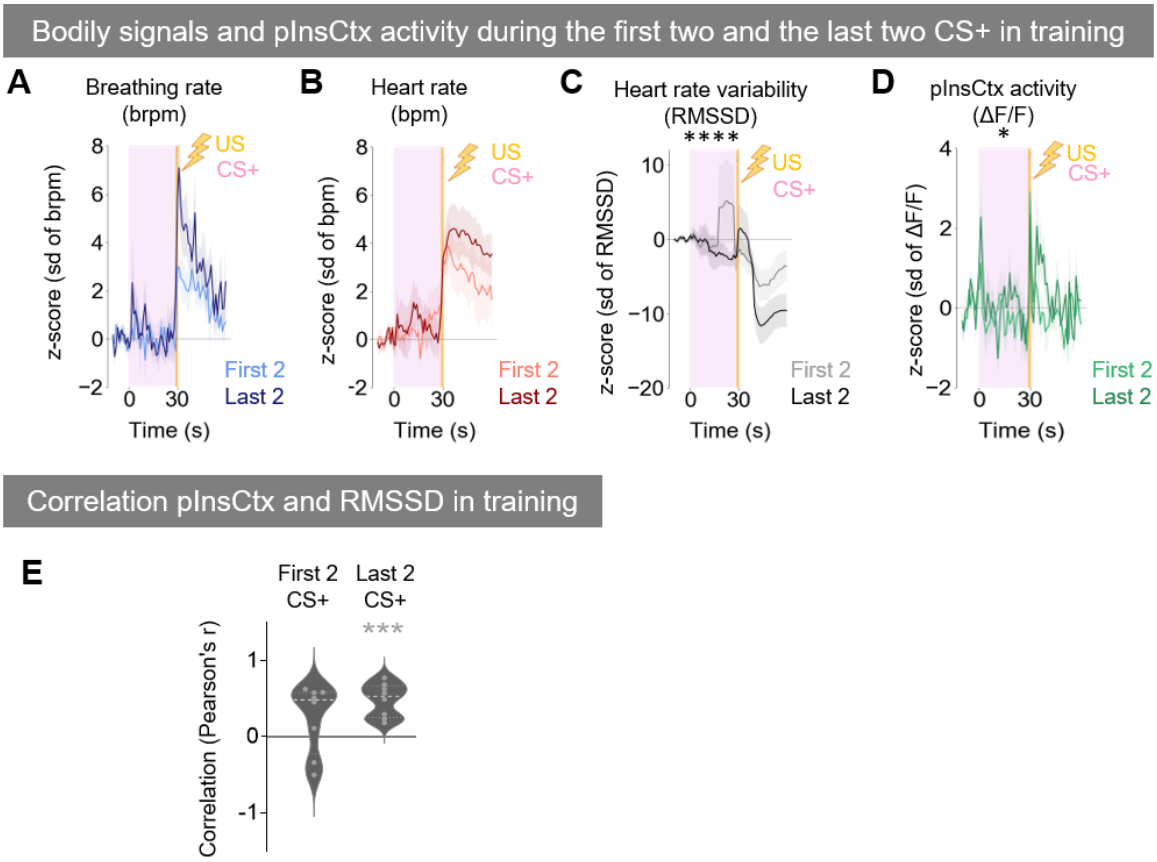

Fig. 15: **Bodily signals and pInsCtx activity during the first two and the last two CS+ in training.**
A - D: Averaged responses of bodily signals of breathing rate (brpm), heart rate (bpm), heart rate variability (RMSSD), and pInsCtx activity of all animals to the first two (lighter color) and last two (darker color) CS+ presentations in training. Responses are z-scored to the 10 seconds of baseline before CS+ onset.
Statistics: comparison of first two CS+ vs. last two CS+ with paired t-test.
A) Response of breathing rate (brpm, n=8), first two CS+ vs. last two CS+ ns.
B) Response of heart rate (bpm, n=11), first two CS+ vs. last two CS+ ns.
C) Response of heart rate variability (RMSSD, n=11), first two CS+ vs. last two CS+ ****p<0.0001.
D) Response of pInsCtx activity (ΔF/F, n=9), first two CS+ vs. last two CS+ *p=0.04.

E) Pearson's correlation of RMSSD and pInsCtx during the first two (left) and last two (right) CS+ presentations. pInsCtx-RMSSD (n=8) first two CS+ mean r=0.25, ns; last two CS+ mean r=0.49, ***p=0.0004.
A - D: Vertical pink bars indicate the duration of CS+ presentations (30 seconds); yellow line and lightning bolt indicate time point of foot shock (US).
Averaged values show the mean, shading and violin plot show SEM.

Since an interaction between pInsCtx and cardiac or breathing variables had not been observed during a neutral state, I next sought to examine whether the correlation between pInsCtx and HRV may emerge during the process of fear learning. To this end, I first assessed if fear acquisition during the training phase was successful, utilizing the time spent freezing to the CS+ as a readout. This showed that animals displayed a significantly higher freezing response during the last two CS+ presentations in training compared to the first two CS+ presentations in training, thus indicating successful learning and a higher fear state during the last two CS+ presentations (*Fig. 13B*).

Strikingly, comparison of correlations between pInsCtx activity and bodily variables at the beginning versus end of the fear conditioning session, revealed that HRV was the only variable, which showed a significant difference between the response during CS+ at beginning of fear learning compared to the end (*Fig. 15A-C*). HRV was significantly lower during the last two CS+ presentations than during the first two CS+ presentations in training (*Fig. 15C*). Additionally, pInsCtx activity displayed a significantly higher activity during the last two compared to the first two CS+ in training (*Fig. 15D*). Furthermore, activity in the pInsCtx showed a significant correlation to HRV during the last two CS+ presentations, which was not present during the first two CS+, indicating that pInsCtx and HRV become correlated throughout fear learning. Taken together, the results obtained from training suggest that fear learning induces a fear-state dependent coupling between HRV and pInsCtx.

3.1.1.2 Laterality of the posterior insular cortex during conditioned stimuli in training

One especially intriguing aspect of interoceptive studies in humans is that they consistently highlight a lateralization of the insular cortex[179,180]. Moreover, hemispheric lateralization has not only been found to occur in humans but also in rodents[181,182]. To gain insights on whether cardiac and respiratory interoception are lateralized in the mouse insular cortex, the dataset was divided into two groups, one for each hemisphere in which neuronal activity had been recorded. Since the calcium indicator used to record neuronal activity has both a fast half-rise (around 5ms) and half-decay time (around 150ms)[177], I averaged only the first three seconds of CS+ presentations for the quantification of differences to ensure a representation of immediate changes of pInsCtx activity to tone onset.

Analysis of hemispheric differences revealed that the left pInsCtx exhibited a significantly stronger response to the CS+ and foot shock (US) compared to the right pInsCtx (*Fig. 16A-B*). Furthermore, investigation of pInsCtx interactions with the body at CS+ onset showed different interactions of the left and right pInsCtx with heart rate (*Fig. 16C*). While heart rate exhibited a strong positive correlation with the left pInsCtx, no correlation with the right pInsCtx was found (*Fig. 16C*). Overall, these results suggest a stronger representation of emotional experiences and a closer interaction with cardiac measures in the left pInsCtx hemisphere during training.

To explore whether fear learning evoked the hemispheric difference, pInsCtx activity and its correlations with bodily signals were assessed separately during the first two versus the last two CS+ onsets in training (*Fig. 16D versus G*). No change in pInsCtx activity was observable during the first two CS+ and US (*Fig. 16D*) or during the first 3 seconds of tone presentations between the hemisphere (*Fig. 16E (right)*). Nonetheless, both, the right and the left pInsCtx, displayed an increase during the US (*Fig. 16D and E (left)*). Neither of the hemispheres were correlated with heart nor breathing rate or RMSSD (*Fig. 16F*). Strikingly, activity in the left pInsCtx was significantly higher than in the right pInsCtx during the last two CS+ and US (*Fig. 16G*) and further showed a markedly higher activity at the onset of CS+ (*Fig. 16H*). Additionally, during the last two CS+ onsets in training, the left pInsCtx was significantly correlated with heart rate (*Fig. 16G*). Intriguingly, these results suggest an emergence of lateralization of the pInsCtx during fear learning.

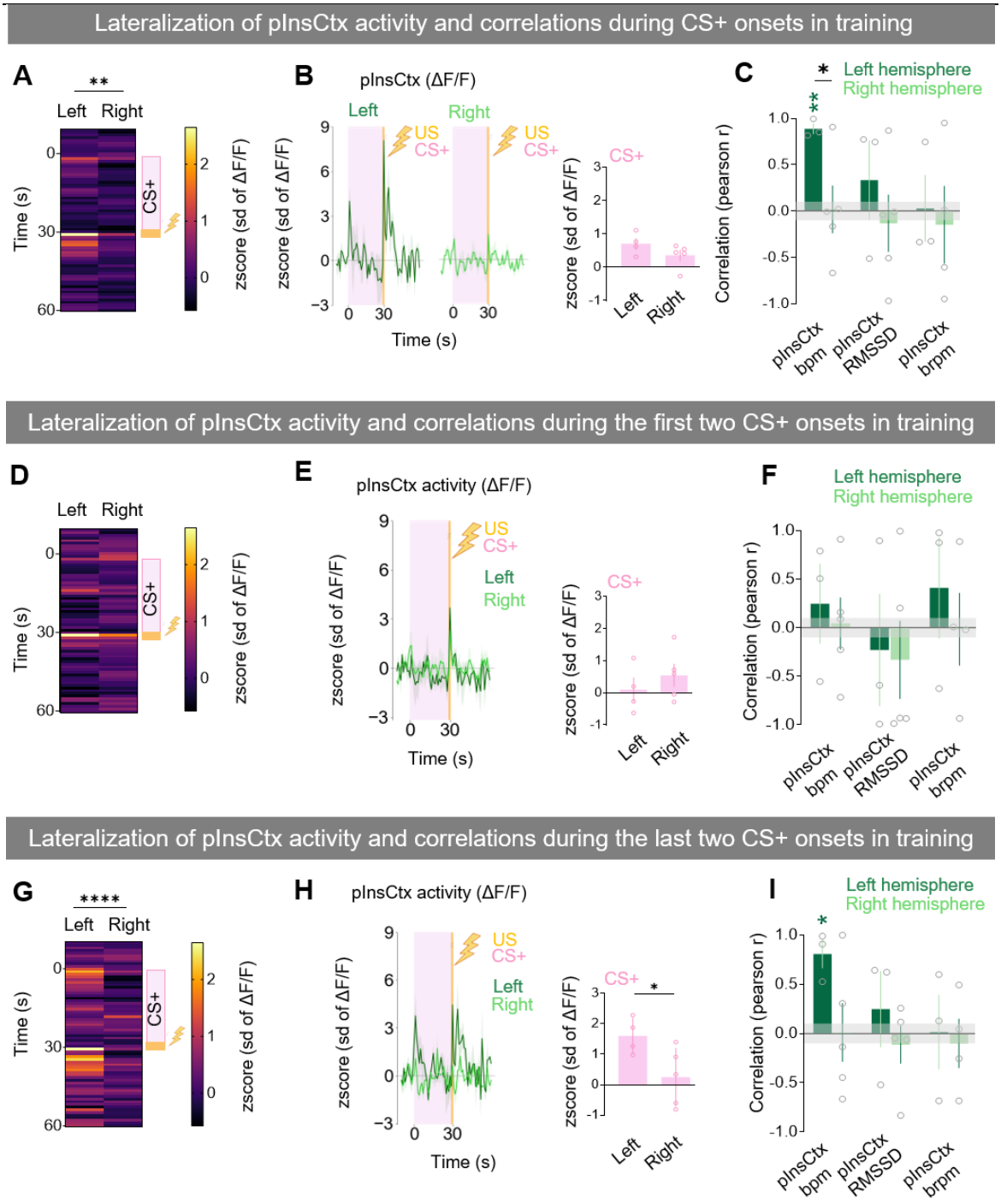

Fig. 16**: Lateralization of pInsCtx activity during fear learning**
A) Comparison of baseline (10 seconds preceding CS+), CS+ and postCS+ (30 seconds post CS+) of average pInsCtx activity (ΔF/F) during training between left (n=4) and right hemisphere (n=5). Unpaired t-test **p=0.002.
B) Average pInsCtx activity (ΔF/F) responses to all 5 CS+ presentations during training of the left (dark green, left) and right (light green, middle) hemisphere. Comparison of responses during the first 3 seconds of CS+ between both hemispheres with unpaired t-test was ns (right).
C) Pearson's correlations between pInsCtx activity (ΔF/F) and the bodily signals of heart rate (bpm), HRV (RMSSD), and breathing rate (brpm) per hemisphere. Left pInsCtx and bpm CS+ mean r=0.89 **p=0.004. All other interactions ns; comparisons between hemispheres with unpaired t-tests: left pInsCtx interaction with heart rate (bpm) vs. right pInsCtx interaction with heart rate (bpm) *p=0.04. Remaining left vs. right pInsCtx interactions with bodily signals were ns.

D) Comparison of baseline (10 seconds preceding CS+), CS+ and postCS+ (30 seconds post CS+) of average pInsCtx activity (ΔF/F) during the first two CS+ presentations in training between left and right hemisphere. Unpaired t-test ns.
E) Average pInsCtx activity (ΔF/F) responses to the first two CS+ presentations in training of the left (dark green) and right (light green) hemisphere (left). Comparison of responses during the first 3 seconds of CS+ between both hemispheres with unpaired t-test was ns (right).
F) Pearson's correlations between pInsCtx activity (ΔF/F) and bodily signals (as in C) during the first two CS+ presentations per hemisphere; all correlations as well as comparisons between hemispheres were ns.
G) Comparison of baseline (10 seconds preceding CS+), CS+ and postCS+ (30 seconds post CS+) of average pInsCtx activity (ΔF/F) during the last two CS+ presentations in training between left and right hemisphere. Unpaired t-test ****p<0.0001.
H) Average pInsCtx activity (ΔF/F) responses to the last two CS+ presentations in training of the left (dark green) and right (light green) hemisphere (left). Comparison of responses during the first 3 seconds of CS+ between both hemispheres with unpaired t-test *p=0.04 (right).
I) Pearson's correlations between pInsCtx activity (ΔF/F) and bodily signals (as in C and F) during the last two CS+ presentations per hemisphere; left pInsCtx and bpm CS+ mean r=0.81, *p=0.03; All other interactions as well as comparisons between hemispheres were ns.
Animal numbers: pInsCtx left hemisphere n=4, pInsCtx right hemisphere n=5. pInsCtx left and bpm n=3, pInsCtx left and RMSSD n=3, pInsCtx left and brpm n=3, pInsCtx right and bpm n=5, pInsCtx right and RMSSD n=5, pInsCtx right and brpm n=4.
Vertical pink bars indicate the duration of CS+ presentations (30 seconds); yellow line and lightning bolt indicate time point of foot shock (US); heatmaps show z-scored pInsCtx activity (ΔF/F); left hemisphere: dark green, right hemisphere: light green.
Averaged values show the mean, shading and error bars show SEM.

3.1.2 Interactions of the posterior insular cortex with the body in extinction learning

Characterization of bodily signals and pInsCtx throughout fear learning elucidated compelling pInsCtx-body interactions. First, I discovered that a coupling between HRV and pInsCtx activity arises during training. Further analyses additionally revealed stronger activation during CS+ as well as stronger correlations with heart rate within the pInsCtx of the left rather than right hemisphere. Since these intriguing relationships emerged during fear learning, I next sought to explore pInsCtx activity, bodily signals and their interactions during the other stage of emotional learning in this paradigm, namely fear extinction learning.

3.1.2.1 Characterization of bodily signals and posterior insular cortex activity during conditioned stimuli in extinction

As mentioned in in *chapter 3.1.1*, fear extinction learning did not result in a significant reduction in time spent freezing, and could therefore not be regarded as successful (*Fig. 13B*). However, bodily signals and pInsCtx activity may still show different responses and interactions to and during CS+ presentations in the process of fear extinction compared to fear learning, as the abundant freezing responses during fear extinction are indicative of a high fear state throughout the entire session.

Analysis of average changes during all eight CS+ presentations in extinction compared to the baseline (10 seconds preceding CS+) showed significant decreases in heart and breathing rates, revealing a strong bodily response during the CS+ presentations (*Fig. 17A-B*). Interestingly, HRV and pInsCtx activity, on the other hand, did not show overall changes during the 30 seconds of all CS+ presentations (*Fig. 17C, D*). However, HRV displayed a trend of an increase over the time course of the CS+ (*Fig. 17C*). Overall, the bodily reactions during CS+ in fear extinction differed markedly from the responses during CS+ during fear learning in training where neither breathing nor heart rate showed significant changes (*Fig. 14A, B*) while HRV was significantly decreased (*Fig. 14C*). These observations suggest different bodily processes during CS+ presentations, depending on the type of emotional learning and internal fear states.

Next, I assessed whether not only the responses, but also the interactions between bodily signals as well as between bodily signals and pInsCtx during CS+ in extinction differed from the interactions in training. While in training, pInsCtx and HRV showed a significant positive correlation (*Fig. 14G, Fig. 15E*), surprisingly, in extinction, no significant interactions between bodily signals and pInsCtx activity were found (*Suppl.* Fig. 3*E*). Nonetheless, correlations between bodily signals revealed significant interactions between heart and breathing rate as well as between heart rate and HRV (*Fig. 17E*). Heart and breathing rate exhibited a significant positive correlation (*Fig. 17E*), which was also observed during neutral state in cage recordings (*Suppl. Fig.* 1*B*) as well as during fear cues (CS+) in training (*Fig. 14F*). The consistent observation of the positive interaction between heart and breathing rate may suggest that their relationship is rather stable across different emotional states. Additionally, heart rate and HRV showed an inverse relationship during CS+ in extinction (*Fig. 17E*), which mimicked their interaction during the neutral baseline state (*Suppl. Fig. 1B*), but differed to their interactions during CS+ in training, where no correlations were found (*Fig. 14F*). These results indicate that interactions amongst bodily signals as well as between bodily signals and pInsCtx, are more similar between fear extinction learning and baseline conditions than between fear extinction learning and fear learning.

To explore whether bodily signals and pInsCtx activity or their interactions during CS+ changed throughout extinction learning, I compared the first two to the last two CS+ presentations in extinction (*Fig. 17F-I*). Interestingly, despite the lack of a significant extinction effect of freezing behavior (*Fig. 13B*), these comparisons revealed different responses of bodily signals and pInsCtx activity to CS+ presentations in the beginning comparted to the end of extinction. Notably, breathing rate, heart rate and pInsCtx activity were significantly lower during CS+ at the end of extinction compared to the beginning (*Fig. 17F, G -*

E). Furthermore, HRV was significantly higher during CS+ presentations at the end of extinction compared to the beginning (*Fig. 17H*). Interestingly, this separation revealed that the peak response of HRV shifted throughout fear extinction. While at the beginning of the extinction session, HRV displayed a peak at the offset of the CS+ where the foot shock was expected, at the end of extinction learning, the peak response was found during the CS+ presentation.

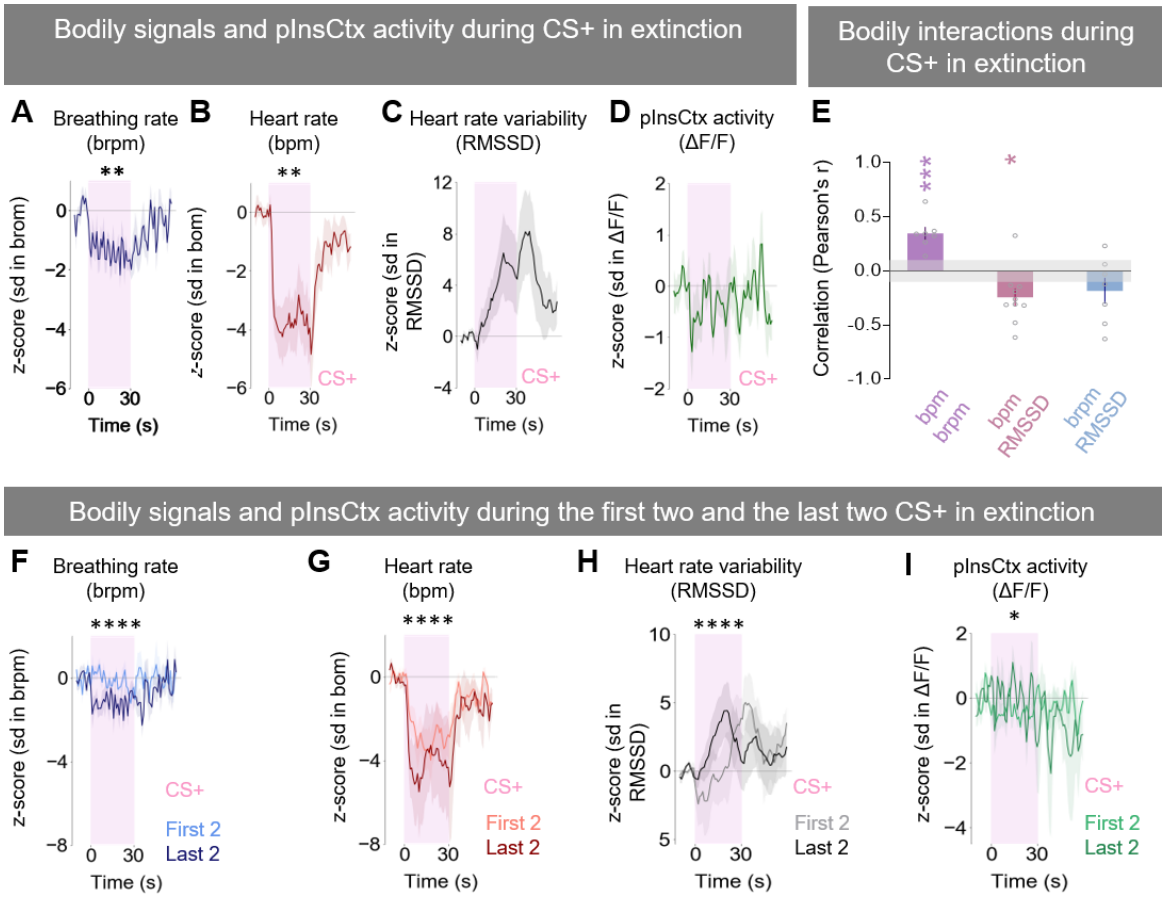

Fig. 17: **Fear extinction learning**
A - D: Averaged responses of bodily signals of breathing rate (brpm), heart rate (bpm), heart rate variability (RMSSD) and pInsCtx activity (ΔF/F) of all animals to all 8 CS+ presentations in fear extinction. Responses are z-scored to the 10 seconds of baseline before CS+ onset. Statistics: comparison of baseline (10 seconds preceding CS+) vs. CS+ with paired t-test.
A) Response of breathing rate (brpm, n=8), baseline vs. CS+ **p=0.004.
B) Response of heart rate (bpm, n=11), baseline vs. CS+ **p=0.001.
C) Response of heart rate variability (RMSSD, n=11), baseline vs. CS+ ns.
D) Response of pInsCtx activity (ΔF/F, n=9), baseline vs. CS+ ns.
E) Pearson's correlations between bodily signals (as in A) during CS+; bpm and brpm (n=7) mean r=0.35, ***p=0.0009; bpm and RMSSD (n=10), mean r=-0.24, *p=0.01; brpm and RMSSD (n=10) ns.
F - I: Averaged responses of bodily signals (as in A) and pInsCtx activity (ΔF/F) of all animals to the first two (lighter color) and last two (darker color) CS+ presentations in extinction. Responses are z-scored to the 10 seconds of baseline before CS+ onset. Statistics: comparison of first two CS+ vs. last two CS+ with paired t-test.
F) Response of breathing rate (brpm, n=8), first two CS+ vs. last two CS+ ****p<0.0001.
G) Response of heart rate (bpm, n=11), first two CS+ vs. last two CS+ ****p<0.0001.
H) Response of heart rate variability (RMSSD, n=11), first two CS+ vs. last two CS+ ****p<0.0001.

I) Response of pInsCtx activity (ΔF/F, n=9), first two CS+ vs. last two CS+ *p=0.047.
A - D and F - I: Vertical pink bars indicate the duration of CS+ presentations (30 seconds)
E: Horizontal grey bars between -0.1 and 0.1 indicate area in which the mean Pearson's r values indicate no correlation.
Averaged values show the mean, shading and error bars show SEM.

Together these results showed that whilst there was no significant difference in freezing between the beginning and end of extinction (*Fig. 13B*), responses of the body and pInsCtx to the fear cues changed throughout extinction learning. This suggests that pInsCtx as well as bodily signals may hold additional information about the animal's internal states, and changes thereof, which is not reflected by the time spent freezing.

Since responses to the CS+ were different at the beginning of extinction compared to the end, I next sought to explore if interactions between pInsCtx activity and bodily signals changed throughout extinction learning. However, these analyses showed that bodily signals and pInsCtx did not exhibit significant interactions during the first two CS+, nor during the last 2 CS+ or all 8 CS+ during extinction (*Suppl.* Fig. 3*A, C*). This, once more, highlighted the specificity of HRV and pInsCtx coupling during fear learning (*Fig. 14G, Fig. 15E*). Moreover, bodily signals did not differ in their interaction between the beginning of extinction learning versus the end of extinction learning (*Suppl.* Fig. 3*B*). Overall, these results showed that while bodily signals and pInsCtx activity during CS+ changed over the time course of extinction training, their interactions did not. However, since extinction learning had not been successful (*chapter 3.1.1, Fig. 13B*), it warrants further experiments to investigate whether this may differ if extinction training evokes significant freezing changes.

Since the left pInsCtx activity had shown a higher activity during fear learning (*Fig. 16A*), as well as a stronger correlation with heart rate compared to the right hemisphere (*Fig. 16C*), I examined whether hemispheric differences were present during extinction learning. To compare left and right pInsCtx activity as well as their interactions with bodily signals during extinction to the aforementioned differences observed in training (*chapter 3.1.1.2, Fig. 16*), the same analyses were conducted. Therefore, activity during baseline, CS+, US, and postCS+ (*Suppl. Fig.* 4*A, D, G*) as well as neuronal activity at CS+ onset (*Suppl. Fig.* 4*B, E, H*) and interactions with bodily signals (*Suppl. Fig.* 4*C, F, J*) were assessed for the left and the right hemisphere throughout extinction. Interestingly, those analyses revealed that in extinction, the only difference between hemispheres, was a lower activity in the left pInsCtx during the first two CS+, US and postCS+ (*Suppl. Fig.* 4*D*). Furthermore, a trend towards a strong positive correlation between the left hemisphere and heart rate during all CS+ onsets in extinction was observable (*Suppl. Fig.* 4*C*, mean Pearson's r >0.5). Overall, this showed that while during fear training, a clear lateralization was present (*Fig. 16*), no

significant lateralization effects were present in the same mice during CS+ in fear extinction (*Suppl. Fig.* 4). Taken together, characterizations of bodily signals and pInsCtx activity in extinction revealed differences in activity and interactions compared to training, possibly suggesting different internal states in these two phases of emotional learning.

3.1.2.2 Post extinction learning baseline

Three days after completion of the fear learning and fear extinction paradigm, another recording in the home cage was conducted to investigate whether these emotionally salient experiences changed pInsCtx activity and bodily signals as well as their interactions when animals are in a neutral context (*Fig. 12C Day 7, Suppl. Fig.* 1*D-F*). These recordings revealed that, as observed during the initial baseline (*Fig. 12C Day 0*), there were no differences in bodily signals or pInsCtx activity between active and inactive time periods (*Suppl. Fig.* 1*A, D*). Moreover, no correlations between neuronal activity in the pInsCtx and bodily signals were present (*Suppl. Fig.* 1*F*). Taken together, my results highlighted that out of all characterized times and different emotional states (pre-baseline, fear training, fear extinction, and post-baseline), the pInsCtx and HRV coupling was unique to CS+ presentations in training (*Fig. 14G, Fig. 15E*). Furthermore, similarly as during baseline recordings before fear conditioning, a correlation was observable between breathing and heart rate as well as an anti-correlation between HRV and heart rate (*Suppl.* Fig. 1*B, E*). Together, these results suggest that whilst animals did not successfully extinguish the previously acquired fear, the conditioning had little to no long-lasting effects on interactions of bodily signals and pInsCtx activity during neutral emotional states.

The thorough characterization of body-pInsCtx interactions during neutral baseline conditions versus during fear cues, demonstrated differences which seem to depend on fear states. Throughout fear and extinction conditioning, animals displayed a considerable amount of freezing (*Fig. 13*), which may contribute to the different cardio-respiratory and body-pInsCtx relationships during fear states. Therefore, I next investigated bodily signals and pInsCtx activity during freezing.

3.1.3 Interactions of the posterior insular cortex with the body during freezing

To explore bodily signals and pInsCtx activity as well as their interactions, I selected freezing episodes of a minimum length of five seconds which were separated from each other by at least three seconds. This allowed for the analysis of changes in bodily signals and pInsCtx activity after the onset as well as before the offset of freezing.

3.1.3.1 Bodily signals and posterior insular cortex activity during freezing onsets and offsets

First, to explore responses of bodily signals and pInsCtx activity to freezing onsets, the first five seconds of freezing were compared to the baseline (3 seconds before freezing) (*Fig. 18*). This revealed significant decreases of heart and breathing rate at freezing onset. Moreover, the decrease in breathing rate appeared to occur faster than the heart rate decrease (*Fig. 18A, B*). Interestingly, while the average pInsCtx activity response for the first 3 seconds after freezing onsets was not significantly different compared to the baseline, visual inspection indicated a stereotyped initial decrease, followed by an increase of activity (*Fig. 18D*). Since during fear leaning, pInsCtx activity was lateralized, displaying a stronger response in the left hemisphere, I compared pInsCtx activity in the left versus the right hemisphere after freezing onset. Surprisingly, this comparison revealed that activity in the right hemisphere seemed to be more strongly modulated at freezing onset than the activity in the left hemisphere (*Fig. 18E*). However, this trend did not reach significance (p = 0.057). Overall, characterization of bodily signals and pInsCtx activity at freezing onset revealed a strong decrease in both heart and breathing rate.

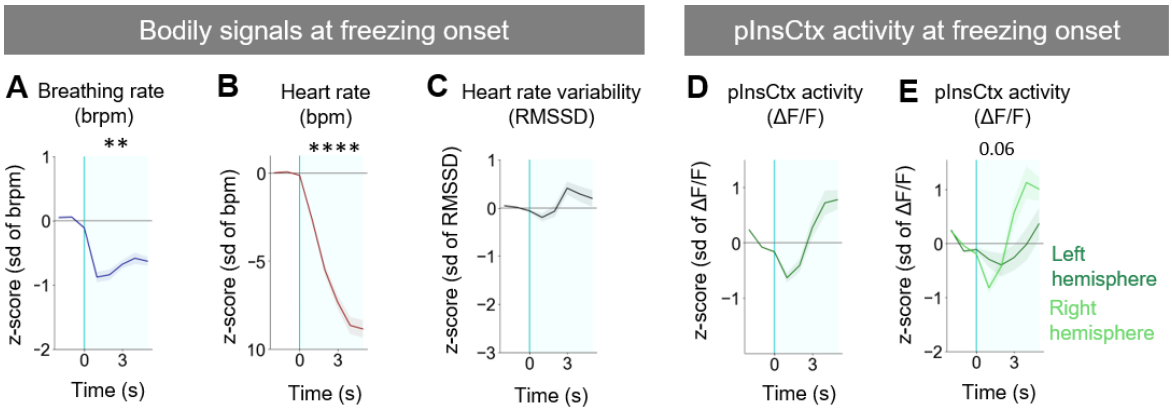

Fig. 18 **: Bodily signals and pInsCtx activity at freezing onset**
A-D: Averaged responses of bodily signals of breathing rate (brpm), heart rate (bpm), heart rate variability (RMSSD) and pInsCtx activity (ΔF/F) of all animals at freezing onsets. Freezing episodes: length ≥ 5 seconds that were ≥ 3 seconds apart from other freezing episodes. Responses are z-scored to the 3 seconds of baseline before freezing.
Statistics: comparison of baseline (3 seconds before freezing) vs. freezing with paired t-test.
A) Response of breathing rate (brpm, n=8), baseline vs. freezing **p=0.009.
B) Response of heart rate (bpm, n=11), baseline vs. freezing ****p<0.0001.
C) Response of heart rate variability (RMSSD, n=11), baseline vs. freezing ns.
D) Response of pInsCtx activity (ΔF/F, n=9), baseline vs. freezing ns.
E) Response of pInsCtx activity (ΔF/F) divided into left (dark green, n=4) and right (light green, n=5) hemisphere; comparison of responses during freezing between both hemispheres with unpaired t-test: p=0.057 (ns).
Averaged values show the mean, shading and error bars show SEM. Light blue shaded area in all panels indicates timespan of freezing.

Subsequently, to explore dynamics of bodily signals before the end of freezing, responses of the body and pInsCtx activity before freezing offsets were compared to the post-baseline (3 seconds after freezing) (*Fig. 19*). These comparisons revealed that both cardiac measures (heart rate and HRV) were significantly lower during freezing than after freezing (*Fig. 19B*). On the other hand, breathing rate and pInsCtx showed no significant changes (*Fig. 19A, D*). Visual inspection, however, revealed a trend towards lower activity during freezing with an increase around three seconds before freezing offset for both pInsCtx and breathing rate, suggesting that both breathing rate and pInsCtx activity increases may predict the end of freezing. These observations may hint towards an interaction between pInsCtx and breathing rate at freezing offset which was not present at freezing onset. To investigate this possibility, body-brain correlations during freezing were assed subsequently (*chapter 3.1.3.2*). Furthermore, comparison of pInsCtx activity in the left versus the right hemisphere before freezing offset revealed a significantly lower activity in the left hemisphere compared to the right (*Fig. 19E*). Intriguingly, at freezing onset, a trend in the same direction had been visible without reaching significance (*Fig. 18E, p=0.06*). This suggests an overall stronger activity decrease in the left pInsCtx compared to the right pInsCtx during freezing.

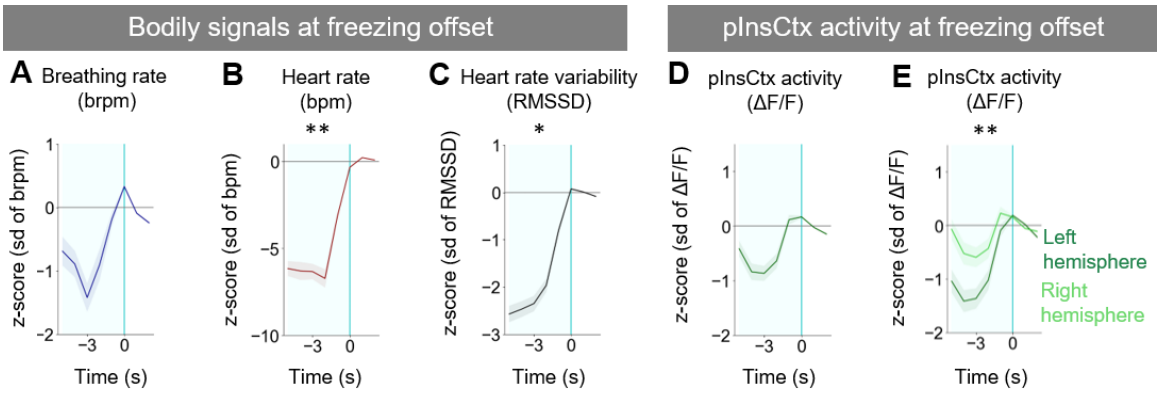

Fig. 19: **Bodily signals and pInsCtx activity at freezing offset**
A-D: Averaged responses of bodily signals of breathing rate (brpm), heart rate (bpm), heart rate variability (RMSSD) and pInsCtx activity (ΔF/F) of all animals at freezing offsets. Freezing episodes: length ≥ 5 seconds that were ≥ 3 seconds apart from other freezing episodes. Responses are z-scored to the 3 seconds of post-baseline after freezing.
Statistics: comparison of post-baseline (3 seconds after freezing) vs. freezing with paired t-test.
A) Response of breathing rate (brpm, n=8), post-baseline vs. freezing ns.
B) Response of heart rate (bpm, n=11), post-baseline vs. freezing **p<0.002.
C) Response of heart rate variability (RMSSD, n=11), post-baseline vs. freezing *p=0.01.
D) Response of pInsCtx activity (ΔF/F, n=9), baseline vs. freezing ns.
E) Response of pInsCtx activity (ΔF/F) divided into left (dark green, n=4) and right (light green, n=5) hemisphere; Comparison of responses during freezing between both hemispheres with unpaired t-test: **p=0.007 (ns). Averaged values show the mean, shading and error bars show SEM. Light blue shaded area in all panels indicates timespan of freezing.

Characterization of bodily signals and pInsCtx activity at freezing onset and offset, revealed stereotyped dynamics. To investigate if these responses would additionally be accompanied by distinct cardio-respiratory or pInsCtx-body interactions, I next analysed their correlations.

3.1.3.2 Brain-body correlations during freezing

To explored how heart rate, breathing rate and HRV interact during freezing and whether those interactions differ between the onsets and offsets of freezing (*Fig. 20*), I correlated the signals with each other and further compared these between freezing on- and offset.

Since heart rate and HRV exhibited a strong anticorrelation during baseline conditions (*Suppl.* Fig. 1*B*) and CS+ presentations in fear extinction (*Fig. 17E*) but none during CS+ in fear learning (*Fig. 14F*), their relationship was analyzed first. Strikingly, the correlation between heart rate and HRV exhibited a shift between the onset and offset of freezing. While at freezing onset, a trend towards an anticorrelation was observable, at freezing offset, these two variables were significantly positively correlated (*Fig. 20A, middle*). Interestingly, a similar shift was observed in the interaction between breathing rate and heart rate. However, neither the correlation at freezing onset nor the correlation at freezing offset reached significance and can therefore only be interpreted as trends (*Fig. 20A, left*). Together, these observations highlight a positive interaction between heart rate and HRV before freezing offset. Interestingly, this represents not only the opposite of the inverse relationship between those cardiac measures, as observed during baseline and extinction (*Suppl.* Fig. 1*B, Fig. 17E*), but additionally differs from the lack of correlation observed during training (*Fig. 14F*). Therefore, it could be hypothesized that the positive heart rate and HRV relationship may be initiated by freezing and constitute a unique feature of this fear behaviour. However, further, targeted investigations would be necessary to confirm this hypothesis.

Subsequently, interaction of bodily variables with pInsCtx activity was assessed. Interestingly, heart rate and pInsCtx activity correlations differed significantly between freezing onset and offset (*Fig. 20B, left*). While heart rate and pInsCtx showed a strong negative correlation at freezing onset, no significant interaction was present at the offset. Interestingly, interactions between pInsCtx activity and HRV, revealed a strong positive correlation at freezing onset (*Fig. 20B, middle*), which, however, was not significantly different to the interaction at freezing offset. Lastly, pInsCtx and breathing rate were highly correlated at freezing offset (*Fig. 20B, right*). Intriguingly, this correlation confirms the observed similarities between pInsCtx and breathing rate dynamics at freezing offset, which showed an

increase around three seconds preceding freezing termination (*Fig. 19A, D*). Taken together, correlation analyses revealed that during freezing onsets pInsCtx interacted with cardiac measures, while during freezing offsets, pInsCtx exhibited a strong correlation with breathing. This may suggest that a different body-pInsCtx connectivity is recruited during freezing initiation than during freezing termination.

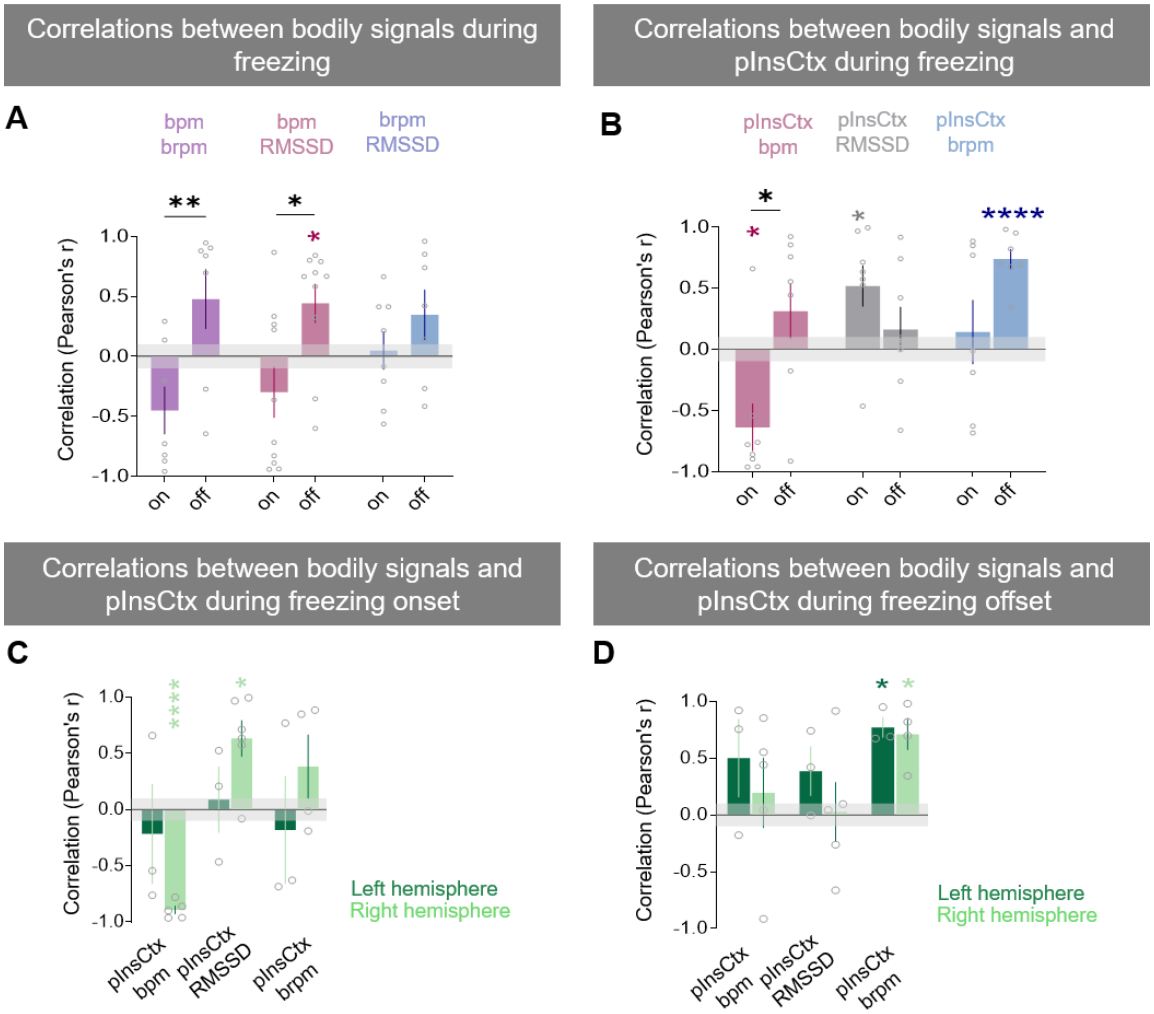

Fig. 20 **: Body-brain interactions differ between freezing onset and offset**
A) Pearson's correlations between bodily signals of breathing rate (brpm), heart rate (bpm), heart rate variability (RMSSD). Pearson's correlation bpm and RMSSD at freezing offset mean r=0.44, *p=0.02. All other interactions between the bodily signals at freezing onset and offset ns. Comparisons between the interactions of bodily signals at freezing onset and offset: bpm and brpm (n=7) **p=0.006; bpm and RMSSD (n=10) *p=0.03. brpm and RMSSD (n=7) ns.
B) Pearson's correlations between bodily signals (as in A) with pInsCtx; Pearson's correlations at freezing onsets: pInsCtx and bpm (n=8) mean r=-0.64 *p=0.01, pInsCtx and RMSSD (n=8) mean r =0.52 *p=0.02; Pearson's correlations at freezing offsets: pInsCtx and brpm (n=7) mean r=0.74 ****p<0.0001; All other interactions between the bodily signals and pInsCtx at freezing onset and offset: ns. Comparisons between the interactions of bodily signals with pInsCtx at freezing onset and offset: pInsCtx and bpm *p=0.02; pInsCtx and RMSSD ns, pInsCtx and brpm ns.
C) Pearson's correlations between pInsCtx activity (ΔF/F) bodily signals (as in A) at freezing onset in the right hemisphere (light green, n=5, right pInsCtx and brpm n=4) and left hemisphere (dark green, n=3). right pInsCtx and bpm mean r=0.89 ****p<0.0001. right pInsCtx and RMSSD mean r=0.76 ***p=0.0009. All other interactions as well as comparisons between hemispheres with unpaired t-tests were ns.

D) Pearson's correlations between pInsCtx activity bodily signals (as in A) at freezing onset in the right hemisphere (light green, n=5, right pInsCtx and brpm n=4) and left hemisphere (dark green, n=3). left pInsCtx and brpm mean r=0.77 *p<0.01. right pInsCtx and brpm mean r=0.71 *p=0.01. All other interactions as well as comparisons between hemispheres with unpaired t-tests were ns. Comparison between interactions at on- versus offset with paired t-tests. Averaged values show the mean, error bars show SEM. Horizontal grey bars between -0.1 and 0.1 indicate area in which the mean Pearson's r values indicate no correlation.

Since pInsCtx activity differed between the hemispheres during freezing compared to the time after freezing offset (*Fig. 19E*), I next explored possible hemispheric differences in interactions between the body and pInsCtx activity. To this end, correlation analyses were conducted on the left and right hemisphere groups, separately. Analyses revealed that during freezing offset, both hemispheres were strongly correlated with breathing rate and displayed no hemispheric differences (*Fig. 20D*). Interestingly, during freezing onset the right pInsCtx was highly anti-correlated with heart rate and strongly correlated with HRV while the left hemisphere showed no correlations with bodily signals (*Fig. 20C*). Remarkably, the pInsCtx hemisphere which displayed a strong correlation with heart rate during CS+ in fear learning was not the right but the left hemisphere (*Fig. 16*). This might suggest that the hemispheres of pInsCtx may have different roles during fear. It could be hypothesized that the left pInsCtx has its predominant role in the interaction with the body during fear learning (CS+ presentations), while the interaction of the right pInsCtx with the body is most crucial during the initiation of fear behaviour (freezing). However, with the present dataset this hypothesis cannot be tested and would require further experiments.

Overall, characterizations during freezing revealed that pInsCtx and the body are strongly interacting both at the beginning and at the end of freezing episodes. On one hand, at freezing onset, the strongest interaction can be found between the pInsCtx and cardiac measures. On the other hand, at freezing offset, breathing rate and pInsCtx as well as heart rate and heart rate variability exhibit the strongest interactions.

After the observation of significant interactions between pInsCtx and bodily signals during fear cues and fear behaviour, I next explored how distinct the signaling in the pInsCtx was during these processes compared to the brainstem region of the nucleus of the solitary tract (NTS).

3.1.4 Comparison between posterior insular cortex and nucleus of the solitary tract activity during fear and extinction conditioning

Characterization of the interaction between pInsCtx and the body during fear conditioning highlighted an emotion-state dependent modulation of the pInsCtx by cardiac and respiratory signals. Bodily signals first get relayed by the NTS before eventually reaching the pInsCtx via multi-synaptic pathways (*see chapter 1.2.4 Neuronal regulation of cardiorespiratory*

activity). At each of the steps in this pathway, bodily signals are processed and represented differently [108,114]. To compare how bodily signals are processed in the NTS compared to the pInsCtx, activity was recorded in both brain regions simultaneously during fear and extinction conditioning in a subset of animals (n=4, Fig. 21B). Since the NTS is a brain structure which stretches along the rostro-caudal axis, thus presenting several possible target sites for recordings[183], anterograde viral tracings from the pInsCtx were conducted to identify a recording site which would have the potential to be involved in the interaction between cardiac and respiratory signaling and pInsCtx activity. Interestingly, tracings consistently showed strong projections from the pInsCtx to the NTS, and especially its caudal parts (*Fig. 21A*). Furthermore, a study showed that fibers of lung, and heart innervating vagal sensory neurons can be found in the NTS [184]. Utilizing the knowledge obtained from the tracing experiment, as well as from literature, recordings of NTS activity were conducted in the caudal NTS at an anatomical location which has been shown to not only receive direct input from the pInsCtx but also the periphery, and compared to activity in the pInsCtx in fear and extinction learning.

As described in a previous chapter (*3.1.1*), during CS+ in fear learning, pInsCtx activity displayed significantly higher activity during the last compared to the first two CS+ (Fig. 21*C*). Simultaneous recordings of NTS activity on the other hand, was significantly higher during the first two CS+ than the last two CS+ in training (Fig. 21*D*). Moreover, NTS and pInsCtx activity during CS+ in training were neither correlated during the first two, the last two or all 5 CS+ presentations (*Fig. 21E, F*). Together these results demonstrate that NTS and pInsCtx activity are not reflective of similar processes during CS+ in fear learning. During CS+ in extinction learning (*see: chapter 3.1.2*), neither pInsCtx nor NTS activity differed compared to baseline (10 seconds preceding CS+ presentations) (*Fig. 21G, H*). Like in fear learning, pInsCtx and NTS activity were not correlated during CS+ in extinction (Fig. 21*E, F, I*). These results demonstrated that observed activity in pInsCtx during fear cues differed from activity in the NTS during both fear and extinction learning.

After no interactions between activity in these two brain regions were found during fear cues (CS+), I next assessed responses of neuronal activity during freezing. Comparisons of pInsCtx and NTS response at freezing onsets and offsets revealed no overall difference (Fig. 21*J*). Interestingly, however, a trend towards an increase of NTS after freezing onset was visible which went into the opposite direction of pInsCtx response (Fig. 21*J, left*). Finally, no correlation between NTS and pInsCtx activity during freezing onset or offset were found (Fig. 21*K*). Together, this data showed that not only during fear cues but also during freezing, NTS and pInsCtx activity appear to represent different processes.

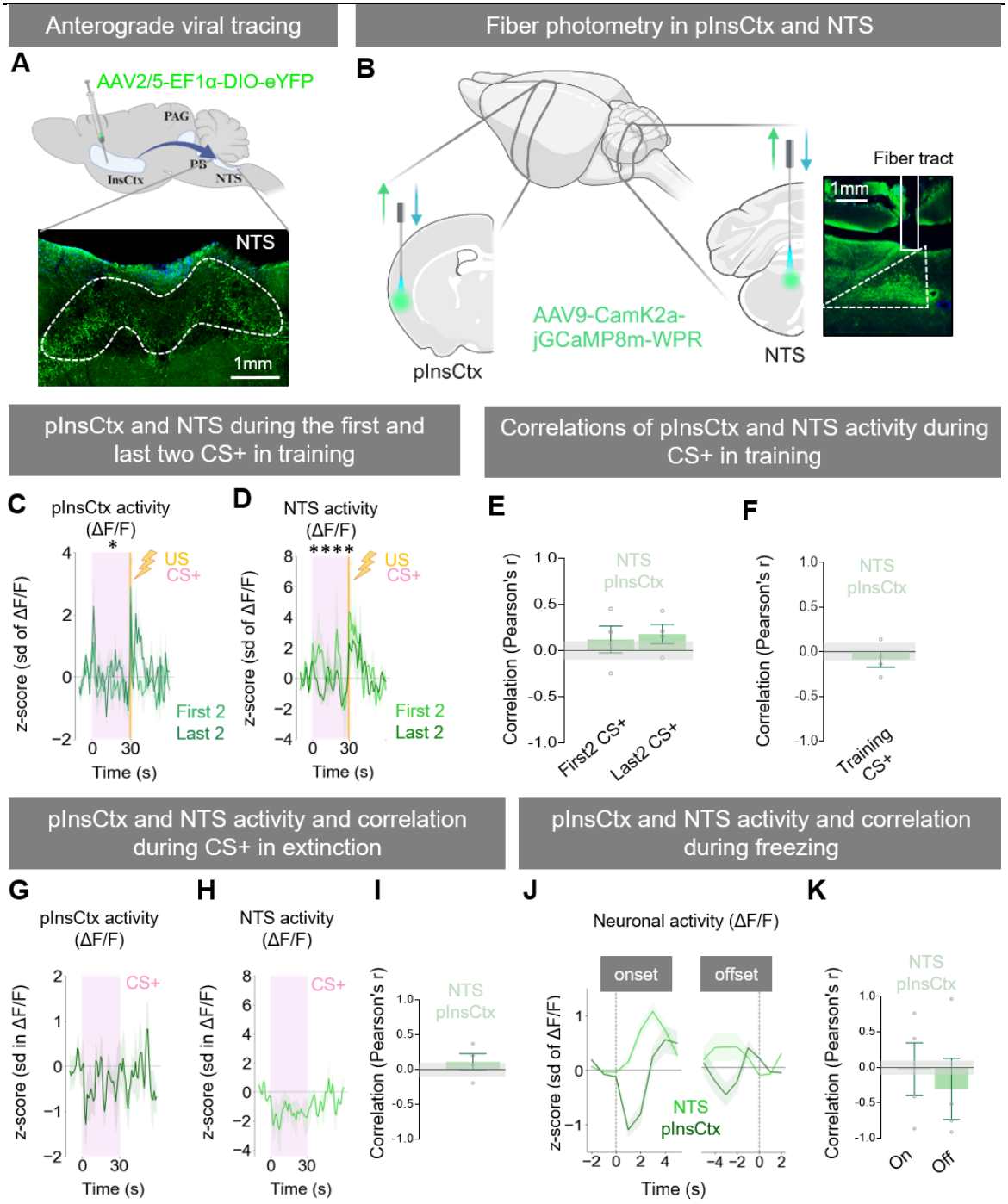

Fig. 21: **pInsCtx and NTS activity do not correlate during fear conditioning, extinction or freezing.**
A) Schematic of anterograde tracing (top); Fibers in the nucleus of the solitary tract (NTS) that receive direct input from CamK2a neurons in the pInsCtx. NTS location is indicated in white
B) Schematic of injection and implantation site in the pInsCtx and NTS for fiber photometry (left) and example of injection and implantation in the NTS, fiber placement is indicated in white (right).
C) Averaged pInsCtx activity (ΔF/F, n=9) during the first two (lighter color) and last two (darker color) CS+ presentations in training. Responses are z-scored to the 10 seconds of baseline before CS+ onset. Statistics: comparison of first two CS+ vs. last two CS+ with paired t-test *p=0.04
D) Averaged NTS activity (ΔF/F, n=4) during the first two (lighter color) and last two (darker color) CS+ presentations in training. Responses are z-scored to the 10 seconds of baseline before CS+ onset. Statistics: comparison of first two CS+ vs. last two CS+ with paired t-test ****p<0.0001

E) Pearson's correlation between NTS (n=4) and pInsCtx (n=4) activity during the first 2 CS+ (left) and last 2 CS+ (right) in training. One sample t-test ns.
F) Pearson's correlation between NTS (n=4) and pInsCtx (n=4) activity during all 5 CS+ in training. One sample t-test ns.
G) Averaged pInsCtx activity (ΔF/F, n=9) during all 8 CS+ presentations in extinction. Responses are z-scored to the 10 seconds of baseline before CS+ onset. Statistics: comparison of baseline vs. CS+ with paired t-test: ns.
H) Averaged NTS activity (ΔF/F, n=4) during all 8 CS+ presentations in extinction. Responses are z-scored to the 10 seconds of baseline before CS+ onset. Statistics: comparison of baseline vs. CS+ with paired t-test: ns.
I) Pearson's correlation between NTS (n=4) and pInsCtx (n=4) activity during all 8 CS+ in extinction. One sample t-test ns.
J left) Averaged responses of NTS (n=4) and pInsCtx (n=4) activity (ΔF/F) within the same animal at freezing onsets. Freezing episodes: length ≥ 5 seconds that were ≥ 3 seconds apart from other freezing episodes. Responses are z-scored to the 3 seconds of baseline before freezing. Statistics: comparison of pInsCtx activity during freezing vs. NTS activity during freezing with paired t-test ns.
J right) Averaged responses of NTS (n=4) and pInsCtx (n=4) activity (ΔF/F) within the same animal at freezing offsets. Freezing episodes: length ≥ 5 seconds that were ≥ 3 seconds apart from other freezing episodes. Responses are z-scored to the 3 seconds of post-baseline after freezing. Statistics: comparison of pInsCtx activity during freezing vs. NTS activity during freezing one sample t-test ns.
K) Pearson's correlation between NTS and pInsCtx activity during freezing onset (left) and freezing offset (right). One sample t-test ns.
Averaged values show the mean, shading and error bars show SEM. Vertical pink bars indicate the duration of CS+ presentations (30 seconds); yellow line and lightning bolt indicate time point of foot shock (US); horizontal grey bars between -0.1 and 0.1 indicate area in which the mean Pearson's r values indicate no correlation. pInsCtx: dark green, NTS: light green. A and B created with *BioRender*. Animal numbers: pInsCtx n=9, NTS n=4, pInsCtx in correlations and in J: n=4

Overall, results suggest that the neuronal activity observed in the pInsCtx and therefore its interactions with bodily signals, are not simply representative of lower order autonomic processes but might rather represent new properties and processes.

3.2 Interaction between neuronal and physiological signals during innate fear

Having observed how activity in the pInsCtx is modulated during fear and extinction learning and how its activity may be modulated by inputs from the body, I next explored how the insular cortex encodes innate fear-like states.

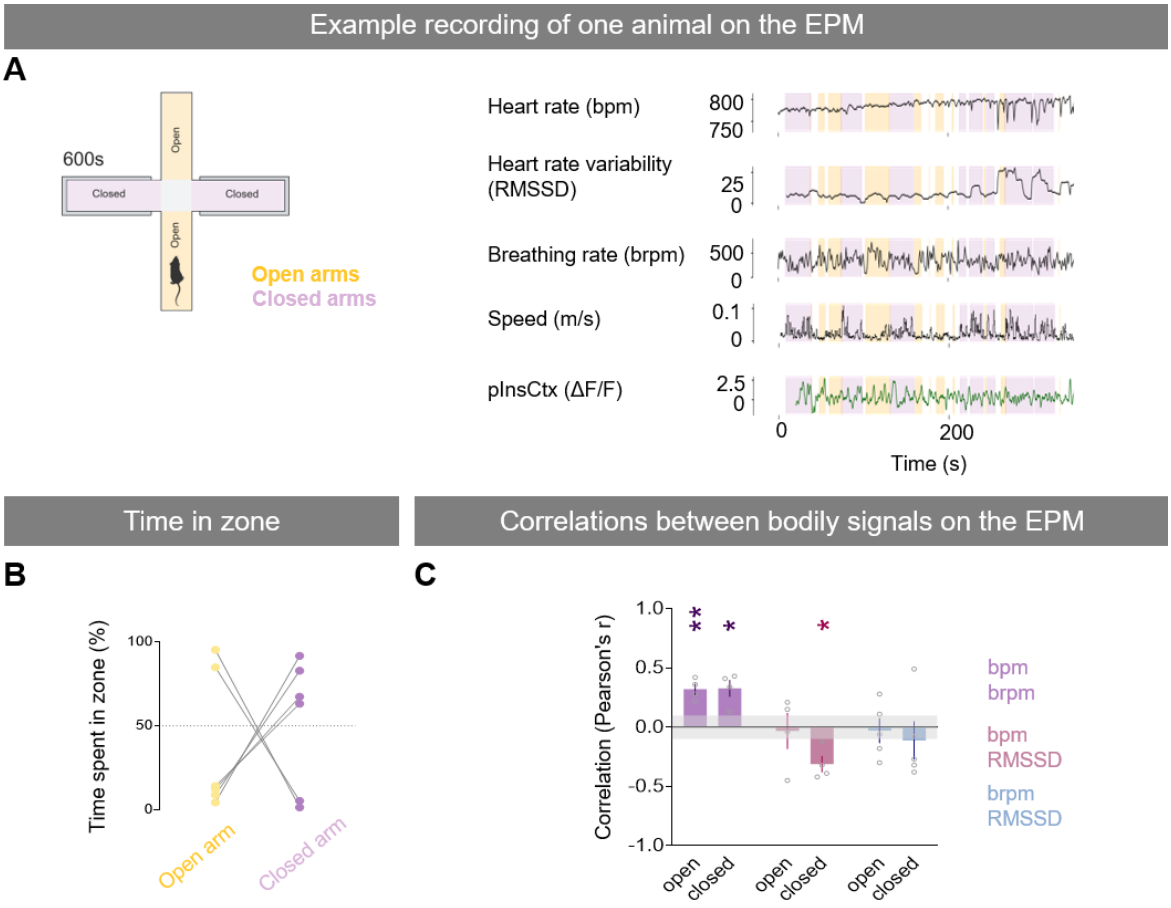

Fig. 22 **: Bodily signals and pInsCtx activity during innate fear.**
A) Schematic drawing of the elevated plus maze (EPM) (left, created with BioRender); example traces of the first 300 seconds on the EPM of one animal.
B) Percentage time spent in each zone (open arm in yellow, closed arm in violet) per animal. Statistics animals with a high time on open arms (n=2) vs. animals with a low time on open arms (n=4) unpaired t-test: ****p<0.0001
C) Pearson's correlations between bodily signals (breathing rate (brpm), heart rate (bpm), heart rate variability (RMSSD)) on the open arms (open) and closed arms (closed); Statistics: Pearson's correlation analyses were conducted per animal to obtain within-individual correlations (points represent correlations of different animals). Afterwards, one sampled t-tests were run to assess significance of individual correlations on a population level. Open arm: bpm and brpm mean r=0.32, **p=0.005; Closed arm: bpm and brpm mean r=0.33 *p=0.02, bpm and RMSSD mean r=-0.31, *p=0.02. All other interactions as well as comparisons between interactions on the open versus the closed arms with unpaired t-tests: ns. Averaged values show the mean, error bars show SEM. Horizontal grey bars between -0.1 and 0.1 indicate area in which the mean Pearson's r values indicate no correlation. Animal numbers: bpm: n=5, RMSSD: n=5, brpm: n=5, pInsCtx: n=5, speed: n=6; bpm-brpm: n=4, brpm-RMSSD: n=4, pInsCtx-bpm: n=4, pInsCtx-RMSSD: n=4, pInsCtx-brpm: n=4, bpm-RMSSD: n=5

To assess bodily and neuronal signals in an environment which gauges innate fear, animals were placed in the center of an elevated plus maze (EPM) five days after fear and extinction conditioning and were left to explore freely for 10 minutes (*Fig.* 22*A, left*). During this time, bodily signals, speed, and pInsCtx activity were recorded (*Fig.* 22*A, right*). Out of the six animals that were tested on the EPM, four spent more than 50% of the time on the closed arms, while two mice spent above 80% of the total time on the EPM on the open arms (*Fig.* 22*B*). Interestingly, although a significant difference in time spent on the open versus the closed arms was observed between the groups, there was no difference in bodily signals or pInsCtx in either of the arms between those groups. Furthermore, animals who spent more time on the open than the closed arm did neither consistently represent the highest nor lowest values of bodily signals or pInsCtx (*Suppl. Fig.* 5*A*). Therefore, data from all animals was analysed together. Overall, no significant differences between average bodily signals, pInsCtx activity or speed was found when comparing open and closed arms (*Suppl. Fig.* 5*A*).

On both, the open and the closed arms, heart rate and breathing rate were significantly correlated (*Fig.* 22*C*). This heart and breathing rate interaction has consistently been found in all previous characterizations. Observation of the positive interaction on both arms further highlighted that breathing and heart rate coupling seems to be stable and independent of internal state. Interestingly, a significant anti-correlation between heart rate and HRV was present in the closed arm but not in the open arm (*Fig.* 22*C*). Intriguingly, the only other times where heart rate and HRV were not anticorrelated, apart from times on the open arm, was during CS+ in training and during freezing (*Fig. 14, Fig. 20*). This suggests that cardiac signal interaction, or lack thereof, on the open arm may be similar to their interaction during fear learning and freezing. Thus, the decoupling of heart rate and HRV might be a useful read-out for fear-like states. Analysis of correlations between pInsCtx activity and bodily signals found no significant interactions on either of the arms (*Suppl. Fig.* 5*B*).

Given the differences in heart rate to HRV correlations in the open versus closed arm of the EPM, I next sought to investigate how bodily signals and insular activity changed at the transition points between the open and closed arms. Analyses aligned to the transitions between the two zones revealed that all recorded variables of breathing rate, heart rate, HRV, pInsCtx activity but also speed of locomotion, displayed changes in opposite directions for open arm → closed arm transitions versus closed arm → open arm transitions, suggesting opposite behavioral, bodily, and likely internal state changes (*Fig. 23A-E*). However, only the measures of speed, heart rate and pInsCtx activity differed significantly depending on zone change (*Fig. 23B, D, E*). In such, transitions from the exposed to the safe zone (open arm → closed arms) resulted in a decrease of both heart rate and pInsCtx

activity (*Fig. 23B, D*) as well as a bimodal change in speed, namely an initial short increase followed by a decrease of speed (*Fig. 23E*). Inversely, transitions into the exposed zone (closed arm → open arms) showed an overall increase in heart rate that started prior to the entry as well as a decrease in speed (*Fig. 23B, D, E*).Interestingly, HRV showed the same trends as heart rate for both transitions, without reaching significance (*p=0.06, Fig. 23C*).

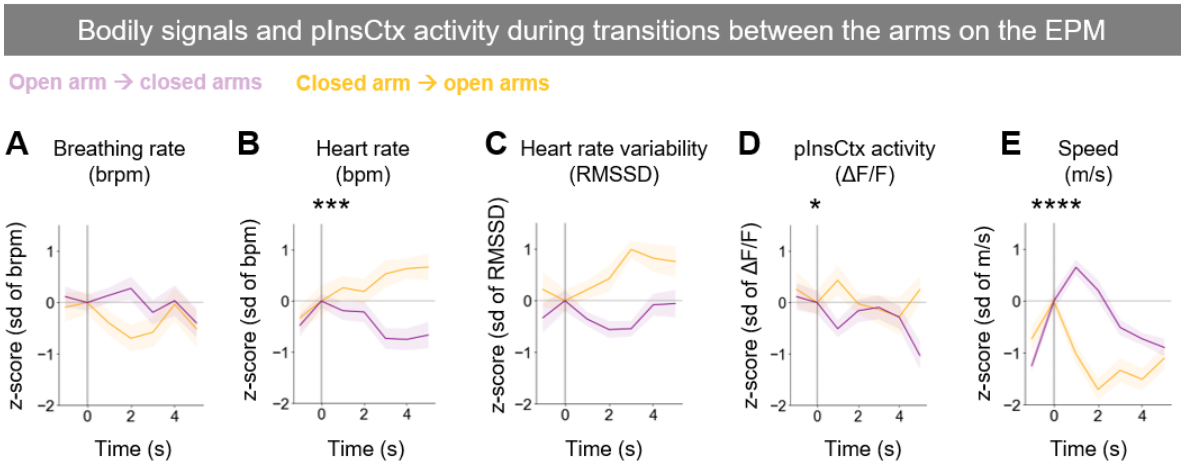

Fig. 23**: Bodily signals and pInsCtx activity during zone transitions.**
A - E: Bodily signals of breathing rate (brpm), heart rate (bpm), heart rate variability (RMSSD), and pInsCtx activity (ΔF/F) before and after transitions from one zone to the other (open arm → closed arm, violet, and closed arms → open arm, yellow); z-scored to whole trace and centered at 0 at timepoint of transition.
Statistics: Comparison between the dynamics of transitions to the open arm versus transitions to the closed arm: Mixed-effects analysis, Row Factor x Column Factor.
A) Breathing rate in brpm during arm transitions (n=5); ns.
B) Heart rate in bpm during arm transitions (n=5); ***p=0.0005.
C) Heart rate variability in RMSSD during arm transitions (n=5); p=0.06.
D) pInsCtx activity in ΔF/F during arm transitions (n=5); *p=0.03.
E) Speed in m/s during arm transitions (n=6); ****p<0.0001.
Averaged values show the mean, shading shows SEM.

Since transitions between zones were accompanied by dynamics that changed directionality, correlation analyses of signals during the time following the zone transition were conducted to investigate possible interactions between the different measures. Interestingly, this revealed a positive correlation between heart and breathing rate after entry of the closed arm but not after entry of the open arm (*Suppl. Fig.* 5*D*). Furthermore, no significant anticorrelation between heart rate and HRV was observed following either of the arm transitions, suggesting that transitions may evoke the fear-like state specific decoupling between heart rate and HRV (*Suppl. Fig.* 5*D*). Correlations between all other measures revealed no significant interactions (Suppl. Fig. 5D-F).

Overall, characterization of bodily signals and pInsCtx on the EPM suggest that the change of safety context (transition between closed and open arms) is an emotionally salient event, evoking stereotyped changes in heart rate, speed, and pInsCtx activity. Together these results suggest that changes in bodily signals and pInsCtx activity as well as their interactions, are part of stereotyped behavioral patterns that accompany different internal states. Thus, I next sought to probe possible predictive values of the interplay between pInsCtx and the body.

3.3 Predictive value of brain-body interactions

After characterization of the different body-brain interactions, the question if these interactions and variables could be leveraged to predict future emotion states and behaviour was addressed.

3.3.1 Directionality of neuronal and physiological signals

First, directionality of the different measures was investigated utilizing Multivariate Granger causality (MVGC), to provide a hypothesis about the direction of information flow between the body and the pInsCtx. Granger causality (GC) is a useful tool to elucidate whether a possible driver signal can improve forecasting of a target signal. This logic can further be applied to multiple variables. In this study, GC was calculated per individual for all of the CS+ presentations per stage of fear conditioning and subsequently averaged to represent the population mean (*Fig. 24A*, *chapter 2.7.2* Multivariate Granger Causality). Results showed a consistent lag of one second for all of the significant feedback interactions, meaning the driving signal was useful for predicting how the target signal would look in the following second (*Fig. 24B-D*). Bidirectional relationships arose whenever both the driver and target signals held equally useful information in predicting each other. Since during recall and retrieval, CS+ was only presented twice and directionality analysis requires a minimum amount of data, only habituation, training and extinction were assessed.

Analyses revealed different brain-body interactions dependent on the stage of fear conditioning (*Fig. 24B-D*). However, two bodily interactions remained unchanged throughout habituation, fear, and extinction learning. First, heart rate and HRV displayed a strong mutual influence on each other, irrespective of the emotional context during the aforementioned stages of fear and extinction conditioning. Secondly, breathing rate consistently had a strong influence on heart rate throughout all stages (*Fig. 24B-D*). Interestingly, most stage-dependent differences were observed in the interaction between pInsCtx and bodily signals.

Breathing rate and pInsCtx interactions displayed different interactions between all three stages. While during CS+ presentations in habituation, pInsCtx and breathing rate showed a strong bidirectional influence (Fig. 24B), during training, pInsCtx activity predicted breathing rate unidirectionally (Fig. 24C). Strikingly, during extinction this relationship was reversed such that breathing unidirectionally predicted pInsCtx activity (Fig. 24D). Together, these results suggest that breathing rate and pInsCtx interactions not only change between neutral and emotional states, but further change depending on the type of emotional learning.

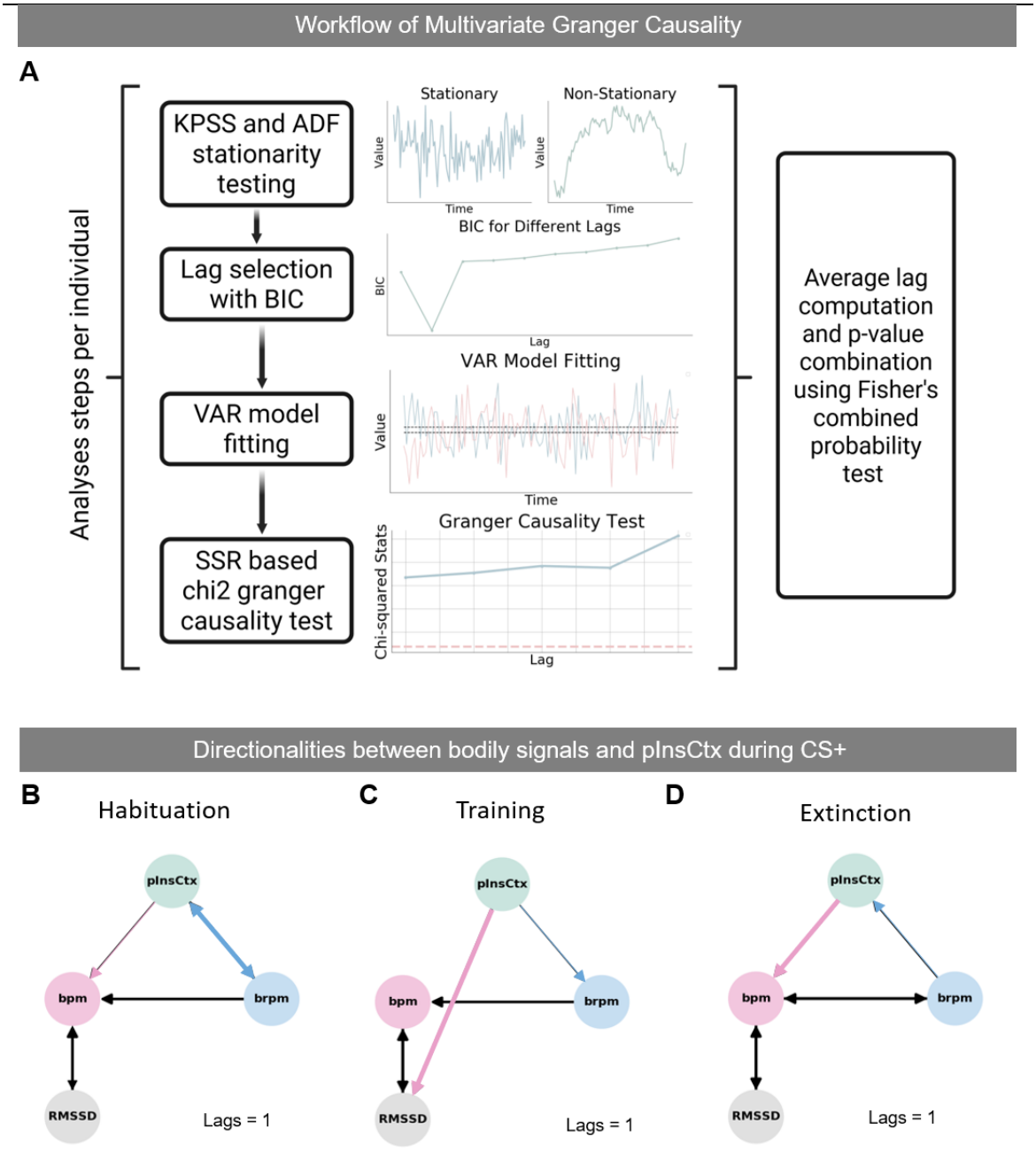

Fig. 24**: Multivariate Granger causality**
A) Workflow describing the steps that were applied to data from individual animals and subsequent combination of all results; Abbreviations: KPSS test: Kwiatkowski–Phillips–Schmidt–Shin test, ADF test: Augmented Dickey-Fuller test, BIC: Bayesian information criterion, VAR model: Vector Auto-regression model, SSR: Sum of Squared Residuals,
B-D) Multivariate Granger causality (MVGC) of pInsCtx activity (ΔF/F, green), heart rate (bpm, pink), breathing rate (brpm, blue) and heart rate variability (RMSSD, grey) during CS+ presentations in habituation, training and extinction (left to right). Arrows indicate direction of influence, thickness of lines indicate p-value: thin lines *p<0.05, thick lines **p<0.01. All significant lags=1; n=6. Black arrows indicate unchanged interactions, blue arrows indicates changed pInsCtx-brpm interaction, pink arrows indicates changed cardiac-pInsCtx interaction.

Interactions between cardiac measures and pInsCtx activity differed between training and the other two stages, namely habituation and extinction. During CS+ presentations in habituation and extinction, pInsCtx displayed a unidirectional influence on heart rate and no interaction between pInsCtx and RMSSD (*Fig. 24B, D*). Intriguingly, during CS+ in training, pInsCtx displayed a strong unidirectional influence on HRV, whilst no interaction with heart rate was observed (*Fig. 24C*).

Overall, pInsCtx and body interactions resembled each other during habituation and extinction while showing a more distinct interaction during fear training. Interestingly, the only time pInsCtx had a direct influence on HRV was during CS+ in training, which was the only time these measures were correlated. Therefore, MVGC suggests that the correlation between pInsCtx and HRV may be a top-down process.

3.3.2 Prediction of fear extinction success

Although the cohort did not display a significant reduction in time freezing, during extinction retrieval compared to fear recall (*chapter 3.1.1, Fig. 13B*), differences between individual extinction learning performance were observable. To quantify individual extinction success, an extinction performance index, based on freezing in recall and freezing in extinction (*for formula see: Methods chapter 2.7.3*), was calculated for each animal. Interestingly, this index revealed two significantly different groups (*Fig. 25A, B*). While one group showed a positive extinction performance, which was characterized by a reduction in time spent freezing after extinction, the other group failed to show a change in time spent freezing (*Fig. 25B*).

Splitting animals into these groups revealed that there was no difference between freezing in any of the fear conditioning stages apart from the recall phase in which freezing was significantly higher in the group with a positive extinction performance (mean 71%) compared to the group of animals exhibiting a negative extinction performance (mean 33%) (*Fig. 25B*).

Since freezing to CS+ in recall is used as a measure of fear learning success, I hypothesized that bodily signals and pInsCtx activity may already show differences during training, which are not reflected in behaviour, but would ultimately predict extinction performance. Intriguingly, even though the extinction performance index is calculated based on freezing during CS+ in stages taking place after training, bodily responses to the CS+ onset differed significantly between the groups during fear learning (*Fig. 25C*). Responses to CS+ were significantly higher in both bodily signals and pInsCtx activity of animals that would later display a negative extinction performance (*Fig. 25C*). Moreover, no significant difference

was observed in responses to the shock, indicating that perception of the aversive unconditioned stimulus did not differ between the groups. These analyses suggested that different bodily processes as well as different reactivity of pInsCtx towards fear cues in training could be useful in predicting extinction performance. Since bodily signals and pInsCtx exhibited significant interaction during fear and extinction learning, I next investigated whether the interactions between pInsCtx activity and bodily signals differed between the different extinction performance groups.

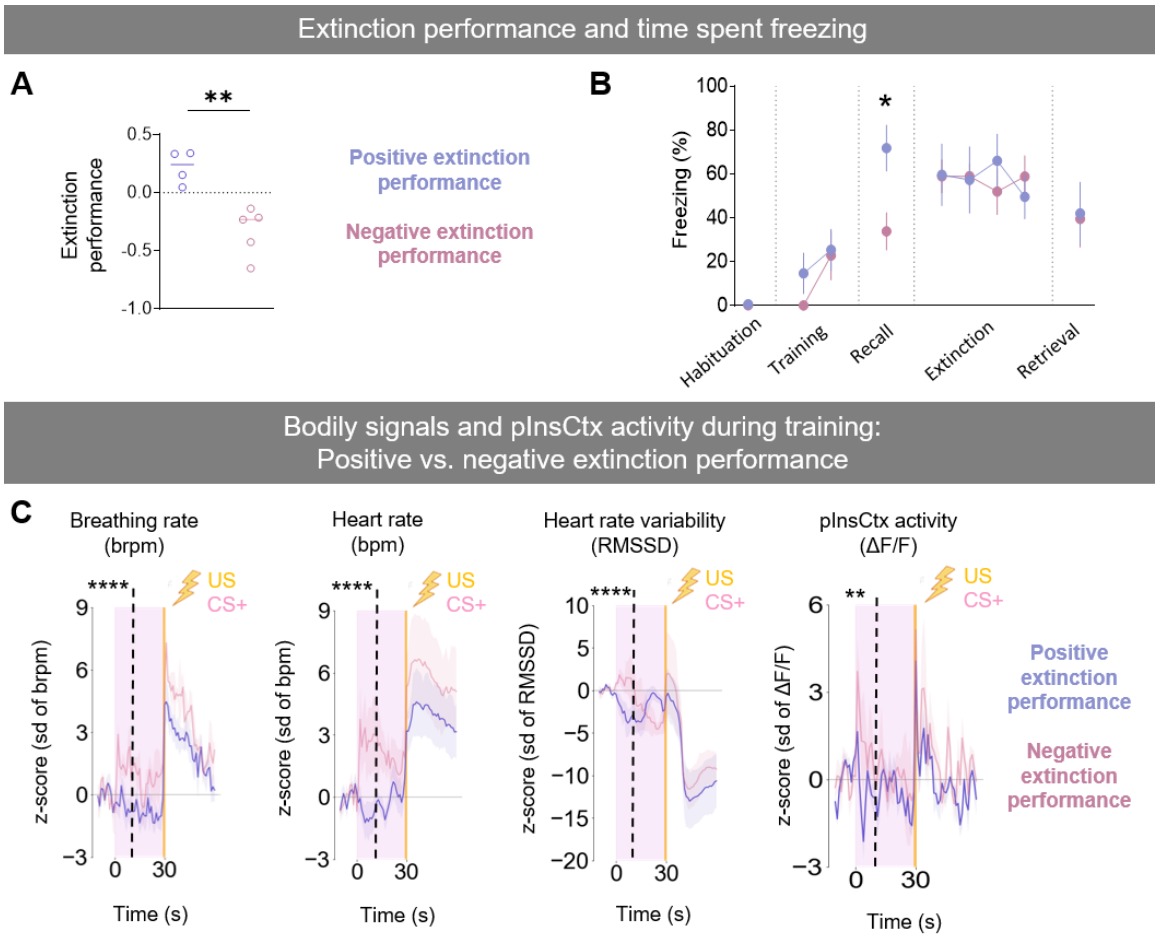

Fig. 25: **Individual extinction performance**
A) Comparison of extinction performance groups (positive, blue, n=4 vs. negative, pink, n=5), unpaired t-test **p=0.0028
B) Percentage of time spent freezing to CS+ presentations. Each data point represents two pooled CS+ presentations. Paired t-test of Positive (blue, n=4) vs. negative (pink, n=5) extinction performance during Recall *p=0.0234
C) Averaged responses of bodily signals of breathing rate (brpm), heart rate (bpm), heart rate variability (RMSSD) and pInsCtx activity (ΔF/F) of positive (blue, n=4) vs. negative extinction performance (pink, n=5) animals to the first 10 seconds of all 5 CS+ presentations in training compared to baseline (10 seconds preceding CS+); unpaired t-test: brpm ****p<0.0001, bpm ****p<0.0001, RMSSD ****p<0.0001, pInsCtx **p=0.0027. Vertical pink bars indicate the duration of CS+ presentations (30 seconds); yellow line and lightning bolt indicate time point of foot shock
Averaged values show the mean, shading and error bars show SEM.

Analyses of body-pInsCtx interactions after grouping of the animals based on positive or negative extinction performance, revealed that the correlation between pInsCtx activity and breathing rate during CS+ presentations in recall was lower in animals with positive extinction performance compared to those with a negative extinction performance (*Fig.* 26*A*). Interestingly, this dynamic was in the opposite direction of freezing differences, which showed animals with a positive extinction performance to display more time freezing (*Fig.* 26*A*). However, both cardiac measures of heart rate and HRV did not show differences in correlation with pInsCtx between groups during CS+ in recall (*Fig.* 26*B*). Intriguingly, correlation of extinction performance with the interaction of breathing rate with pInsCtx activity revealed negative linear relationship (*Fig.* 26*C*). Together these results may suggest that the interaction between breathing rate and pInsCtx contribute to the extinction performance of an individual. However, since during recall, extinction performance groups differed by the amount of time animals spent freezing, the difference in pInsCtx interaction with breathing rate could also be explained by freezing.

Utilizing MVGC over the entire recall session further highlights two differences in pInsCtx-body interactions between the extinction performance groups (*Fig.* 26*D*), while interactions of bodily signals with each other were consistent between the groups. Strikingly, the group with a negative extinction performance demonstrated a mutual influence between pInsCtx and breathing rate as well as a unidirectional influence of HRV on pInsCtx (*Fig.* 26*D right*) which were not found in the group with a positive extinction performance (*Fig.* 26*D left*). Overall, analyses highlighted that the interaction between pInsCtx and breathing rate during recall might hold value in predicting extinction performance.

However, since the extinction performance index is derived from the amount of time animals spent freezing, a possible explanation for group differences may be a different reaction by individuals during freezing per se. To evaluate this possibility, I analyzed responses of bodily signals and pInsCtx activity during freezing for both groups separately (*Fig.* 27*A-D*). This analysis revealed no difference in heart rate, HRV or pInsCtx activity in response to freezing onset. However, animals with a positive extinction performance showed a significantly lower breathing rate during freezing than animals with a negative extinction performance (*Fig.* 27*A*). Interestingly, before freezing offset, breathing rate was no longer lower in animals with a positive extinction performance (*Fig.* 27*E*), instead, heart rate and HRV was significantly higher in this group compared to the animals with a negative extinction performance (*Fig.* 27*F, G*). However, comparison between interactions of breathing rate with pInsCtx activity at freezing offset, showed a trend towards a higher correlation in the group with a negative extinction performance (*Suppl. Fig. 6B).* All other correlations of

the pInsCtx with the body during freezing onset and offset did not differ between extinction performance groups (*Suppl. Fig. 6*). These results suggest that bodily processes during freezing may differ between individuals and influence the fear extinction success, while highlighting the relationship between breathing rate and pInsCtx.

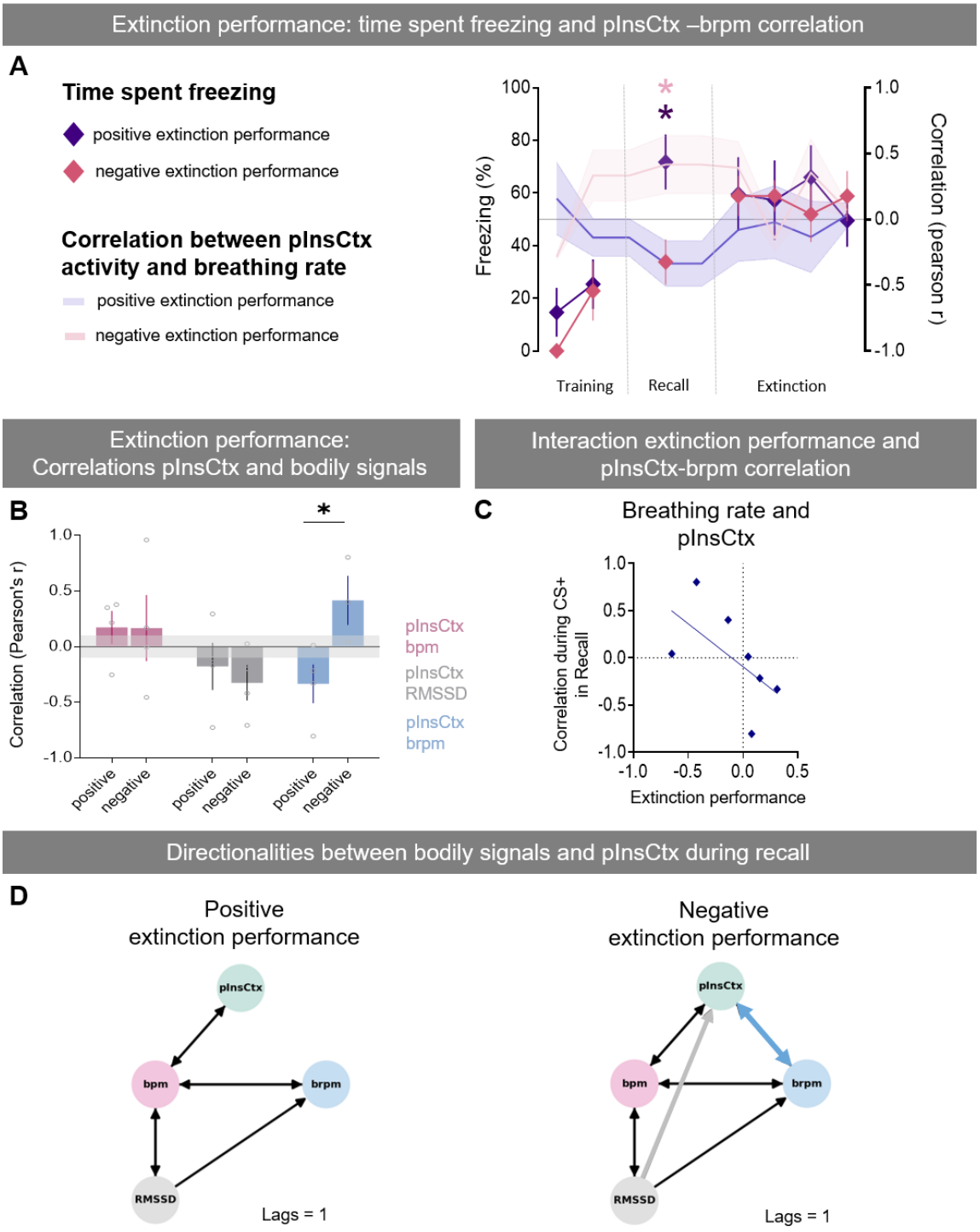

Fig. 26**: Interaction between breathing rate and pInsCtx activity differs between extinction performance groups.**

A) Diamonds: Percentage of time spent freezing to CS presentations; unpaired t-test. Recall (light blue Asterix) *p=0.02; for more details see *Fig. 25*. Lines: correlation between breathing rate (in brpm) and pInsCtx (in ΔF/F) during the pooled CS+ presentations shown with the diamonds; unpaired t-test in Recall (pink Asterix) *p=0.04
B) Pearson's correlations between bodily signals of heart rate (bpm), heart rate variability (RMSSD) and breathing rate (brpm), and pInsCtx (ΔF/F); Paired t-test: pInsCtx and brpm positive vs. negative *p=0.04. Horizontal grey bars between -0.1 and 0.1 indicate area in which the mean Pearson's r values indicate no correlation.
C) Pearson's correlation between extinction performance and pInsCtx correlation with brpm in recall; Simple linear regression r^2=0.36 p=0.16
D) MVGC of pInsCtx activity (ΔF/F, green), heart rate (bpm, pink), breathing rate (brpm, blue) and heart rate variability (RMSSD, grey) over the entire recall session of animals with a positive extinction performance (left) and animals with a negative extinction performance (right); Arrows indicate direction of influence, thickness of lines indicate p-value: thin lines *p<0.05, thick lines **p<0.01. All significant lags=1. Black arrows indicate unchanged interactions, blue arrow indicates changed pInsCtx-brpm interaction, grey arrow indicates changed HRV-pInsCtx interaction. Animal numbers: positive extinction performance n=4, negative extinction performance n=5; pInsCtx-bpm and pInsCtx-RMSSD: each group n=4; pInsCtx-brpm: positive extinction performance n=4, negative extinction performance n=3. Positive extinction performance: blue, negative extinction performance: pink. Averaged values show the mean, shading and error bars show SEM.

Taken together, extinction performance analyses revealed four distinct differences between the groups. First, animals exhibiting negative extinction performance displayed stronger bodily reactions and pInsCtx activity increases to the fear cue (CS+) in training (*Fig. 25C*). Second, during recall, animals with a negative extinction performance displayed stronger coupling of breathing rate and pInsCtx as well as less time spent freezing (*Fig.* 26*A*). Third, those animals further showed a bidirectional influence between pInsCtx and breathing rate as well as a direct influence of HRV on pInsCtx during recall, which was not the case in animals with a positive extinction performance (*Fig.* 26*C*). Fourth, during freezing, animals with a negative extinction performance displayed a higher breathing rate at freezing onset and a higher correlation with pInsCtx at freezing offset (*Fig.* 27*A, Suppl. Fig. 6B*). In conclusion, the data suggests that the interaction between pInsCtx activity and breathing rate may play a crucial role in extinction performance.

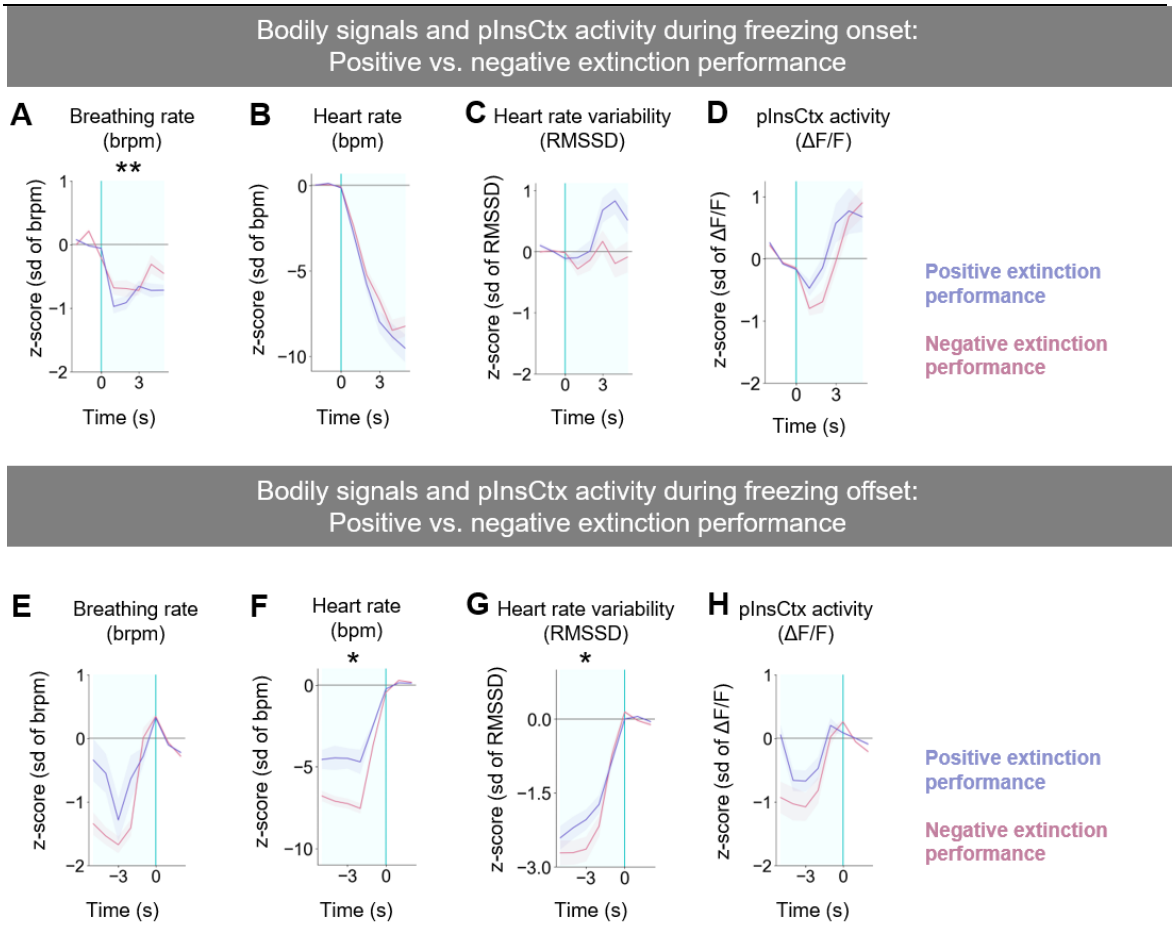

Fig. 27: **Breathing rate differs during freezing dependent on extinction performance**
A - D: Averaged responses of bodily signals of breathing rate (brpm), heart rate (bpm), heart rate variability (RMSSD), and pInsCtx activity of animals with a positive extinction performance (n=4, blue) and a negative extinction performance (n=5, pink) at freezing onsets. Freezing episodes: length ≥ 5 seconds that were ≥ 3 seconds apart from other freezing episodes. Responses are z-scored to the 3 seconds of baseline before freezing. Statistics: unpaired t-tests between positive and negative extinction performance of time after freezing onset.
A) Response of breathing rate, positive vs. negative extinction performance **p=0.008.
B) Response of heart rate, positive vs. negative extinction performance ns.
C) Response of heart rate variability, positive vs. negative extinction performance ns.
D) Response of pInsCtx activity, positive vs. negative extinction performance ns.
E-F: Averaged responses of bodily signals of breathing rate (brpm), heart rate (bpm), heart rate variability (RMSSD), and pInsCtx activity of animals with a positive extinction performance (n=4, blue) and a negative extinction performance (n=5, pink) at freezing offsets. Freezing episodes: length ≥ 5 seconds that were ≥ 3 seconds apart from other freezing episodes. Responses are z-scored to the 3 seconds of post-baseline after freezing. Statistics: comparison of post-baseline (3 seconds after freezing) vs. freezing with paired t-test.
E) Response of breathing rate, positive vs. negative extinction performance ns.
F) Response of heart rate, positive vs. negative extinction performance*p=0.01.
G) Response of heart rate variability, positive vs. negative extinction performance *p=0.02.
H) Response of pInsCtx activity, positive vs. negative extinction performance ns.
Averaged values show the mean, shading show SEM. Light blue shaded area in all panels indicates timespan of freezing.

4. Discussion

In this study, brain-body interactions of female mice were characterized during emotional behaviour. More precisely, breathing rate, heart rate, HRV, pInsCtx activity, their interactions with each other, and the directionality thereof were investigated during conditioned as well as innate fear. Furthermore, pInsCtx activity during fear cues and fear behaviour was compared with activity in the downstream brainstem region of the NTS. Finally, bodily signals and pInsCtx activity as well as their interactions were probed for their potential in predicting extinction learning success.

4.1 Activity in posterior insular cortex reflects different dynamics than in nucleus of the solitary tract

The brainstem is known to be predominantly involved in the regulation of vital bodily functions[185,186]. To explore how activity in the pInsCtx was distinct from downstream activity in the brainstem, recordings of neuronal activity were simultaneously obtained in the pInsCtx and the NTS.

Overall, no correlations between pInsCtx and NTS activity could be found when investigating responses to fear cues and freezing. However, NTS activity showed an increased response to fear cues in training and a trend of an increase at freezing onset. Interestingly, the NTS activity increase during CS+ in fear learning was stronger at the beginning of the training session than at the end, which might indicate a role of the NTS in processing of saliency of the stimulus. Nevertheless, as characterization of NTS responses in fear conditioning was not the main objective of this study, the sample size was low. Thus, no speculations about its contribution to fear conditioning can be made from this data. Nonetheless, these findings suggest an additional but different role of the NTS in fear conditioning. Which matches with previous studies which have suggested an involvement of the NTS in fear and stress[187–189]. However, the exact role of the NTS in fear is still unclear and requires further investigation. Taken together, it can however be concluded that activity in the pInsCtx reflects processes that differ from the ones computed in the NTS.

4.2 The relationship between the body and the posterior insular cortex is fear state dependent

Characterizations of bodily signals and pInsCtx activity in undisturbed settings revealed no meaningful interactions between the pInsCtx and the body, regardless of prior experiences (before versus after fear and extinction conditioning). Furthermore, when testing innate fear, no differences of bodily or pInsCtx signals were observed when comparing the exposed with the safe zone. Nonetheless, pInsCtx activity, heart rate and speed responded differently to zone transitions. Interestingly, the different responses of speed and heart rate to the zone change confirmed findings from Signoret-Genest et al. (2023)[42]. In their study, they proposed that heart rate changes into opposite directions to zone switches reflected internal state changes. The present study additionally showed that pInsCtx activity displays a decrease in activity upon entry of the safe zone and thus appears to be reflective of these zone or state changes. It has to be noted that Signoret-Genest et al. (2023)[42] found a lower average heart rate in the safe zone compared to the exposed zone. While in the present study, no differences were found, this may however be due to the relatively sample size in this study (*n=5*) which was lower than that in the study of Signoret-Genest et al. (2023)[42] (n=20). Together, in neutral conditions as well as during innate fear, no interactions between pInsCtx activity were found. This might suggest that during emotionally neutral conditions, cardiac and respiratory signals do not strongly influence pInsCtx activity.

Measurements during fear and extinction conditioning, on the other hand, elucidated how bodily and pInsCtx signals are not only altered during responses to fear cues and behaviour, but also displayed an overarching interaction change between different fear stages. Characterization of fear learning revealed a significant change in pInsCtx activity and HRV in response to CS+ at the end of learning compared to the beginning, indicating that both measures were reflective of emotional association of the tone with the shock. This was further supported by a significant correlation between pInsCtx and HRV. Directionality analyses further suggested that this change may be top-down controlled, since pInsCtx shows a direct predictive influence on HRV. Moreover, this influence was exclusively found during training, highlighting body-brain interaction as distinctly different compared to habituation and extinction.

Presentation of CS+ in fear extinction, on the other hand, had more widespread effects on the body. All bodily signals and pInsCtx showed a change from responses to CS+ at the beginning of extinction as compared to at the end. This indicated a change which was not

reflected by time spent freezing. It further highlighted the potential of bodily and pInsCtx signals in reflecting processes during fear extinction that go beyond freezing detection. These findings are in line with previous literature, showing that physiological measures in rodent research hold additional information about fear[78,190]. Thus, this study highlights the importance of using multiple readout dimensions, if feasible, to gain a comprehensive understanding of state changes.

In addition to cue-elicited pInsCtx-body interactions, freezing elicited changes were found as well. Studies have shown specific and stereotyped responses and interactions between the periphery and the brain during freezing, including a freezing-induced bradycardic response as well as a decrease breathing rate[42,88,89,91,134,191]. In line with these previously reported changes, initial decreases in heart rate and breathing rate in response to freezing onset were found in this study. Overall, decreases of heart and respiratory rates along with increase of heart rate variability suggests a predominant activity of the parasympathetic nervous system in response to freezing onset. These results support studies which highlight a dominance of the parasympathetic nervous system during the fear response of freezing[192–195]. Furthermore, results showed that interaction of bodily signals with each other but also with pInsCtx activity differed between the beginning of a freezing episode compared to the end of a freezing episode. At the start of freezing, cardiac signals were most strongly interacting with pInsCtx activity, whereas at the end of freezing a significant interaction between pInsCtx and respiratory rate was present. Overall, freezing elicited strong pInsCtx-body interactions, highlighting an important role of the pInsCtx in processing of bodily signals during fear.

These alterations further exhibited more intricate dynamics that are explored in more detail in the subchapter of lateralization. Moreover, directionality analyses additionally suggested that these changes underlie general dynamics between the body and pInsCtx that change depending on internal fear state. Livneh and Andermann (*2021*)[196] hypothesized that fast insular cortex activity changes may reflect prediction of future bodily states, while differences in activity over longer timescales may represent current physiological states. The current findings, showing short term interaction changes during CS+ and freezing, as well as long term interactions changes between fear states, support the concept that pInsCtx and body interactions play important roles on both timescales.

4.3 Heart rate variability is interacting strongly with the posterior insular cortex during fear

The bodily signal that showed especially pronounced interactions with the pInsCtx was the HRV. HRV has been linked to emotional arousal, emotion regulation as well as interoceptive sensitivity and accuracy in humans[197–199]. Additionally, studies with patients suffering from anxiety disorders showed a decreased HRV compared to healthy controls[200–203]. Likewise, in rodent studies, low HRV has been shown to be indicative of high fear[204–206].
Most insights on the relationship between HRV and higher order brain regions have been derived from imaging and lesion studies in humans. Functional connectivity studies in humans revealed associations of HRV with several regions including the prefrontal cortex, the amygdala, and insular cortex[207–210]. Additionally, lesion studies found that heart rate variability was affected by damage to the insula, resulting in a decreased HRV [211,212], thus indicating the insular cortex as in important region in the regulation of HRV.

This study now provided evidence of a tight link between HRV and pInsCtx in mice. As discussed in the previous sub-chapter (*4.2*), HRV and pInsCtx showed a likely top-down controlled, strong correlation during fear training. Furthermore, this interaction was the most pronounced distinguishing factor between fear learning and extinction learning. Lastly, an influence of HRV on pInsCtx activity during fear recall was only detectable in animals that extinguished fear poorly. These results may suggest that the role of the pInsCtx in interoception during fear learning is not to simply to reflect autonomic processes but rather represent an internal fear state.

4.4 Indications of emotional lateralization in the posterior insular cortex

Among other findings, this study highlighted a lateralization of the pInsCtx during fear. Studies about hemispheric differences have traditionally been conducted in humans, since for a long time, it was assumed that lateralization is a uniquely human feature. This has since been refuted[68,213]. It is, therefore, of high relevance to combine findings in humans about lateralization with findings in rodents to aid in the increase of translational value of research. Currently, several theories about lateralization of emotions exist[214,215]. On the one hand, there is evidence from lesion and interoception studies highlighting a dominance of activity in the right hemisphere during interoceptive tasks[129,179,216–218]. On the other hand,

there is also evidence for more nuanced interactions by studies showing associations between emotional valence and dominance of hemispheres[180,219–221]. Findings in animal research show similar variability in observations. For example, even though hemispheric differences in the amygdala have been found to be involved in memory, stress, and anxiety the exact dynamics are still unclear[222–227]. Overall, the most consistent finding in both humans and several different animal species is a predominant involvement of the right hemisphere in sympathetic functions[66–68,228,229].

This study adds to the existing body of literature by suggesting a lateralization in the mouse posterior insular cortex during fear. More precisely, the results showed how fear learning evoked a lateralization in the pInsCtx. The left hemisphere showed an increased activity in response to the CS+ after learning to associate this tone with the foot shock, whereas the right hemisphere only showed a small response. Furthermore, the left hemisphere showed a strong correlation with heart rate during CS+ which was not present in the right hemisphere. Together, these findings suggest separate roles of the hemispheres during fear acquisition with a dominant involvement of the left hemisphere. In extinction learning only a weak lateralization of pInsCtx activity was detectable with the left hemisphere showing a lower activity during CS+, US, and postCS+ in the beginning of the session. These results may suggest that the hemispheric difference is most pertinent during fear learning. Interestingly, during freezing onset the right hemisphere showed significant interactions with the body, while the left hemisphere did not. These results indicate that fear acquisition and fear expression may be processed in different hemispheres of the pInsCtx. However, to test this hypothesis and to comprehensively tie these results into existing findings and theories, a more targeted investigation of the hemispheric differences in pInsCtx during fear are required.

4.5 Extinction success

Based on the extinction performance index, which had been introduced in our laboratory[134], two distinct groups were found. Regarding their behaviour, the only difference was observable during fear recall which was reflected in time freezing to CS+. Interestingly, bodily signals and pInsCtx activity responses to the CS+ during training differed depending on extinction performance. This is especially noteworthy since there was no difference in freezing behaviour observed during this stage. Moreover, responses during fear training were not considered in the calculation of the extinction performance index. These findings

suggest that pInsCtx activity and bodily signals provide information about internal processes which may predict subsequent emotional states. In addition, the different amount of time spent freezing during fear recall was accompanied by different pInsCtx and breathing rate interactions. Results revealed that high freezing levels and a negative relationship of respiration and pInsCtx during fear recall were both indicative of a positive extinction performance. Furthermore, breathing rate at the beginning of freezing and cardiac signals at the end of freezing differed between the groups, indicating that not only the amount but also the autonomic processes during freezing play a role in extinction success.

A previous study from this laboratory showed evidence of interactions between pInsCtx and the body during fear extinction[134]. The study reported that pInsCtx activity was the driving factor determining extinction success. It additionally highlighted that heart rate and pInsCtx responses to freezing did not differ. Results described in the current study not only corroborated these earlier findings but also added to them, by showing that breathing rate displayed a significantly different response to freezing depending on extinction success.

Together these findings suggest that the influence of the pInsCtx on respiration could be an important feature of fear extinction success. However, further dissections of the relationship between respiration and pInsCtx are required to probe this systematically. An outlook on this is given in chapter *4.7 Future directions*.

4.6 Limitations of the study

Historically, female animals were oftentimes excluded from studies, citing hormonal changes throughout their estrous cycle as a main source of concern[14]. In this study, which was performed with female animals, estrous cycles of the mice were not tracked. However, human studies, which have focused on a possible relationship between fear learning and the menstrual phase, have not found differences in behaviour during fear acquisition dependent on estradiol levels[230–232]. These findings are in accordance with results from rodents[21,23]. On the other hand, both human and rodent studies point towards beneficial effects of low estradiol levels during extinction training on extinction success[23,233,234]. Overall, since these studies indicate that while tracking estradiol levels would have certainly added another dimension, it was not a necessity for meaningful analysis and interpretation of the data acquired in the present study.

Next, it must be noted that the subject numbers were relatively low in some of the subgroups which makes analyses sensitive to statistical errors, especially type II errors, resulting in false negatives[235,236]. Therefore, even though effect sizes were sufficient to elucidate strong interactions, increasing the number of animals would help to additionally clarify robustness of trends that were observed in this study.

Lastly, the EPM test for assessing innate fear was conducted only 5 days after conclusion of fear and extinction conditioning. Since no full extinction of fear was achieved, it cannot be ruled out that this previous experience had an influence on the mice's behaviour or bodily or neuronal signaling on the EPM. Therefore, an addition of innate fear tests without previous fear experiences may provide further insights.

4.7 Future directions

A first suggestion would be to extend the characterizations of pInsCtx-body interactions during emotional behaviour to include male mice. This addition would be valuable for a more comprehensive understanding of differences and similarities between sexes. There are some key points that might suggest differences between the sexes. First, sex differences in physiological measures of heart rate, heart rate variability, and breathing rate have been found in both humans and rodents[237–241]. Concerning rodent studies, females typically have a higher breathing rate, heart rate, and heart rate variability[242–245]. Additionally, links between physiological interactions and behaviour have shown sex differences in both humans and rodents[246]. Moreover, women and men show a different prevalence for the development and severity of anxiety disorders[11–13]. Therefore, it would be beneficial to explore potential differences in their responses of bodily signals and pInsCtx activity to fear.

Furthermore, a targeted investigation of lateralization effects of fear in the pInsCtx would be a compelling next step. Starting with a corroboration of existing findings, this could further be extended to investigate whether pInsCtx lateralization interacts with other brain regions involved in fear learning. As a first target for such experiments, I suggest the amygdala-pInsCtx interaction, for several reasons. The amygdala is not only known for its prominent role in fear and anxiety[247–249], but has also been shown to exhibit lateralization[250,251] as well as strong connections with the insular cortex[121,252]. Therefore, the amygdala would present a promising initial interaction site to probe.

Finally, after highlighting the important interaction between breathing rate and pInsCtx during freezing offset and during fear recall, another future direction would be to systematically probe this relationship, applying manipulation techniques like peripheral or central optogenetics. This direction of further research could be divided into two parts.

First, disturbance of pInsCtx and breathing coupling during freezing by means of optogenetic manipulations, could clarify the role of this interaction. Previous research has shown that breathing at a 4Hz rhythm occurs during freezing, which is further closely interacting with oscillations in various brain regions[88,89,91]. Furthermore, studies have found important roles of the periaqueductal gray[42] and dorsomedial prefrontal cortex[88] in maintenance of freezing in combination with bodily signals. As this study indicated a strong interplay between the pInsCtx and breathing rate at the end of freezing, it could be hypothesized that pInsCtx signaling contributes to the termination of freezing behaviour alongside the aforementioned regions.

Second, the predictive value of breathing rate and pInsCtx interaction during fear recall could potentially be utilized to change outcomes of extinction training on an individual basis. In humans, breathing exercises or meditation techniques have been shown to improve overall well-being but also help in reduction of anxiety[253–255]. Artificial induction or disturbance of pInsCtx and breathing coupling during fear recall, using peripheral optogenetics, could aid in the understanding of underlying mechanisms.

Considering all findings, I propose that heart rate variability and breathing rate interactions with the posterior insular cortex comprise a fear state dependent synergy, which can be leveraged to predict and potentially alter fear extinction success in females.

References

1. Tovote P, Fadok JP, Lüthi A. Neuronal circuits for fear and anxiety. *Nat Rev Neurosci*. 2015;16(6):317-331. doi:10.1038/nrn3945
2. Benun J, Lewis C, Siegel M. Fears and phobias. *Pediatr Rev*. 2008;29(7):250-251. doi:10.1542/pir.29-7-250
3. Davis M, Walker DL, Miles L, Grillon C. Phasic vs sustained fear in rats and humans: Role of the extended amygdala in fear vs anxiety. *Neuropsychopharmacology*. 2010;35(1):105-135. doi:10.1038/npp.2009.109
4. Grupe DW, Nitschke JB. Uncertainty and anticipation in anxiety: An integrated neurobiological and psychological perspective. *Nat Rev Neurosci*. 2013;14(7):488-501. doi:10.1038/nrn3524
5. Chen S, Huang W, Zhang M, et al. Dynamic changes and future trend predictions of the global burden of anxiety disorders: analysis of 204 countries and regions from 1990 to 2021 and the impact of the COVID-19 pandemic. *eClinicalMedicine*. 2025;79(12):103014. doi:10.1016/j.eclinm.2024.103014
6. Osborn TL, Wasanga CM, Ndetei DM. *Transforming Mental Health for All*.; 2022. doi:10.1136/bmj.o1593
7. Mangolini VI, Andrade LH, Lotufo-Neto F, Wang YP. Treatment of anxiety disorders in clinical practice: A critical overview of recent systematic evidence. *Clinics*. 2019;74(11):e1316. doi:10.6061/clinics/2019/e1316
8. Olatunji BO, Cisler JM, Deacon BJ. Efficacy of cognitive behavioral therapy for anxiety disorders: A review of meta-analytic findings. *Psychiatr Clin North Am*. 2010;33(3):557-577. doi:10.1016/j.psc.2010.04.002
9. Knowles KA, Tolin DF. Mechanisms of Action in Exposure Therapy. *Curr Psychiatry Rep*. 2022;24(12):861-869. doi:10.1007/s11920-022-01391-8
10. Calhoon GG, Tye KM. Resolving the neural circuits of anxiety. *Nat Neurosci*. 2015;18(10):1394-1404. doi:10.1038/nn.4101
11. Javaid SF, Hashim IJ, Hashim MJ, Stip E, Samad MA, Ahbabi A Al. Epidemiology of anxiety disorders: global burden and sociodemographic associations. *Middle East Curr Psychiatry*. 2023;30(1). doi:10.1186/s43045-023-00315-3
12. McLean CP, Asnaani A, Litz BT, Hofmann SG. Gender differences in anxiety disorders: Prevalence, course of illness, comorbidity and burden of illness. *J Psychiatr Res*. 2011;45(8):1027-1035. doi:10.1016/j.jpsychires.2011.03.006
13. Breslau N. Epidemiologic studies of trauma, posttraumatic stress disorder, and other psychiatric disorders. *Can J Psychiatry*. 2002;47(10):923-929. doi:10.1177/070674370204701003
14. Zucker I, Prendergast BJ, Beery AK. Pervasive Neglect of Sex Differences in Biomedical Research. *Cold Spring Harb Perspect Med*. 2022;14(4):1-17. doi:10.1101/cshperspect.a039156
15. Becker JB, Prendergast BJ, Liang JW. Female rats are not more variable than male rats: A meta-analysis of neuroscience studies. *Biol Sex Differ*. 2016;7(1):1-7. doi:10.1186/s13293-016-0087-5
16. Prendergast BJ, Onishi KG, Zucker I. Female mice liberated for inclusion in neuroscience and biomedical research. *Neurosci Biobehav Rev*. 2014;40:1-5. doi:10.1016/j.neubiorev.2014.01.001
17. Baran SE, Armstrong CE, Niren DC, Hanna JJ, Conrad D. NIH Public Access. 2010;91(3):323-332. doi:10.1016/j.nlm.2008.11.005.Chronic

18. Day HLL, Stevenson CW. The neurobiological basis of sex differences in learned fear and its inhibition. *Eur J Neurosci*. 2020;52(1):2466-2486. doi:10.1111/ejn.14602

19. Borkar CD, Dorofeikova M, Le QSE, et al. Sex differences in behavioral responses during a conditioned flight paradigm. *Behav Brain Res*. 2020;389(March):112623. doi:10.1016/j.bbr.2020.112623

20. Clark JW, Drummond SPA, Hoyer D, Jacobson LH. Sex differences in mouse models of fear inhibition: Fear extinction, safety learning, and fear–safety discrimination. *Br J Pharmacol*. 2019;176(21):4149-4158. doi:10.1111/bph.14600

21. Blume SR, Freedberg M, Vantrease JE, et al. Sex- And estrus-dependent differences in rat basolateral amygdala. *J Neurosci*. 2017;37(44):10567-10586. doi:10.1523/JNEUROSCI.0758-17.2017

22. Voulo ME, Parsons RG. Response-specific sex difference in the retention of fear extinction. *Learn Mem*. 2017;24(6):245-251. doi:10.1101/lm.045641.117

23. Gruene TM, Roberts E, Thomas V, Ronzio A, Shansky RM. Sex-specific neuroanatomical correlates of fear expression in prefrontal-amygdala circuits. *Biol Psychiatry*. 2015;78(3):186-193. doi:10.1016/j.biopsych.2014.11.014

24. Bauer EP. Sex differences in fear responses: Neural circuits. *Neuropharmacology*. 2023;222(July 2022):109298. doi:10.1016/j.neuropharm.2022.109298

25. Krueger JN, Sangha S. On the basis of sex: Differences in safety discrimination vs. conditioned inhibition. *Behav Brain Res*. 2021;400(December 2020):113024. doi:10.1016/j.bbr.2020.113024

26. Rattel JA, Wegerer M, Miedl SF, et al. Peritraumatic unconditioned and conditioned responding explains sex differences in intrusions after analogue trauma. *Behav Res Ther*. 2019;116(July 2018):19-29. doi:10.1016/j.brat.2019.01.009

27. Tovote P, Fadok JP, Lüthi A. Neuronal circuits for fear and anxiety. *Nat Rev Neurosci*. 2015;16(6):317-331. doi:10.1038/nrn3945

28. Wilensky AE, Schafe GE, Kristensen MP, LeDoux JE. Rethinking the fear circuit: The central nucleus of the amygdala is required for the acquisition, consolidation, and expression of pavlovian fear conditioning. *J Neurosci*. 2006;26(48):12387-12396. doi:10.1523/JNEUROSCI.4316-06.2006

29. Ledoux JE, Ledoux JE. Emotion Circuits in the Brain. *Annu Rev Neurosci*. 2000;23:155-184.

30. Janak PH, Tye KM, Sciences B, Sciences C. From circuits to behaviour in the amygdala : Nature : Nature Publishing Group. *NatureCom*. 2015;517(7534):284-292. doi:10.1038/nature14188.From

31. Herry C, Trifilieff P, Micheau J, Lüthi A, Mons N. Extinction of auditory fear conditioning requires MAPK/ERK activation in the basolateral amygdala. *Eur J Neurosci*. 2006;24(1):261-269. doi:10.1111/j.1460-9568.2006.04893.x

32. Kwon JT, Nakajima R, Kim HS, Jeong Y, Augustine GJ, Han JH. Optogenetic activation of presynaptic inputs in lateral amygdala forms associative fear memory. *Learn Mem*. 2014;21(11):627-633. doi:10.1101/lm.035816.114

33. Krabbe S, Paradiso E, d'Aquin S, et al. Adaptive disinhibitory gating by VIP interneurons permits associative learning. *Nat Neurosci*. 2019;22(11):1834-1843. doi:10.1038/s41593-019-0508-y

34. LeDoux JE, Iwata J, Cicchetti P, Reis DJ. Different projections of the central amygdaloid nucleus mediate autonomic and behavioral correlates of conditioned fear. *J Neurosci*. 1988;8(7):2517-2529. doi:10.1523/jneurosci.08-07-02517.1988

35. Ressler RL, Maren S. Synaptic encoding of fear memories in the amygdala. *Curr Opin Neurobiol*. 2019;54:54-59. doi:10.1016/j.conb.2018.08.012

36. Johansen JP, Hamanaka H, Monfils MH, et al. Optical activation of lateral amygdala pyramidal cells instructs associative fear learning. *Proc Natl Acad Sci U S A*. 2010;107(28):12692-12697. doi:10.1073/pnas.1002418107

37. Paré D, Quirk GJ, Ledoux JE. New vistas on amygdala networks in conditioned fear. *J Neurophysiol*. 2004;92(1):1-9. doi:10.1152/jn.00153.2004

38. Giustino TF, Maren S. The role of the medial prefrontal cortex in the conditioning and extinction of fear. *Front Behav Neurosci*. 2015;9(NOVEMBER):1-20. doi:10.3389/fnbeh.2015.00298

39. Chaitoff KA, Toner F, Tedesco A, Maher TJ, Ally A. Effects of inducible nitric oxide synthase blockade within the periaqueductal gray on cardiovascular responses during mechanical, heat, and cold nociception. *Neurol Sci*. 2012;33(1):69-78. doi:10.1007/s10072-011-0661-x

40. Deng H, Xiao X, Wang Z. Periaqueductal gray neuronal activities underlie different aspects of defensive behaviors. *J Neurosci*. 2016;36(29):7580-7588. doi:10.1523/JNEUROSCI.4425-15.2016

41. Back FP, Carobrez AP. Periaqueductal gray glutamatergic, cannabinoid and vanilloid receptor interplay in defensive behavior and aversive memory formation. *Neuropharmacology*. 2018;135:399-411. doi:10.1016/j.neuropharm.2018.03.032

42. Signoret-Genest J, Schukraft N, L. Reis S, Segebarth D, Deisseroth K, Tovote P. Integrated cardio-behavioral responses to threat define defensive states. *Nat Neurosci*. 2023;26(3):447-457. doi:10.1038/s41593-022-01252-w

43. Fanselow MS, Dong HW. Are the Dorsal and Ventral Hippocampus Functionally Distinct Structures? *Neuron*. 2010;65(1):7-19. doi:10.1016/j.neuron.2009.11.031

44. Xu C, Krabbe S, Gründemann J, et al. Distinct Hippocampal Pathways Mediate Dissociable Roles of Context in Memory Retrieval. *Cell*. 2016;167(4):961-972.e16. doi:10.1016/j.cell.2016.09.051

45. Courtin J, Bienvenu TCM, Einarsson EÖ, Herry C. Medial prefrontal cortex neuronal circuits in fear behavior. *Neuroscience*. 2013;240:219-242. doi:10.1016/j.neuroscience.2013.03.001

46. Cho JH, Deisseroth K, Bolshakov VY. Synaptic encoding of fear extinction in mPFC-amygdala circuits. *Neuron*. 2013;80(6):1491-1507. doi:10.1016/j.neuron.2013.09.025

47. Etkin A, Wager TD. Functional neuroimaging of anxiety: A meta-ana lysis of emotional processing in PTSD, social anxiety disorder, and specific phobia. *Am J Psychiatry*. 2007;164(10):1476-1488. doi:10.1176/appi.ajp.2007.07030504

48. Nummenmaa L, Glerean E, Hari R, Hietanen JK. Bodily maps of emotions. *Proc Natl Acad Sci U S A*. 2014;111(2):646-651. doi:10.1073/pnas.1321664111

49. Ashhad S, Kam K, Del Negro CA, Feldman JL. Breathing Rhythm and Pattern and Their Influence on Emotion. *Annu Rev Neurosci*. 2022;45:223-247. doi:10.1146/annurev-neuro-090121-014424

50. Daubenmier J, Sze J, Kerr CE, Kemeny M, Mehling W. Follow your breath. *Psychophysiology*. 2013;50(8):777-789. doi:10.1111/psyp.12057.Follow

51. Gibson J. Mindfulness, Interoception, and the Body: A Contemporary Perspective. *Front Psychol*. 2019;10(September). doi:10.3389/fpsyg.2019.02012

52. Maleki A, Ravanbakhsh M, Saadat M, Bargard MS, Latifi SM. Effect of breathing exercises on respiratory indices and anxiety level in individuals with generalized anxiety disorder: a randomized double-blind clinical trial. *J Phys Ther Sci*. 2022;34(4):247-251. doi:10.1589/jpts.34.247

53. Chalmers JA, Quintana DS, Abbott MJA, Kemp AH. Anxiety disorders are associated with reduced heart rate variability: A meta-analysis. *Front Psychiatry*. 2014;5(JUL):1-11. doi:10.3389/fpsyt.2014.00080

54. Beauchaine TP, Thayer JF. Heart rate variability as a transdiagnostic biomarker of psychopathology. *Int J Psychophysiol*. 2015;98(2):338-350. doi:10.1016/j.ijpsycho.2015.08.004

55. Fagioli S, Watanabe DK, Koenig J, et al. Heart Rate Variability Predicts Therapy Outcome in Anxiety Disorders: The Role of Inhibitory Learning. *Appl Psychophysiol Biofeedback*.

Published online 2025. doi:10.1007/s10484-025-09686-1

56. Steimer T. The biology of fear- and anxiety-related behaviors. *Dialogues Clin Neurosci*. 2002;4(3):231-249. doi:10.31887/dcns.2002.4.3/tsteimer

57. AM Roest, PhD1, P de Jonge, PhD1, C Lim, MSc2, DJ Stein, MD, PhD3, A Al-Hamzawi, MD4, J Alonso, MD, DrPH5, C Benjet, PhD6, R Bruffaerts, PhD7, B Bunting, PhD8, JM Caldas-deAlmeida, MD, PhD9, M Ciutan, MD10, G de Girolamo, MD11, C Hu, MD, PhD12, D Levinson P. Fear and distress disorders as predictors of heart disease: a temporal perspective. *Physiol Behav*. 2017;176(3):139-148. doi:10.1002/hep.30150.Ductular

58. Emdin CA, Odutayo A, Wong CX, Tran J, Hsiao AJ, Hunn BHM. Meta-Analysis of Anxiety as a Risk Factor for Cardiovascular Disease. *Am J Cardiol*. 2016;118(4):511-519. doi:10.1016/j.amjcard.2016.05.041

59. Wilhelm FH, Gevirtz R, Roth WT. Respiratory dysregulation in anxiety, functional cardiac, and pain disorders: Assessment, phenomenology, and treatment. *Behav Modif*. 2001;25(4):513-545. doi:10.1177/0145445501254003

60. Karami N, Kazeminia M, Karami A, Salimi Y, Ziapour A, Janjani P. Global prevalence of depression, anxiety, and stress in cardiac patients: A systematic review and meta-analysis. *J Affect Disord*. 2023;324(January 2023):175-189. doi:10.1016/j.jad.2022.12.055

61. Hynninen KMJ, Breitve MH, Wiborg AB, Pallesen S, Nordhus IH. Psychological characteristics of patients with chronic obstructive pulmonary disease: A review. *J Psychosom Res*. 2005;59(6):429-443. doi:10.1016/j.jpsychores.2005.04.007

62. Jaenig W. *Neurosciences - From Molecule to Behavior: A University Textbook*.; 2013. doi:10.1007/978-3-642-10769-6

63. Sternini C. Organization of the peripheral nervous system: Autonomic and sensory ganglia. *J Investig Dermatology Symp Proc*. 1997;2(1):1-7. doi:10.1038/jidsymp.1997.2

64. Guyton AC, Hall JE, D P. *Of Medical of Medical*.

65. Koopman FA, Stoof SP, Straub RH, Van Maanen MA, Vervoordeldonk MJ, Tak PP. Restoring the balance of the autonomic nervous system as an innovative approach to the treatment of rheumatoid arthritis. *Mol Med*. 2011;17(9-10):937-948. doi:10.2119/molmed.2011.00065

66. Dono F, Evangelista G, Frazzini V, et al. Interictal Heart Rate Variability Analysis Reveals Lateralization of Cardiac Autonomic Control in Temporal Lobe Epilepsy. *Front Neurol*. 2020;11(August):1-12. doi:10.3389/fneur.2020.00842

67. Critchley HD, Elliott R, Mathias CJ, Dolan RJ. Neural activity relating to generation and representation of galvanic skin conductance responses: A functional magnetic resonance imaging study. *J Neurosci*. 2000;20(8):3033-3040. doi:10.1523/jneurosci.20-08-03033.2000

68. Gainotti G. The difficult integration between human and animal studies on emotional lateralization: A perspective article. *Brain Sci*. 2021;11(8). doi:10.3390/brainsci11080975

69. Gehrmann J, Hammer PE, Maguire CT, Wakimoto H, Triedman JK, Berul CI. Phenotypic screening for heart rate variability in the mouse. *Am J Physiol - Hear Circ Physiol*. 2000;279(2 48-2):733-740. doi:10.1152/ajpheart.2000.279.2.h733

70. Georgakopoulos D, Kass DA. Minimal force-frequency modulation of inotropy and relaxation of in situ murine heart. *J Physiol*. 2001;534(2):535-545. doi:10.1111/j.1469-7793.2001.00535.x

71. Turner D, Kang C, Mesirca P, et al. Electrophysiological and Molecular Mechanisms of Sinoatrial Node Mechanosensitivity. *Front Cardiovasc Med*. 2021;8(August). doi:10.3389/fcvm.2021.662410

72. Shaffer F, Ginsberg JP. An Overview of Heart Rate Variability Metrics and Norms. *Front Public Heal*. 2017;5(September):1-17. doi:10.3389/fpubh.2017.00258

73. Malik M, John Camm A, Thomas Bigger J, et al. Heart rate variability: Standards of measurement, physiological interpretation, and clinical use. *Circulation*. 1996;93(5):1043-1065. doi:10.1161/01.cir.93.5.1043

74. Thireau J, Zhang BL, Poisson D, Babuty D. Heart rate variability in mice: A theoretical and practical guide. *Exp Physiol*. 2008;93(1):83-94. doi:10.1113/expphysiol.2007.040733

75. DeGiorgio CM, Miller P, Meymandi S, et al. RMSSD, a measure of vagus-mediated heart rate variability, is associated with risk factors for SUDEP: The SUDEP-7 Inventory. *Epilepsy Behav*. 2010;19(1):78-81. doi:10.1016/j.yebeh.2010.06.011

76. Peabody JE, Ryznar R, Ziesmann MT, Gillman L. A Systematic Review of Heart Rate Variability as a Measure of Stress in Medical Professionals. *Cureus*. 2023;15(1):1-11. doi:10.7759/cureus.34345

77. Gullett N, Zajkowska Z, Walsh A, Harper R, Mondelli V. Heart rate variability (HRV) as a way to understand associations between the autonomic nervous system (ANS) and affective states: A critical review of the literature. *Int J Psychophysiol*. 2023;192(August):35-42. doi:10.1016/j.ijpsycho.2023.08.001

78. Liu J, Wei W, Kuang H, Zhao F, Tsien JZ. Changes in Heart Rate Variability Are Associated with Expression of Short-Term and Long-Term Contextual and Cued Fear Memories. *PLoS One*. 2013;8(5):1-14. doi:10.1371/journal.pone.0063590

79. Pizzo E, Berrettoni S, Kaul R, et al. Heart Rate Variability Reveals Altered Autonomic Regulation in Response to Myocardial Infarction in Experimental Animals. *Front Cardiovasc Med*. 2022;9(May):1-15. doi:10.3389/fcvm.2022.843144

80. Lakin R, Guzman C, Izaddoustdar F, Polidovitch N, Goodman JM, Backx PH. Changes in heart rate and its regulation by the autonomic nervous system do not differ between forced and voluntary exercise in mice. *Front Physiol*. 2018;9(JUL):1-14. doi:10.3389/fphys.2018.00841

81. Card JW, Carey MA, Bradbury JA, et al. Gender Differences in Murine Airway Responsiveness and Lipopolysaccharide-Induced Inflammation. *J Immunol*. 2006;177(1):621-630. doi:10.4049/jimmunol.177.1.621

82. Hainsworth R. Ventricular and Coronary Receptors. Published online 1995:157-174.

83. Ito J, Roy S, Liu Y, et al. Whisker barrel cortex delta oscillations and gamma power in the awake mouse are linked to respiration. *Nat Commun*. 2014;5:1-10. doi:10.1038/ncomms4572

84. Heck DH, McAfee SS, Liu Y, et al. Breathing as a fundamental rhythm of brain function. *Front Neural Circuits*. 2017;10(January):1-8. doi:10.3389/fncir.2016.00115

85. Tort ABL, Brankačk J, Draguhn A. Respiration-Entrained Brain Rhythms Are Global but Often Overlooked. *Trends Neurosci*. 2018;41(4):186-197. doi:10.1016/j.tins.2018.01.007

86. Tort ABL, Ponsel S, Jessberger J, Yanovsky Y, Brankačk J, Draguhn A. Parallel detection of theta and respiration-coupled oscillations throughout the mouse brain. *Sci Rep*. 2018;8(1):1-14. doi:10.1038/s41598-018-24629-z

87. Moberly AH, Schreck M, Bhattarai JP, Zweifel LS, Luo W, Ma M. Olfactory inputs modulate respiration-related rhythmic activity in the prefrontal cortex and freezing behavior. *Nat Commun*. 2018;9(1). doi:10.1038/s41467-018-03988-1

88. Bagur S, Lefort JM, Lacroix MM, et al. Breathing-driven prefrontal oscillations regulate maintenance of conditioned-fear evoked freezing independently of initiation. *Nat Commun*. 2021;12(1):1-15. doi:10.1038/s41467-021-22798-6

89. Karalis N, Sirota A. Breathing coordinates cortico-hippocampal dynamics in mice during offline states. *Nat Commun*. 2022;13(1):1-20. doi:10.1038/s41467-022-28090-5

90. Karalis N, Dejean C, Chaudun F, et al. 4-Hz oscillations synchronize prefrontal-amygdala circuits during fear behavior. *Nat Neurosci*. 2016;19(4):605-612. doi:10.1038/nn.4251

91. Ozawa M, Davis P, Ni J, Maguire J, Papouin T, Reijmers L. Experience-dependent resonance in amygdalo-cortical circuits supports fear memory retrieval following extinction. *Nat Commun*. 2020;11(1). doi:10.1038/s41467-020-18199-w

92. Schreck MR, Zhuang L, Janke E, et al. State-dependent olfactory processing in freely behaving mice. *Cell Rep*. 2022;38(9):1-31. doi:10.1016/j.celrep.2022.110450

93. Ruffoli R, Giorgi FS, Pizzanelli C, Murri L, Paparelli A, Fornai F. The chemical neuroanatomy of vagus nerve stimulation. *J Chem Neuroanat*. 2011;42(4):288-296. doi:10.1016/j.jchemneu.2010.12.002

94. Gallager DW, Pert A. Afferents to brain stem nuclei (brain stem raphe, nucleus reticularis pontis caudalis and nucleus gigantocellularis) in the rat as demonstrated by microiontophoretically applied horseradish peroxidase. *Brain Res*. 1978;144(2):257-275. doi:10.1016/0006-8993(78)90153-1

95. Steriade M, McCarley RW. Afferent and Efferent Connections of Brainstem and Forebrain Modulatory Systems. *Brain Control Wakefulness Sleep*. Published online 2007:55-138. doi:10.1007/0-387-26270-9_3

96. Cutsforth-Gregory JK, Benarroch EE. Nucleus of the solitary tract, medullary reflexes, and clinical implications. *Neurology*. 2017;88(12):1187-1196. doi:10.1212/WNL.0000000000003751

97. Huang TX, Wang S, Ran C. Interoceptive processing in the nucleus of the solitary tract. *Curr Opin Neurobiol*. 2025;93:103021. doi:10.1016/j.conb.2025.103021

98. Palkovits M, Záborszky L. Neuroanatomy of Central Cardiovascular Control. Nucleus Tractus Solitarii: Afferent and Efferent Neuronal Connections in Relation to the Baroreceptor Reflex Arc. *Prog Brain Res*. 1977;47(C):9-34. doi:10.1016/S0079-6123(08)62709-0

99. Breit S, Kupferberg A, Rogler G, Hasler G. Vagus nerve as modulator of the brain-gut axis in psychiatric and inflammatory disorders. *Front Psychiatry*. 2018;9(MAR). doi:10.3389/fpsyt.2018.00044

100. Aicher SA, Kurucz OS, Reis DJ, Milner TA. Nucleus tractus solitarius efferent terminals synapse on neurons in the caudal ventrolateral medulla that project to the rostral ventrolateral medulla. *Brain Res*. 1995;693(1-2):51-63. doi:10.1016/0006-8993(95)00660-I

101. Zanutto BS, Frías BC, Valentinuzzi ME. Blood pressure long term regulation: A neural network model of the set point development. *Biomed Eng Online*. 2011;10(1):54. doi:10.1186/1475-925X-10-54

102. Bastianini S, Silvani A. Clinical implications of basic research. *Clin Transl Neurosci*. 2018;2(2):2514183X1878932. doi:10.1177/2514183x18789327

103. Schreihofer AM, Sved AF. Nucleus tractus solitarius and control of blood pressure in chronic sinoaortic denervated rats. *Am J Physiol - Regul Integr Comp Physiol*. 1992;263(2 32-2). doi:10.1152/ajpregu.1992.263.2.r258

104. Alheid GF, McCrimmon DR. The chemical neuroanatomy of breathing. *Respir Physiol Neurobiol*. 2008;164(1-2):3-11. doi:10.1016/j.resp.2008.07.014

105. Kubin L, Alheid GF, Zuperku EJ, McCrimmon DR. Central pathways of pulmonary and lower airway vagal afferents. *J Appl Physiol*. 2006;101(2):618-627. doi:10.1152/japplphysiol.00252.2006

106. Michael Spyer K, Gourine A V. Chemosensory pathways in the brainstem controlling cardiorespiratory activity. *Philos Trans R Soc B Biol Sci*. 2009;364(1529):2603-2610. doi:10.1098/rstb.2009.0082

107. Bauer J, Devinsky O, Rothermel M, Koch H. Autonomic dysfunction in epilepsy mouse models with implications for SUDEP research. *Front Neurol*. 2023;13. doi:10.3389/fneur.2022.1040648

108. van der Heijden ME, Zoghbi HY. Development of the brainstem respiratory circuit. *Wiley Interdiscip Rev Dev Biol*. 2020;9(3):1-15. doi:10.1002/wdev.366

109. Hayward LF, Castellanos M, Davenport PW. Parabrachial neurons mediate dorsal periaqueductal gray evoked respiratory responses in the rat. *J Appl Physiol*. 2004;96(3):1146-1154. doi:10.1152/japplphysiol.00903.2003

110. Martelli D, Stanić D, Dutschmann M. The emerging role of the parabrachial complex in the generation of wakefulness drive and its implication for respiratory control. *Respir Physiol Neurobiol*. 2013;188(3):318-323. doi:10.1016/j.resp.2013.06.019

111. Carrive P. The periaqueductal gray and defensive behavior: Functional representation and neuronal organization. *Behav Brain Res*. 1993;58(1-2):27-47. doi:10.1016/0166-4328(93)90088-8

112. Keay KA, Bandler R. Parallel circuits mediating distinct emotional coping reactions to different types of stress. *Neurosci Biobehav Rev*. 2001;25(7-8):669-678. doi:10.1016/S0149-7634(01)00049-5

113. Klaassen FH, de Voogd LD, Hulsman AM, et al. The neurocomputational link between defensive cardiac states and approach-avoidance arbitration under threat. *Commun Biol*. 2024;7(1). doi:10.1038/s42003-024-06267-6

114. Cechetto DF. Cortical control of the autonomic nervous system. *Exp Physiol*. 2014;99(2):326-331. doi:10.1113/expphysiol.2013.075192

115. Yasui Y, Breder CD, Safer CB, Cechetto DF. Autonomic responses and efferent pathways from the insular cortex in the rat. *J Comp Neurol*. 1991;303(3):355-374. doi:10.1002/cne.903030303

116. Cechetto DF, Saper CB. Evidence for a viscerotopic sensory representation in the cortex and thalamus in the rat. *J Comp Neurol*. 1987;262(1):27-45. doi:10.1002/cne.902620104

117. Zhang Z, Oppenheimer SM. Characterization, distribution and lateralization of baroreceptor-related neurons in the rat insular cortex. *Brain Res*. 1997;760(1-2):243-250. doi:10.1016/S0006-8993(97)00284-9

118. Shura RD, Hurley RA, Taber KH. Insular cortex: Structural and functional neuroanatomy. *J Neuropsychiatry Clin Neurosci*. 2014;26(4):277-282. doi:10.1176/appi.neuropsych.260401

119. Gogolla N. The insular cortex. *Curr Biol*. 2017;27(12):R580-R586. doi:10.1016/j.cub.2017.05.010

120. McGregor MS, LaLumiere RT. Still a “hidden island”? The rodent insular cortex in drug seeking, reward, and risk. *Neurosci Biobehav Rev*. 2023;153(July):105334. doi:10.1016/j.neubiorev.2023.105334

121. Gehrlach DA, Weiand C, Gaitanos TN, et al. A whole-brain connectivity map of mouse insular cortex. *Elife*. 2020;9:1-78. doi:10.7554/ELIFE.55585

122. Quabs J, Caspers S, Schöne C, et al. Cytoarchitecture, probability maps and segregation of the human insula. *Neuroimage*. 2022;260(June):119453. doi:10.1016/j.neuroimage.2022.119453

123. Zinn PO, Habib A, Deng H, et al. Uncovering Interoceptive Human Insular Lobe Function through Intraoperative Cortical Stimulation—A Review. *Brain Sci*. 2024;14(7). doi:10.3390/brainsci14070646

124. Allen G V., Saper CB, Hurley KM, Cechetto DF. Organization of visceral and limbic connections in the insular cortex of the rat. *J Comp Neurol*. 1991;311(1):1-16. doi:10.1002/cne.903110102

125. McDonald AJ, Shammah-Lagnado SJ, Shi C, Davis M. Cortical afferents to the extended amygdala. In: *Annals of the New York Academy of Sciences*. Vol 877. New York Academy of Sciences; 1999:309-338. doi:10.1111/j.1749-6632.1999.tb09275.x

126. Chen J, Gao Y, Bao ST, et al. Insula→Amygdala and Insula→Thalamus Pathways Are Involved in Comorbid Chronic Pain and Depression-Like Behavior in Mice. *J Neurosci*. 2024;44(15):1-17. doi:10.1523/JNEUROSCI.2062-23.2024

127. Özkan M, Altınöz D, Erkan E, Güneş YC, Algın O, Çavdar S. Thalamo-insular cortex connections in the rat and human. *Neurosci Lett*. 2025;847(October 2024). doi:10.1016/j.neulet.2024.138111

128. A.D. Craig. How do you feel? Interoception: the sense of the physiological condition of the body. *Nat Rev Neurosci*. 2002;3(August):655-666.

129. Critchley HD, Wiens S, Rotshtein P, Öhman A, Dolan RJ. Neural systems supporting interoceptive awareness. *Nat Neurosci*. 2004;7(2):189-195. doi:10.1038/nn1176

130. Oppenheimer S, Cechetto D. The insular cortex and the regulation of cardiac function. *Compr Physiol*. 2016;6(2):1081-1133. doi:10.1002/cphy.c140076

131. Lucina Q. Uddin1,2,*, Jason S. Nomi1, Benjamin Hebert-Seropian3, Jimmy Ghaziri4,5, and Olivier Boucher3 *. Structure and function of the human insula. *J Clin Neurophysiol*. 2017;34(4):300-306. doi:10.1016/j.physbeh.2017.03.040

132. Gehrlach DA, Dolensek N, Klein AS, et al. Aversive state processing in the posterior insular cortex. *Nat Neurosci*. 2019;22(9):1424-1437. doi:10.1038/s41593-019-0469-1

133. Casanova JP, Aguilar-Rivera M, Rodríguez M de los Á, Coleman TP, Torrealba F. The activity of discrete sets of neurons in the posterior insula correlates with the behavioral expression and extinction of conditioned fear. *J Neurophysiol*. 2018;120(4):1906-1913. doi:10.1152/jn.00318.2018

134. Klein AS, Dolensek N, Weiand C, Gogolla N. Fear balance is maintained by bodily feedback to the insular cortex in mice. *Science (80-)*. 2021;374(6570):1010-1015. doi:10.1126/science.abj8817

135. Foilb AR, Flyer-Adams JG, Maier SF, Christianson JP. Posterior insular cortex is necessary for conditioned inhibition of fear. *Neurobiol Learn Mem*. 2016;134(Part B):317-327. doi:10.1016/j.nlm.2016.08.004

136. Casanova JP, Aguilar-Rivera M, Rodríguez M de los Á, Coleman TP, Torrealba F. The activity of discrete sets of neurons in the posterior insula correlates with the behavioral expression and extinction of conditioned fear. *J Neurophysiol*. 2018;120(4):1906-1913. doi:10.1152/jn.00318.2018

137. de Paiva JPQ, Bueno APA, Dos Santos Corrêa M, Oliveira MGM, Ferreira TL, Fornari R V. The posterior insular cortex is necessary for the consolidation of tone fear conditioning. *Neurobiol Learn Mem*. 2021;179(August 2020). doi:10.1016/j.nlm.2021.107402

138. Critchley HD, Garfinkel SN. Interoception and emotion. *Curr Opin Psychol*. 2017;17:7-14. doi:10.1016/j.copsyc.2017.04.020

139. Chen WG, Schloesser D, Arensdorf AM, et al. The Emerging Science of Interoception: Sensing, Integrating, Interpreting, and Regulating Signals within the Self. *Trends Neurosci*. 2021;44(1):3-16. doi:10.1016/j.tins.2020.10.007

140. Khalsa SS, Adolphs R, Cameron OG, et al. Interoception and Mental Health: A Roadmap. *Biol Psychiatry Cogn Neurosci Neuroimaging*. 2018;3(6):501-513. doi:10.1016/j.bpsc.2017.12.004

141. Desmedt O, Luminet O, Maurage P, Corneille O. Discrepancies in the Definition and Measurement of Human Interoception: A Comprehensive Discussion and Suggested Ways Forward. *Perspect Psychol Sci*. Published online 2023. doi:10.1177/17456916231191537

142. Khalsa SS, Lapidus RC. Can interoception improve the pragmatic search for biomarkers in psychiatry? *Front Psychiatry*. 2016;7(JUL):1-19. doi:10.3389/fpsyt.2016.00121

143. Kleiman A, Kramer KA, Wegener I, et al. Psychophysiological decoupling in alexithymic pain disorder patients. *Psychiatry Res*. 2016;237:316-322. doi:10.1016/j.psychres.2016.01.021

144. Murphy J, Brewer R, Catmur C, Bird G. Interoception and psychopathology: A developmental neuroscience perspective. *Dev Cogn Neurosci*. 2017;23:45-56. doi:10.1016/j.dcn.2016.12.006

145. Khoury NM, Lutz J, Schuman-Olivier Z. Interoception in Psychiatric Disorders: A Review of Randomized, Controlled Trials with Interoception-Based Interventions. *Harv Rev Psychiatry*. 2018;26(5):250-263. doi:10.1097/HRP.0000000000000170

146. Schandry R. Heart Beat Perception and Emotional Experience. *Psychophysiology*. 1981;18(4):483-488.

147. Zhao W, Martin AD, Davenport PW. Detection of inspiratory resistive loads in double-lung transplant recipients. *J Appl Physiol*. 2002;93(5):1779-1785. doi:10.1152/japplphysiol.00210.2002

148. Garfinkel SN, Zorab E, Navaratnam N, et al. Anger in brain and body: The neural and

physiological perturbation of decision-making by emotion. *Soc Cogn Affect Neurosci*. 2015;11(1):150-158. doi:10.1093/scan/nsv099

149. Mehling W. Differentiating attention styles and regulatory aspects of self-reported interoceptive sensibility. *Philos Trans R Soc B Biol Sci*. 2016;371(1708). doi:10.1098/rstb.2016.0013

150. Zoellner LA, Craske MG. Interoceptive accuracy and panic. *Behav Res Ther*. 1999;37(12):1141-1158. doi:10.1016/S0005-7967(98)00202-2

151. Pollatos O, Traut-Mattausch E, Schandry R. Differential effects of anxiety and depression on interoceptive accuracy. *Depress Anxiety*. 2009;26(2):167-173. doi:10.1002/da.20504

152. Ricciardi L, Demartini B, Crucianelli L, Krahé C, Edwards MJ, Fotopoulou A. Interoceptive awareness in patients with functional neurological symptoms. *Biol Psychol*. 2016;113:68-74. doi:10.1016/j.biopsycho.2015.10.009

153. Garfinkel SN, Tiley C, O'Keeffe S, Harrison NA, Seth AK, Critchley HD. Discrepancies between dimensions of interoception in autism: Implications for emotion and anxiety. *Biol Psychol*. 2016;114:117-126. doi:10.1016/j.biopsycho.2015.12.003

154. Critchley HD. Neural mechanisms of autonomic, affective, and cognitive integration. *J Comp Neurol*. 2005;493(1):154-166. doi:10.1002/cne.20749

155. Craig ADB. How do you feel — now? The anterior insula and human awareness. *Nat Rev Neurosci*. 2009;10(January). doi:10.1038/nrn2555

156. Hassanpour MS, Simmons WK, Feinstein JS, et al. The insular cortex dynamically maps changes in cardiorespiratory interoception. *Neuropsychopharmacology*. 2018;43(2):426-434. doi:10.1038/npp.2017.154

157. Wang L, Gillis-Smith S, Peng Y, et al. The coding of valence and identity in the mammalian taste system. *Nature*. 2018;558(7708):127-131. doi:10.1038/s41586-018-0165-4

158. Paulus MP, Stein MB. Interoception in anxiety and depression. *Brain Struct Funct*. 2010;214(5-6):451-463. doi:10.1007/s00429-010-0258-9

159. Paulus MP, Stein MB. An Insular View of Anxiety. *Biol Psychiatry*. Published online 2006. doi:10.1016/j.biopsych.2006.03.042

160. Simmons A, Strigo I, Matthews SC, Paulus MP, Stein MB. Anticipation of Aversive Visual Stimuli Is Associated With Increased Insula Activation in Anxiety-Prone Subjects. *Biol Psychiatry*. 2006;60(4):402-409. doi:10.1016/j.biopsych.2006.04.038

161. Carlson JM, Greenberg T, Rubin D, Mujica-Parodi LR. Feeling anxious: Anticipatory amygdalo-insular response predicts the feeling of anxious anticipation. *Soc Cogn Affect Neurosci*. 2011;6(1):74-81. doi:10.1093/scan/nsq017

162. Simmons AN, Stein MB, Strigo IA, Arce E, Hitchcock C, Paulus MP. Anxiety positive subjects show altered processing in the anterior insula during anticipation of negative stimuli. *Hum Brain Mapp*. 2011;32(11):1836-1846. doi:10.1002/hbm.21154

163. Alvarez RP, Kirlic N, Misaki M, et al. Increased anterior insula activity in anxious individuals is linked to diminished perceived control. *Transl Psychiatry*. 2015;5(6):1-9. doi:10.1038/tp.2015.84

164. Stewart JL, May AC, Tapert SF, Paulus MP. Hyperactivation to pleasant interoceptive stimuli characterizes the transition to stimulant addiction. *Drug Alcohol Depend*. 2015;154:264-270. doi:10.1016/j.drugalcdep.2015.07.009

165. Tan Y, Wei D, Zhang M, Yang J, Jelinčić V, Qiu J. The role of mid-insula in the relationship between cardiac interoceptive attention and anxiety: evidence from an fMRI study. *Sci Rep*. 2018;8(1):1-12. doi:10.1038/s41598-018-35635-6

166. Harrison OK, Köchli L, Marino S, et al. Interoception of breathing and its relationship with anxiety. *Neuron*. 2021;109(24):4080-4093.e8. doi:10.1016/j.neuron.2021.09.045

167. Parkitna JR, Bilbao A, Rieker C, et al. Loss of the serum response factor in the dopamine system leads to hyperactivity: D1-Cre, D1-CreERT2. *FASEB J*. 2010;24(7):2427-2435.

doi:10.1096/fj.09-151423

168. Nord CL, Lawson RP, Dalgleish T. Disrupted Dorsal Mid-Insula Activation During Interoception Across Psychiatric Disorders. *Am J Psychiatry*. 2021;178(8):761-770. doi:10.1176/appi.ajp.2020.20091340

169. Livneh Y, Sugden AU, Madara JC, et al. Estimation of Current and Future Physiological States in Insular Cortex Article Estimation of Current and Future Physiological States in Insular Cortex. *Neuron*. Published online 2020:1-18. doi:10.1016/j.neuron.2019.12.027

170. Wu Y, Chen C, Chen M, et al. The anterior insular cortex unilaterally controls feeding in response to aversive visceral stimuli in mice. *Nat Commun*. 2020;11(1). doi:10.1038/s41467-020-14281-5

171. Aguilar-Rivera M, Kim S, Coleman TP, Maldonado PE, Torrealba F. Interoceptive insular cortex participates in sensory processing of gastrointestinal malaise and associated behaviors. *Sci Rep*. 2020;10(1):1-12. doi:10.1038/s41598-020-78200-w

172. Livneh Y, Sugden AU, Madara JC, et al. Estimation of Current and Future Physiological States in Insular Cortex. *Neuron*. 2020;105(6):1094-1111.e10. doi:10.1016/j.neuron.2019.12.027

173. Hsueh B, Chen R, Jo YJ, et al. Cardiogenic control of affective behavioural state. *Nature*. 2023;615(7951):292-299. doi:10.1038/s41586-023-05748-8

174. Gunaydin LA, Grosenick L, Finkelstein JC, et al. Natural neural projection dynamics underlying social behavior. *Cell*. 2014;157(7):1535-1551. doi:10.1016/j.cell.2014.05.017

175. Byron N, Sakata S. Fiber photometry-based investigation of brain function and dysfunction. *Neurophotonics*. 2023;11(S1):1-7. doi:10.1117/1.nph.11.s1.s11502

176. Junichi Nakai, Masamichi Ohkura, Keiji Imoto. A high signal-to-noise Ca2+ probe composed of a single green fluorescent protein. *Nat Biotechnol*. 2001;19:137-141. http://biotech.nature.com

177. Zhang Y, Rózsa M, Liang Y, et al. *Fast and Sensitive GCaMP Calcium Indicators for Imaging Neural Populations*. Vol 615. Springer US; 2023. doi:10.1038/s41586-023-05828-9

178. Kazmi SZH, Zhang H, Aziz W, et al. Inverse correlation between heart rate variability and heart rate demonstrated by linear and nonlinear analysis. *PLoS One*. 2016;11(6):1-10. doi:10.1371/journal.pone.0157557

179. Craig AD. Interoception: The sense of the physiological condition of the body. *Curr Opin Neurobiol*. 2003;13(4):500-505. doi:10.1016/S0959-4388(03)00090-4

180. Strigo IA, Bud Craig AD. Interoception, homeostatic emotions and sympathovagal balance. *Philos Trans R Soc B Biol Sci*. 2016;371(1708). doi:10.1098/rstb.2016.0010

181. Nemati SS, Sadeghi L, Dehghan G, Sheibani N. Lateralization of the hippocampus: A review of molecular, functional, and physiological properties in health and disease. *Behav Brain Res*. 2023;454(September):114657. doi:10.1016/j.bbr.2023.114657

182. Levy RB, Marquarding T, Reid AP, Pun CM, Renier N, Oviedo H V. Circuit asymmetries underlie functional lateralization in the mouse auditory cortex. *Nat Commun*. 2019;10(1). doi:10.1038/s41467-019-10690-3

183. Holt MK. The ins and outs of the caudal nucleus of the solitary tract: An overview of cellular populations and anatomical connections. *J Neuroendocrinol*. 2022;34(6):1-14. doi:10.1111/jne.13132

184. Lovelace JW, Ma J, Yadav S, et al. Vagal sensory neurons mediate the Bezold–Jarisch reflex and induce syncope. *Nature*. 2023;623(7986):387-396. doi:10.1038/s41586-023-06680-7

185. Guyenet PG. The sympathetic control of blood pressure. *Nat Rev Neurosci*. 2006;7(5):335-346. doi:10.1038/nrn1902

186. Elvsåshagen T, Bahrami S, van der Meer D, et al. The genetic architecture of human brainstem structures and their involvement in common brain disorders. *Nat Commun*.

2020;11(1). doi:10.1038/s41467-020-17376-1

187. Burhans LB, Schreurs BG. Inactivation of the central nucleus of the amygdala blocks classical conditioning but not conditioning-specific reflex modification of rabbit heart rate. *Neurobiol Dis*. 2013;100:88-97. doi:10.1016/j.nlm.2012.12.011.Inactivation

188. Ji Y, Onwukwe C, Smith J, et al. Noradrenergic Input from Nucleus of the Solitary Tract Regulates Parabrachial Activity in Mice. *eNeuro*. 2023;10(5):1-13. doi:10.1523/ENEURO.0412-22.2023

189. Holt MK, Valderrama N, Polanco MJ, Rinaman L. Modulation of stress-related behaviour by hypothalamic engagement of preproglucagon neurons in the nucleus of the solitary tract. *Mol Metab*. 2024;91(November 2024):2022.02.04.479117. doi:10.1016/j.molmet.2024.102076

190. Battaglia S, Nazzi C, Thayer JF. Fear-induced bradycardia in mental disorders: Foundations, current advances, future perspectives. *Neurosci Biobehav Rev*. 2023;149(March):105163. doi:10.1016/j.neubiorev.2023.105163

191. Vianna DML, Carrive P. Changes in cutaneous and body temperature during and after conditioned fear to context in the rat. *Eur J Neurosci*. 2005;21(9):2505-2512. doi:10.1111/j.1460-9568.2005.04073.x

192. Walker P, Carrive P. Role of ventrolateral periaqueductal gray neurons in the behavioral and cardiovascular responses to contextual conditioned fear and poststress recovery. *Neuroscience*. 2003;116(3):897-912. doi:10.1016/S0306-4522(02)00744-3

193. Roelofs K. Freeze for action: Neurobiological mechanisms in animal and human freezing. *Philos Trans R Soc B Biol Sci*. 2017;372(1718). doi:10.1098/rstb.2016.0206

194. Noordewier MK, Scheepers DT, Hilbert LP. Freezing in response to social threat: a replication. *Psychol Res*. 2020;84(7):1890-1896. doi:10.1007/s00426-019-01203-4

195. Jaswetz L, de Voogd LD, Becker ES, Roelofs K. The relevance of accounting for parasympathetic as well as sympathetic arousal in threat conditioning: methodological and clinical considerations. 2025;4(March).

196. Livneh Y, Andermann ML. Cellular activity in insular cortex across seconds to hours: Sensations and predictions of bodily states. *Neuron*. 2021;4:1-18. doi:10.1016/j.neuron.2021.08.036

197. Pinna T, Edwards DJ. A Systematic Review of Associations Between Interoception, Vagal Tone, and Emotional Regulation: Potential Applications for Mental Health, Wellbeing, Psychological Flexibility, and Chronic Conditions. *Front Psychol*. 2020;11(August):1-15. doi:10.3389/fpsyg.2020.01792

198. Lischke A, Pahnke R, Mau-Moeller A, Weippert M. Heart Rate Variability Modulates Interoceptive Accuracy. *Front Neurosci*. 2021;14(January):1-10. doi:10.3389/fnins.2020.612445

199. Rominger C, Schwerdtfeger AR. Predicting fluctuations in cardiac interoceptive accuracy and sensibility through additional heart rate variability reductions in everyday life. *Physiol Behav*. 2025;296(February):114928. doi:10.1016/j.physbeh.2025.114928

200. Francis JL, Weinstein AA, Krantz DS, et al. Association between Symptoms of Depression and Anxiety with Heart Rate Variability in Patients with Implantable Cardioverter Defibrillators. *Psychosom Med*. 2009;71(8):821-827. doi:10.1097/PSY.0b013e3181b39aa1.Association

201. Thome J, Densmore M, Frewen PA, et al. Desynchronization of autonomic response and central autonomic network connectivity in posttraumatic stress disorder. *Hum Brain Mapp*. 2017;38(1):27-40. doi:10.1002/hbm.23340

202. Ritsert F, Elgendi M, Galli V, Menon C. Heart and Breathing Rate Variations as Biomarkers for Anxiety Detection. *Bioengineering*. 2022;9(11):1-9. doi:10.3390/bioengineering9110711

203. Tomasi J, Zai CC, Zai G, et al. Investigating the association of anxiety disorders with heart rate variability measured using a wearable device. *J Affect Disord*. 2024;351(May

2023):569-578. doi:10.1016/j.jad.2024.01.137

204. Tovote P, Meyer M, Beck-Sickinger AG, et al. Central NPY receptor-mediated alteration of heart rate dynamics in mice during expression of fear conditioned to an auditory cue. *Regul Pept*. 2004;120(1-3):205-214. doi:10.1016/j.regpep.2004.03.011

205. Gaburro S, Stiedl O, Giusti P, Sartori SB, Landgraf R, Singewald N. A mouse model of high trait anxiety shows reduced heart rate variability that can be reversed by anxiolytic drug treatment. *Int J Neuropsychopharmacol*. 2011;14(10):1341-1355. doi:10.1017/S1461145711000058

206. Liu J, Wei W, Kuang H, Tsien JZ, Zhao F. Heart rate and heart rate variability assessment identifies individual differences in fear response magnitudes to earthquake, free fall, and air puff in mice. *PLoS One*. 2014;9(3). doi:10.1371/journal.pone.0093270

207. Thayer JF, Åhs F, Fredrikson M, Sollers JJ, Wager TD. A meta-analysis of heart rate variability and neuroimaging studies: Implications for heart rate variability as a marker of stress and health. *Neurosci Biobehav Rev*. 2012;36(2):747-756. doi:10.1016/j.neubiorev.2011.11.009

208. Mather M, Thayer JF. How heart rate variability affects emotion regulation brain networks. *Physiol Behav*. 2017;176(1):100–106. doi:10.1177/0022146515594631.Marriage

209. Chand T, Li M, Jamalabadi H, et al. Heart Rate Variability as an Index of Differential Brain Dynamics at Rest and After Acute Stress Induction. *Front Neurosci*. 2020;14(July). doi:10.3389/fnins.2020.00645

210. Min J, Koenig J, Nashiro K, et al. Sex Differences in Neural Correlates of Emotion Regulation in Relation to Resting Heart Rate Variability. *Brain Topogr*. 2023;36(5):698-709. doi:10.1007/s10548-023-00974-9

211. Colivicchi F, Bassi A, Santini M, Caltagirone C. Cardiac autonomic derangement and arrhythmias in right-sided stroke with insular involvement. *Stroke*. 2004;35(9):2094-2098. doi:10.1161/01.STR.0000138452.81003.4c

212. Lacuey N, Garg V, Bangert B, Hampson JP, Miller J, Lhatoo S. Insular resection may lead to autonomic function changes. *Epilepsy Behav*. 2019;97:260-264. doi:10.1016/j.yebeh.2019.04.035

213. Bradshaw JL, Rogers LJ. *The Evolution of Lateral Asymmetries, Language, Tool Use, and Intellect.* Academic Press; 1993.

214. Gainotti G. Emotions and the Right Hemisphere: Can New Data Clarify Old Models? *Neuroscientist*. 2019;25(3):258-270. doi:10.1177/1073858418785342

215. Ross ED. Differential hemispheric lateralization of emotions and related display behaviors: Emotion-type hypothesis. *Brain Sci*. 2021;11(8). doi:10.3390/brainsci11081034

216. Gainotti G. Emotional Behavior and Hemispheric Side of the Lesion. *Cortex*. 1972;8(1):41-55. doi:10.1016/S0010-9452(72)80026-1

217. Wang X, Wu Q, Egan L, et al. Anterior insular cortex plays a critical role in interoceptive attention. *Elife*. 2019;8:1-31. doi:10.7554/eLife.42265

218. Chan PYS, Cheng CH, Liu CY, Davenport PW. Cortical Sources of Respiratory Mechanosensation, Laterality, and Emotion: An MEG Study. *Brain Sci*. 2022;12(2). doi:10.3390/brainsci12020249

219. Leliveld LMC, Langbein J, Puppe B. The emergence of emotional lateralization: Evidence in non-human vertebrates and implications for farm animals. *Appl Anim Behav Sci*. 2013;145(1-2):1-14. doi:10.1016/j.applanim.2013.02.002

220. Guo CC, Sturm VE, Zhou J, et al. Dominant hemisphere lateralization of cortical parasympathetic control as revealed by frontotemporal dementia. *Proc Natl Acad Sci U S A*. 2016;113(17):E2430-E2439. doi:10.1073/pnas.1509184113

221. Greco A, Faes L, Catrambone V, Barbieri R, Scilingo EP, Valenza G. Lateralization of directional brain-heart information transfer during visual emotional elicitation. *Am J Physiol - Regul Integr Comp Physiol*. 2019;317(1):R25-R38. doi:10.1152/ajpregu.00151.2018

222. Belcheva I, Belcheva S, Petkov V V., Petkov VD. Asymmetry in behavioral responses to cholecystokinin microinjected into rat nucleus accumbens and amygdala. *Neuropharmacology*. 1994;33(8):995-1002. doi:10.1016/0028-3908(94)90158-9

223. Orman R, Stewart M. Hemispheric differences in protein kinase C βII levels in the rat amygdala: Baseline asymmetry and lateralized changes associated with cue and context in a classical fear conditioning paradigm. *Neuroscience*. 2007;144(3):797-807. doi:10.1016/j.neuroscience.2006.10.017

224. Young EJ, Williams CL. Differential activation of amygdala Arc expression by positive and negatively valenced emotional learning conditions. *Front Behav Neurosci*. 2013;7(DEC):1-13. doi:10.3389/fnbeh.2013.00191

225. Mundorf A, Ocklenburg S. Hemispheric asymmetries in mental disorders: evidence from rodent studies. *J Neural Transm*. 2023;130(9):1153-1165. doi:10.1007/s00702-023-02610-z

226. Ocklenburg S, Peterburs J, Mundorf A. Hemispheric asymmetries in the amygdala: A comparative primer. *Prog Neurobiol*. 2022;214(April):102283. doi:10.1016/j.pneurobio.2022.102283

227. Andersen SL, Teicher MH. Serotonin laterality in amygdala predicts performance in the elevated plus maze in rats. *Neuroreport*. 1999;10(17):3497-3500. doi:10.1097/00001756-199911260-00006

228. Casperd JM, Dunbar RIM. Asymmetries in the visual processing of emotional cues during agonistic interactions by gelada baboons. *Behav Processes*. 1996;37(1):57-65. doi:10.1016/0376-6357(95)00075-5

229. Cechetto DF, Shoemaker JK. Functional neuroanatomy of autonomic regulation. *Neuroimage*. 2009;47(3):795-803. doi:10.1016/j.neuroimage.2009.05.024

230. Milad MR, Orr SP, Klibanski A, et al. Fear conditioning and extinction: Influence of sex and menstrual cycle in healthy humans. *Behav Neurosci*. 2006;120(6):1196-1203. doi:10.1037/0735-7044.120.5.1196

231. Milad MR, Zeidan M a, Contero A, et al. Hormones estradiol fear extinction recall in Healthy Humans. *Biol Psychiatry*. 2011;168(3):652-658. doi:10.1016/j.neuroscience.2010.04.030.The

232. White EC, Graham BM. Estradiol levels in women predict skin conductance response but not valence and expectancy ratings in conditioned fear extinction. *Neurobiol Learn Mem*. 2016;134:339-348. doi:10.1016/j.nlm.2016.08.011

233. Hwang MJ, Zsido RG, Song H, et al. Contribution of estradiol levels and hormonal contraceptives to sex differences within the fear network during fear conditioning and extinction. *BMC Psychiatry*. 2015;15(1):1-12. doi:10.1186/s12888-015-0673-9

234. Chang YJ, Yang CH, Liang YC, Yeh CM, Huang CC, Hsu K Sen. Estrogen modulates sexually dimorphic contextual fear extinction in rats through estrogen receptor β. *Hippocampus*. 2009;19(11):1142-1150. doi:10.1002/hipo.20581

235. Button KS, Ioannidis JPA, Mokrysz C, et al. Power failure: Why small sample size undermines the reliability of neuroscience. *Nat Rev Neurosci*. 2013;14(5):365-376. doi:10.1038/nrn3475

236. Faber J, Fonseca LM. How sample size influences research outcomes. *Dental Press J Orthod*. 2014;19(4):27-29. doi:10.1590/2176-9451.19.4.027-029.ebo

237. Jungbauer S, Buehler PK, Neubauer J, et al. Sex-dependent differences in the in vivo respiratory phenotype of the TASK-1 potassium channel knockout mouse. *Respir Physiol Neurobiol*. 2017;245:13-28. doi:10.1016/j.resp.2016.11.005

238. Zhang TY, Zhao BJ, Wang T, Wang J. Effect of aging and sex on cardiovascular structure and function in wildtype mice assessed with echocardiography. *Sci Rep*. 2021;11(1):1-12. doi:10.1038/s41598-021-02196-0

239. St. Pierre SR, Peirlinck M, Kuhl E. Sex Matters: A Comprehensive Comparison of Female

and Male Hearts. *Front Physiol*. 2022;13(March):1-19. doi:10.3389/fphys.2022.831179

240. Taylor CE, Mendenhall LE, Sunshine MD, et al. Sex and APOE genotype influence respiratory function under hypoxic and hypoxic-hypercapnic conditions. *J Neurophysiol*. 2024;132(1):23-33. doi:10.1152/jn.00255.2023

241. Zanarini MC, Frankenburg FR, DeLuca CJ, Hennen J, Khera GS, Gunderson JG. The pain of being borderline: Dysphoric states specific to borderline personality disorder. *Harv Rev Psychiatry*. 1998;6(4):201-207. doi:10.3109/10673229809000330

242. Yang JN, Tiselius C, Daré E, Johansson B, Valen G, Fredholm BB. Sex differences in mouse heart rate and body temperature and in their regulation by adenosine A1 receptors. *Acta Physiol*. 2007;190(1):63-75. doi:10.1111/j.1365-201X.2007.01690.x

243. Raşid O, Chirita D, Iancu AD, Stavaru C, Radu DL. Assessment of routine procedure effect on breathing parameters in mice by using whole-body plethysmography. *J Am Assoc Lab Anim Sci*. 2012;51(4):469-474.

244. Carnevali L, Barbetti M, Statello R, Williams DWP, Thayer JF, Sgoifo A. Sex differences in heart rate and heart rate variability in rats: Implications for translational research. *Front Physiol*. 2023;14(March):1-10. doi:10.3389/fphys.2023.1170320

245. Emerson JI, Ariel P, Shi W, Conlon FL. Sex Differences in Mouse Cardiac Electrophysiology Revealed by Simultaneous Imaging of Excitation-Contraction Coupling. *J Cardiovasc Dev Dis*. 2023;10(12). doi:10.3390/jcdd10120479

246. Frasier RM, De Oliveira Sergio T, Starski PA, Grippo AJ, Hopf FW. Heart rate variability measures indicating sex differences in autonomic regulation during anxiety-like behavior in rats. *Front Psychiatry*. 2023;14(October). doi:10.3389/fpsyt.2023.1244389

247. Davis M. The role of the amygdala in fear and anxiety. *Annu Rev Neurosci*. 1992;15:353-375. doi:10.1146/annurev.ne.15.030192.002033

248. LeDoux JE. Emotion, memory and the brain. *Sci Am*. 1994;270(6):50-57. doi:10.1038/scientificamerican0694-50

249. LeDoux JE. Coming to terms with fear. *Proc Natl Acad Sci U S A*. 2014;111(8):2871-2878. doi:10.1073/pnas.1400335111

250. Allen HN, Bobnar HJ, Kolber BJ. Left and right hemispheric lateralization of the amygdala in pain. *Prog Neurobiol*. 2021;196(May 2020):101891. doi:10.1016/j.pneurobio.2020.101891

251. Palomero-Gallagher N, Amunts K. A short review on emotion processing: a lateralized network of neuronal networks. *Brain Struct Funct*. 2022;227(2):673-684. doi:10.1007/s00429-021-02331-7

252. Allen G V., Saper CB, Hurley KM, Cechetto DF. Organization of visceral and limbic connections in the insular cortex of the rat. *J Comp Neurol*. 1991;311(1):1-16. doi:10.1002/cne.903110102

253. Bentley TGK, D'Andrea-Penna G, Rakic M, et al. Breathing Practices for Stress and Anxiety Reduction: Conceptual Framework of Implementation Guidelines Based on a Systematic Review of the Published Literature. *Brain Sci*. 2023;13(12). doi:10.3390/brainsci13121612

254. Fincham GW, Strauss C, Montero-Marin J, Cavanagh K. Effect of breathwork on stress and mental health: A meta-analysis of randomised-controlled trials. *Sci Rep*. 2023;13(1):1-14. doi:10.1038/s41598-022-27247-y

255. Luo Q, Li X, Zhao J, Jiang Q, Wei D. The effect of slow breathing in regulating anxiety. *Sci Rep*. 2025;15(1):1-10. doi:10.1038/s41598-025-92017-5

Supplements

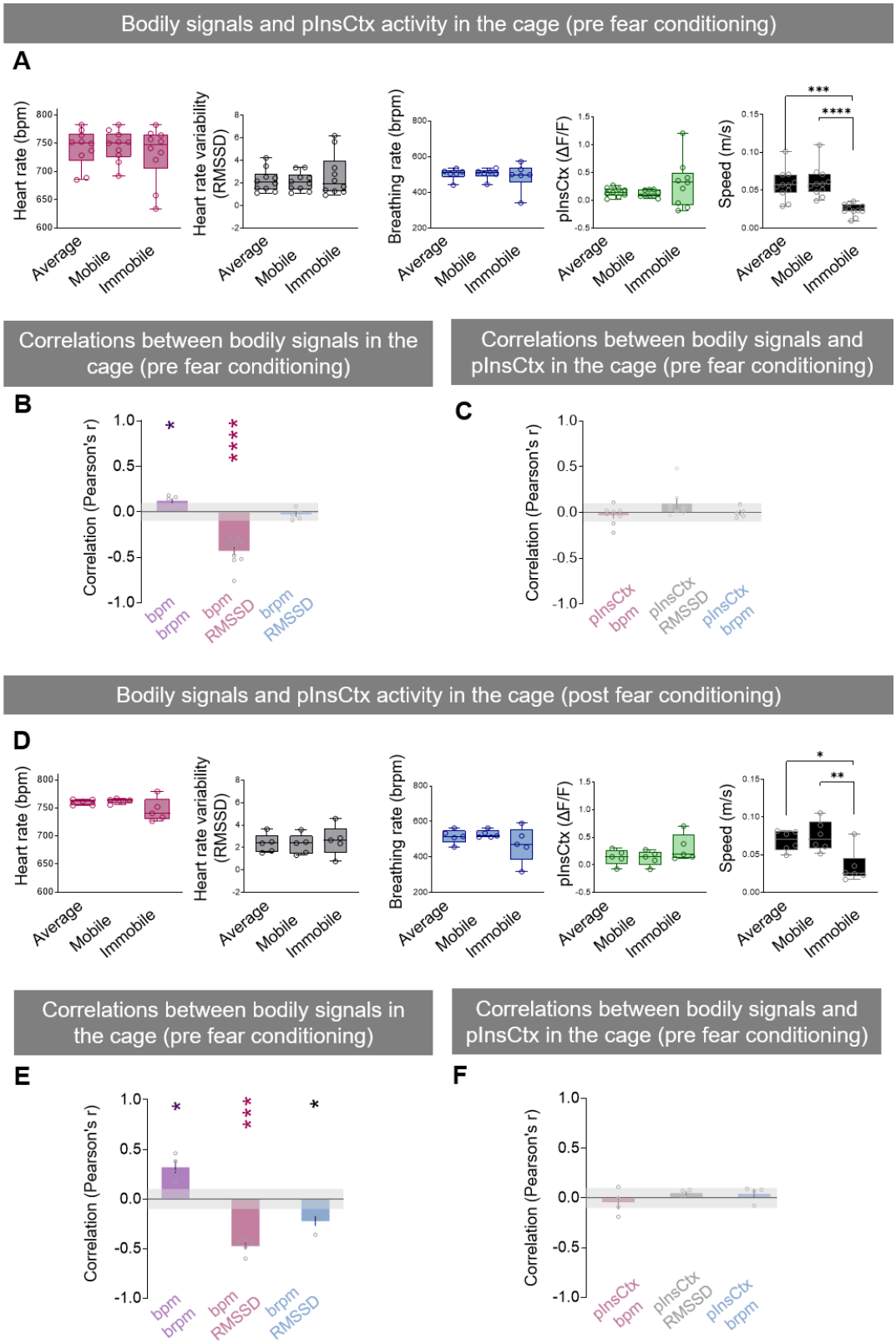

Suppl. Fig. 1**: Bodily signals and pInsCtx activity during cage recordings before and after fear conditioning**

A) Averaged responses of bodily signals (breathing rate (brpm, n=5), heart rate (bpm, n=10), heart rate variability (RMSSD, n=10)), pInsCtx activity (ΔF/F, n=9) and speed (m/s, n=11) of all animals in the home cage the day before fear conditioning (day 1 of experimental timeline). Divided into three measures: during the entire recording time (average), only during times the animals were active (mobile) and only during times the animals were inactive (immobile). Statistics: comparisons between average, mobile and immobile with Ordinary one-way ANOVA, post-hoc Tukey's multiple comparisons test; Speed: average vs. immobile ***p=0.0002, mobile vs. immobile ****p<0.0001. All other comparisons were ns.
B) Pearson's correlations between bodily signals (as in A); Bpm and brpm (n=5) mean r=0.12, **p=0.009, Bpm and RMSSD (n=10) mean r=-0.43, ****p<0.0001; Brpm and RMSSD (n=5) ns.
C) Pearson's correlations between bodily signals (as in A) and pInsCtx; All comparisons ns. pInsCtx-bpm: n=8, pInsCtx-RMSSD: n=8, pInsCtx-brpm: n=5
D) Averaged responses of bodily signals (breathing rate (brpm, n=5), heart rate (bpm, n=5), heart rate variability (RMSSD, n=5)), pInsCtx activity (ΔF/F, n=5) and speed (m/s, n=5) of all animals in the home cage three days after conclusion the fear and extinction conditioning paradigm (day 7 of experimental timeline). Divided into three measures: during the entire recording time (average), only during times the animals were active (mobile) and only during times the animals were inactive (immobile). Statistics: comparisons between average, mobile and immobile with Ordinary one-way ANOVA, post-hoc Tukey's multiple comparisons test; Speed: average vs. immobile *p=0.02, mobile vs. immobile **p=0.005. All other comparisons were ns.
E) Pearson's correlations between bodily signals (as in A and D); Bpm and brpm (n=4) mean r=0.32 *p=0.02, bpm and RMSSD (n=5) mean r=-0.47 ****p<0.0001, Brpm and RMSSD (n=4) mean r=-0.22, *p=0.02.
F) Pearson's correlations between bodily signals (as in A and D) and pInsCtx; All comparisons ns. pInsCtx-bpm: n=4, pInsCtx-RMSSD: n=4, pInsCtx-brpm: n=4.
Averaged values show the mean, error bars show SEM. Horizontal grey bars between -0.1 and 0.1 indicate area in which the mean Pearson's r values indicate no correlation.

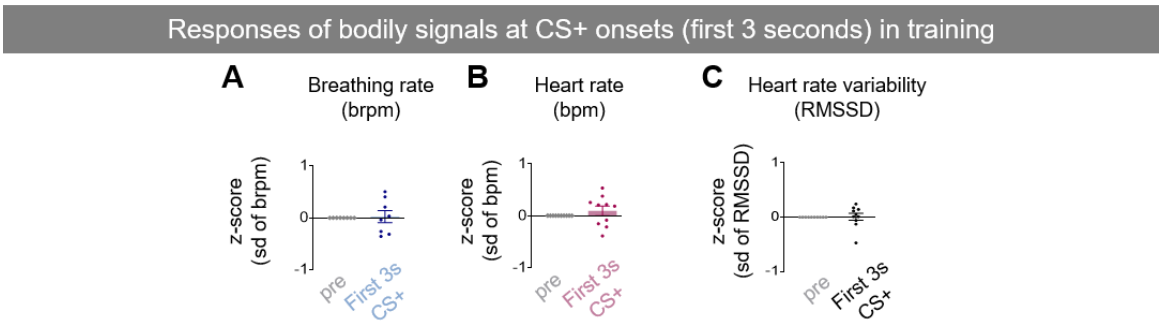

Suppl. Fig. 2: **Bodily signals at CS+ onset (Initial 3 seconds of tone presentation) in training**
A-C) Response of bodily signals (breathing rate (brpm, n=8), heart rate (bpm, n=11), heart rate variability (RMSSD, n=11)) at the onset of CS+ (first 3 seconds) in training, z-scored to the 10 seconds of baseline before CS+ onset (pre). comparison of baseline (10 seconds preceding CS+) vs. CS+ with paired t-test. All comparisons ns. Averaged values show the mean, error bars show SEM.

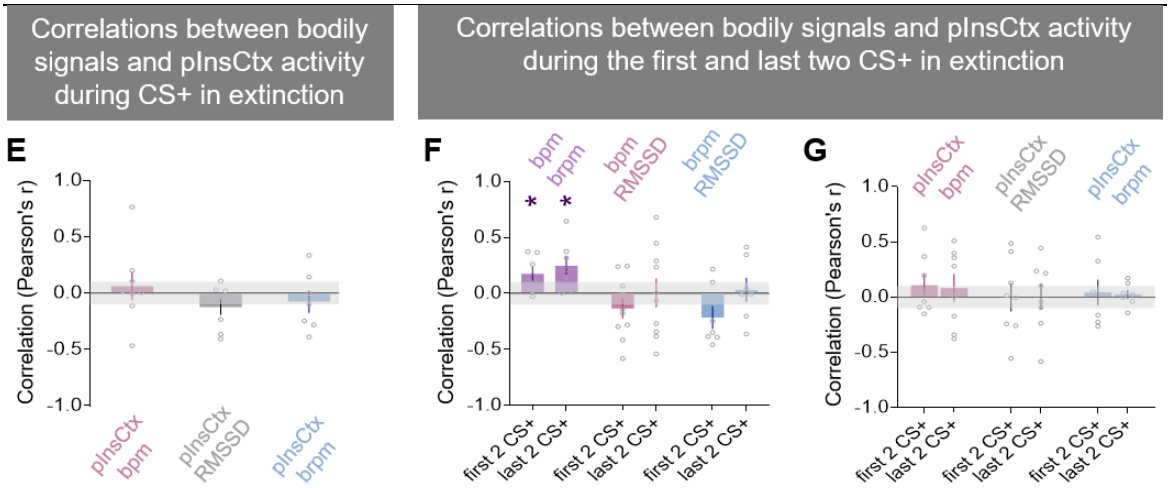

Suppl. Fig. 3: **Bodily signals and pInsCtx activity at CS+ onset (Initial 3 seconds of tone presentation) and correlation between bodily signals and pInsCtx activity in extinction**
A) Pearson's correlations between bodily signals (as in A-C) and pInsCtx in extinction; All correlations ns.
B) Pearson's correlations between bodily signals (as in A-C); during the first 2 CS+ and last 2 CS+ in extinction; Bpm and brpm first 2 CS+ mean r=0.18, *p=0.03; Bpm and brpm last 2 CS+ mean r=0.25, *p=0.03; All other correlations ns.
C) Pearson's correlations between bodily signals (as in A-C) and pInsCtx activity (ΔF/F); during the first 2 CS+ and last 2 CS+ in extinction; All correlations ns.
Averaged values show the mean, shading and error bars show SEM. E-G: Horizontal grey bars between -0.1 and 0.1 indicate area in which the mean Pearson's r values indicate no correlation.
Animal numbers for E-G: bpm-RMSSD: n=10; pInsCtx-bpm: n=8; pInsCtx-RMSSD: n=8; bpm-brpm: n=7; brpm-RMSSD: n=7; pInsCtx-brpm: n=7.

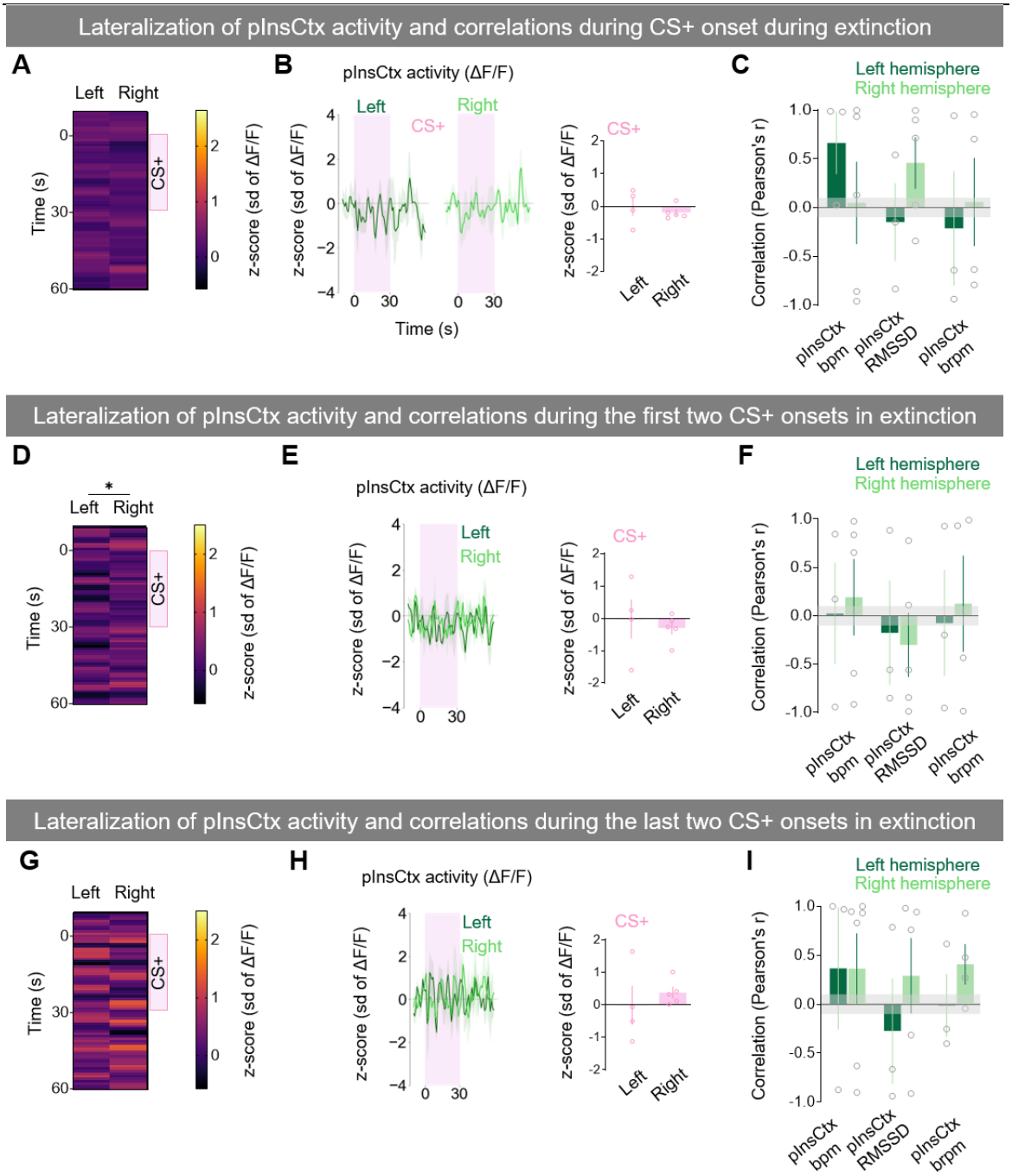

Suppl. Fig. 4**: No strong lateralization effects during CS+ in extinction**
A) Comparison of baseline (10 seconds preceding CS+), CS+ and postCS+ (30 seconds post CS+) of average pInsCtx activity (ΔF/F) in extinction between left (n=4) and right (n=5) hemisphere. Unpaired t-test ns.
B) Average pInsCtx activity (ΔF/F) responses to all 8 CS+ presentations in extinction of the left (dark green, left, n=4) and right (light green, middle, n=5) hemisphere. Comparison of responses during the first 3 seconds of CS+ between both hemispheres with unpaired t-test: ns.
C) Pearson's correlations between pInsCtx activity (ΔF/F) and heart rate (bpm), pInsCtx activity and HRV (RMSSD) and pInsCtx activity and breathing rate (brpm) per hemisphere in extinction. All interactions were ns; Comparisons between hemispheres with unpaired t-tests: All left vs. right pInsCtx interactions with bodily signals were ns. pInsCtx left and bpm n=3, pInsCtx left and RMSSD n=3, pInsCtx left and brpm n=3, pInsCtx right and bpm n=5, pInsCtx right and RMSSD n=5, pInsCtx right and brpm n=4.

D) Comparison of baseline (10 seconds preceding CS+), CS+ and postCS+ (30 seconds post CS+) of average pInsCtx activity (ΔF/F) during the first two CS+ presentations in extinction between left (n=4) and right (n=5) hemisphere. Unpaired t-test *p=0.01.
E) Left: Average pInsCtx activity (ΔF/F) responses to the first two CS+ presentations in extinction of the left (dark green, n=4) and right (light green, n=5) hemisphere. Right: Comparison of responses during the first 3 seconds of CS+ between both hemispheres with unpaired t-test: ns.
F) Pearson's correlations between pInsCtx and bodily signals (as in C) during the first two CS+ presentations per hemisphere; All correlations as well as comparisons between hemispheres were ns. pInsCtx left and bpm n=3, pInsCtx left and RMSSD n=3, pInsCtx left and brpm n=3, pInsCtx right and bpm n=5, pInsCtx right and RMSSD n=5, pInsCtx right and brpm n=4.
G) Comparison of baseline (10 seconds preceding CS+), CS+ and postCS+ (30 seconds post CS+) of average pInsCtx activity (ΔF/F) during the last two CS+ presentations in extinction between left (n=4) and right (n=5) hemisphere. Unpaired t-test ns.
H) Left: Average pInsCtx activity (ΔF/F) responses to the last two CS+ presentations in extinction of the left (dark green, n=4) and right (light green, n=5) hemisphere. Right: Comparison of responses during the first 3 seconds of CS+ between both hemispheres with unpaired t-test: *p=0.04.
I) Pearson's correlations between pInsCtx and bodily signals (as in C and F) during the last two CS+ presentations in extinction per hemisphere; All correlations as well as comparisons between hemispheres were ns. pInsCtx left and bpm n=3, pInsCtx left and RMSSD n=3, pInsCtx left and brpm n=3, pInsCtx right and bpm n=5, pInsCtx right and RMSSD n=5, pInsCtx right and brpm n=4.
Vertical pink bars indicate the duration of CS+ presentations (30 seconds); yellow line and lightning bolt indicate time point of foot shock (US); heatmaps show z-scored pInsCtx activity (ΔF/F); left hemisphere: dark green, right hemisphere: light green.
Averaged values show the mean, shading and error bars show SEM.

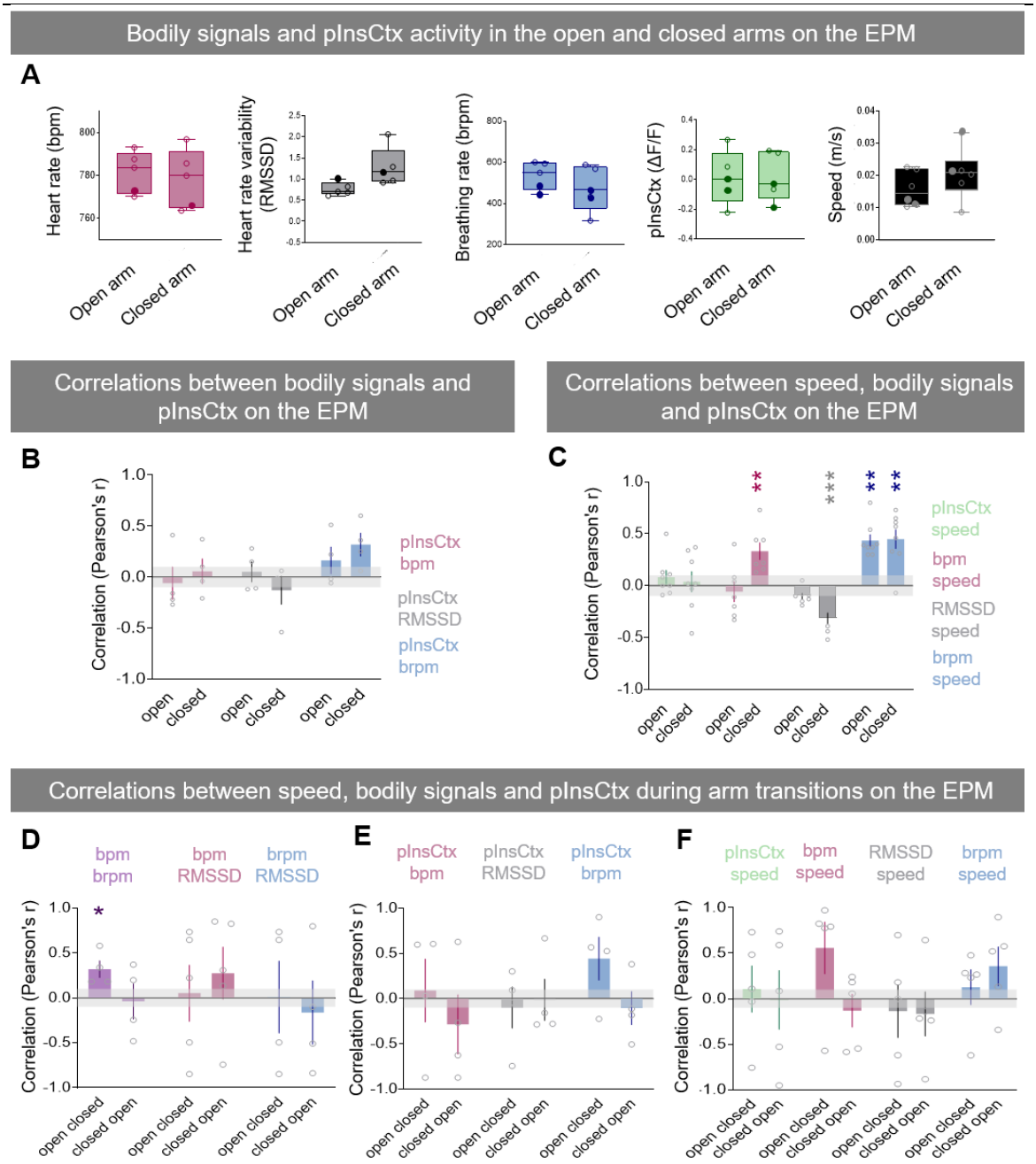

Suppl. Fig. 5**: Averages on open vs. closed arm and correlations on the EPM**
A) Averaged responses of bodily signals (breathing rate (brpm, n=5), heart rate (bpm, n=5), heart rate variability (RMSSD, n=5)), pInsCtx activity (ΔF/F, n=5) and speed (n=6) of all animals on the open arm and closed arm. Animals that spent >50% of the time in the open arms are shown as filled circles, animals that spent <50% of the time in the closed arm are shown in empty circles. Statistics: comparisons between average, mobile and immobile with Ordinary one-way ANOVA, post-hoc Tukey's multiple comparisons test; All comparisons ns.
B) Pearson's correlations between bodily signals (as in A) and pInsCtx activity (ΔF/F) on the EPM in the open arms (open) and closed arms (closed); All correlations ns. pInsCtx-bpm: n=4, pInsCtx-RMSSD: n=4, pInsCtx-brpm: n=4
C) Pearson's correlations between bodily signals (as in A), pInsCtx activity (ΔF/F) and speed (m/s) on the EPM in the open arms (open) and closed arms (closed); Open: Brpm-speed (n=5) mean r=0.45 **p=0.007; Closed: Bpm-speed (n=5) mean r=0.33 **p=0.007, RMSSD-speed (n=5) mean r=-0.32 ***p=0.001, Brpm-speed (n=5) mean r=0.45 **p=0.002; All other correlations ns. pInsCtx-speed (n=5).

D-F: Pearson's correlations during arm transitions. From the open arm to the closed (open closed) and from the closed arm to the open (closed open).
D) Pearson's correlations between bodily signals (as in A) during transitions; Bpm-brpm during transition between open to the closed arm (open closed, n=4) mean r=0.32 *p=0.04 All other correlations ns.
E) Pearson's correlations between bodily signals (as in A) and pInsCtx activity (ΔF/F) during transitions; All correlations ns. bpm-brpm: n=4, brpm-RMSSD: n=4, pInsCtx-bpm: n=4, pInsCtx-RMSSD: n=4, pInsCtx-brpm: n=4, bpm-RMSSD: n=5, speed correlated with any of the bodily signals or pInsCtx: n=5
F) Pearson's correlations between bodily signals (as in A), pInsCtx activity (ΔF/F) and speed (m/s) during transitions; All correlations ns. bpm-brpm: n=4, brpm-RMSSD: n=4, pInsCtx-bpm: n=4, pInsCtx-RMSSD: n=4, pInsCtx-brpm: n=4, bpm-RMSSD: n=5, speed correlated with any of the bodily signals or pInsCtx: n=5
Averaged values show the mean, error bars show SEM. Horizontal grey bars between -0.1 and 0.1 indicate area in which the mean Pearson's r values indicate no correlation.

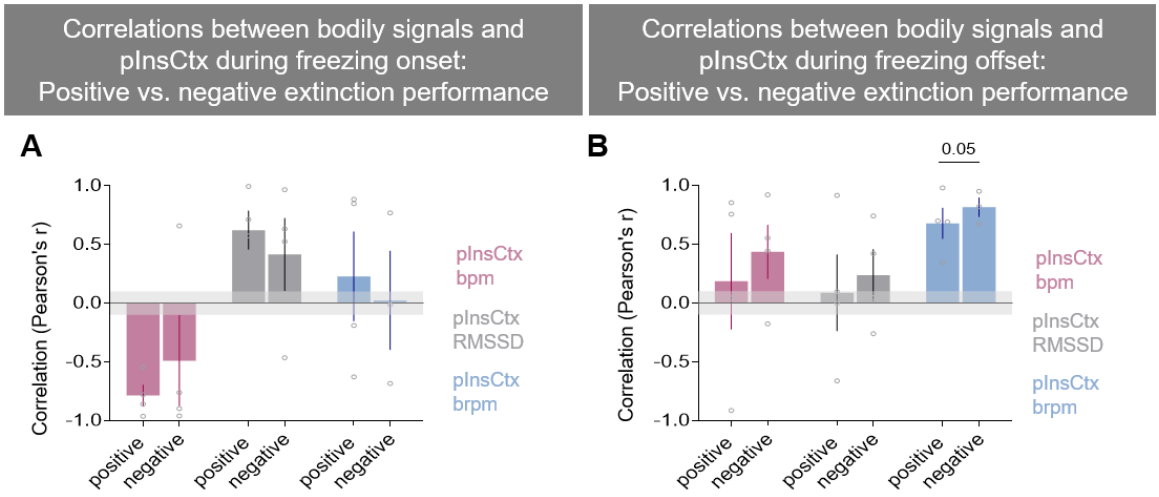

Suppl. Fig. 6: **Correlations between bodily signals and pInsCtx during freezing between animals with a positive vs. animals with a negative extinction performance.**
A) Pearson's correlations of bodily signals (breathing rate (brpm), heart rate (bpm), heart rate variability (RMSSD)) with pInsCtx activity of animals with a positive extinction performance (right bars) and a negative extinction performance (left bars) after freezing onsets. Freezing episodes: length ≥ 5 seconds that were ≥ 3 seconds apart from other freezing episodes. Responses are z-scored to the 3 seconds of baseline before freezing. Statistics: Comparison of correlations with bodily signals of positive vs. negative extinction performance groups. Unpaired t-test. All comparisons ns.
B) Pearson's correlations of bodily signals (breathing rate (brpm), heart rate (bpm), heart rate variability (RMSSD)) with pInsCtx activity of animals with a positive extinction performance (right bars) and a negative extinction performance (left bars) before freezing offsets. Freezing episodes: length ≥ 5 seconds that were ≥ 3 seconds apart from other freezing episodes. Responses ae z-scored to the 3 seconds of post-baseline after freezing. Statistics: Comparison of correlations with bodily signals of positive vs. negative extinction performance groups. Unpaired t-test. All comparisons ns; pInsCtx-brpm p=0.05.
Averaged values show the mean, error bars show SEM. Horizontal grey bars between -0.1 and 0.1 indicate area in which the mean Pearson's r values indicate no correlation.

Acknowledgements

First of all, I want to thank Nadine Gogolla for the warm invitation to the lab. Your guidance and advice throughout my PhD has made a big impact on my research career. Thank you to Elisabeth Binder and Nikos Koutsouleris for being encouraging and supportive TAC members. A big thank you to Victor Spoormaker for his valuable input and help. I want to thank my graduate school IMPRS-TP for giving me the opportunity to learn, network and grow as a scientist. A special thank you, also to our IMPRS-TP coordinator Janhvi, for always being supportive, helpful, and uplifting. A collective thank you goes to all the people in Martinsried at the former Max Planck Institute for Neuroscience and in Schwabing at the Max Planck Institute of Psychiatry who made PhD life a little easier by making sure things are running smoothly. I want to thank Anna for being a great friend to share this PhD journey with. And what a ride this journey has been. The long nights and weekends in the lab and office would have been a lot less fun without you. Thank you to Eunjae, Andrea and Bianca for not only providing advice and support but also being wonderful people. Thank you to Catherine for having been an amazing intern, who helped me so much and was always a joy to be around. Thank you to Ronja for being a great desk neighbor and the best stats support one could wish for.

On a more personal note, I want to thank my parents, who always believe in me and support me through everything life throws at me. A heartfelt thank you to Vanni, who I'm fortunate enough to have in my life since kindergarten times. Thank you Schlumpfi, for being an important part of my life. A big thank you to Rayan, who has always been my fiercest supporter. You hold a special place in my heart. Thank you to C.S. for helping me through the rough patches, celebrating the wins with me and always being in my corner. A massive thank you to Karow, Lars, Alexandra and Torsten for being my feelgood people. Thank you, Matthew, for all your patience with me and my moods and all the great times together. Thank you, Eyk and Hera, for all the love and strength you gave me. A big thank you to my beloved pets Aladdin, Luna and Salem, who were and are by my side, being a constant source of joy and love every single day.

Last but certainly not least, I want to thank all the mice, without whom none of this work would have been possible.

LMU LUDWIG-MAXIMILIANS-UNIVERSITÄT MÜNCHEN

Dean's Office Medical Faculty
Faculty of Medicine

Affidavit

Weiand, Caroline

Surname, first name

I hereby declare, that the submitted thesis entitled

Role of the posterior insular cortex in cardiorespiratory interoception during fear

is my own work. I have only used the sources indicated and have not made unauthorised use of services of a third party. Where the work of others has been quoted or reproduced, the source is always given.

I further declare that the dissertation presented here has not been submitted in the same or similar form to any other institution for the purpose of obtaining an academic degree.

München, 28.01.2026

Place, Date

Caroline Weiand

Signature doctoral candidate

LMU LUDWIG-MAXIMILIANS-UNIVERSITÄT MÜNCHEN

Dean's Office Medical Faculty
Doctoral Office

Confirmation of congruency between printed and electronic version of the doctoral thesis

Weiand, Caroline

Surname, first name

I hereby declare that the electronic version of the submitted thesis, entitled

Role of the posterior insular cortex in cardiorespiratory interoception during fear

is congruent with the printed version both in content and format.

München, 28.01.2026

Place, Date

Caroline Weiand

Signature doctoral candidate